ECHOES AND SCATTERING
FROM PLASMA IN A MAGNETIC FIELD

Fred A. Blum

Technical Report No. 39

May 1968

Research sponsored

by the U. S. Office of Naval Research

Contract Nonr 220(50)

California Institute of Technology

Pasadena, California

ACKNOWLEDGEMENTS

The writing of this thesis marks the culmination of many years of work toward a long standing goal. My achievements during these years are due in part to the advice, encouragement, and training of many people. In a real sense, all of these people contributed to this thesis. To each of them I extend my sincere thanks. However, two people stand out conspicuously: Professor R. N. Little of the University of Texas and Professor L. Davis of Caltech. The open office doors, obvious concern and generous spirit of these men gave invaluable impetus to my career as a student and physicist.

There are several people who have contributed in a more direct sense to the accomplishment embodied in this thesis. I am thoroughly grateful and indebted to Professor R. W. Gould for his profound influence on my professional advancement and achievement in recent years. His direct contributions to the work, willingness to collaborate, and patience are exceptional. In addition, I wish to thank my colleague L. O. Bauer for his cooperation and invaluable contributions to the material in this paper. My thanks go also to others of the Plasma Laboratory and Caltech who have played a useful role at one time or another during the course of this work. Particularly, I thank Professor R. S. Harp for his enlightened comments and advice, and R. Stenzel for collaboration and the use of his radiometer.

I am indebted to Hughes Aircraft Company and the National Science Foundation for financial support during the course of my

graduate studies. My sincere thanks go to Mrs. Ruth Stratton for the patience, loving care and efficiency she exercised in typing this manuscript. Finally, I am deeply grateful to my wife, Joy; her love and devotion as a wife and mother have made the task at hand palatable and worth while.

ABSTRACT

A study of the high frequency properties of a low temperature plasma column in a longitudinal magnetic field is described. The experimental observations give a relatively complete picture of the microwave (extraordinary mode) properties of the plasmas studied, encompassing continuous wave scattering and noise emission measurements, as well as the demonstration of the occurrence of related echo processes. Theoretical developments deal largely with a physical model consisting of a one-dimensional slab of cold (zero temperature) plasma which is nonuniform in the steady state and immersed in a uniform magnetic field. Data on the continuous wave reflection and noise emission from some afterglow rare gas discharges are given. The electron temperature in these plasmas is low, approaching room temperature. The reflection and emission are measured as a function of magnetic field in the vicinity of electron cyclotron resonance with electron density as a parameter. The electron densities are such that $(\omega_p/\omega) \leq 1$, where ω_p is the electron plasma frequency and ω is the signal frequency. Both types of experiment show the presence of collective effects which yield a normal mode spectrum strongly dependent on the electron density. A broad peak is observed in the region $(\omega_c/\omega) \leq 1$ where ω_c is the electron cyclotron frequency. This peak shifts to lower values of (ω_c/ω) and broadens as the electron density increases. For all values of electron density, a sharp peak is found very close to $(\omega_c/\omega) = 1$, the cyclotron resonance condition. The experimental and theoretical results suggest that the phenomena observed involve resonance effects

at the upper hybrid frequencies ($\omega_h^2 = \omega_c^2 + \omega_p^2$) of the plasma. Data are also given on a new two-pulse echo process which occurs in these afterglow plasmas. The results establish the intimate relation between the echoes and the upper hybrid normal modes studied in the CW experiments, demonstrating the dominant role played by collective effects in the formation of this echo. A weakly nonlinear cold plasma theory yields upper hybrid echoes which are strongest in a narrow band of frequencies near the maximum upper hybrid frequency of the nonuniform plasma, in agreement with experiment. Furthermore, large signal computations of the dependence of the echo amplitude on excitation pulse separation and amplitude show a complex behavior in qualitative agreement with experiment. As a supplementary topic, the properties of echoes from a general collection of anharmonic oscillators are discussed. The oscillators in this discussion are a general mathematical analog of the upper hybrid normal modes of a cold nonuniform plasma. Through emphasis of effects due to the finite width of the excitation pulses, the calculations show explicitly the role of the various characteristics of the oscillators in echo processes, further delineating the general features thought requisite of classical multiple-pulse echo systems.

TABLE OF CONTENTS

I. INTRODUCTION

The interest and activity in both experimental and theoretical studies of the high frequency electromagnetic properties of electron plasmas in a magnetic field have grown tremendously in the last ten years. The early theoretical studies dealt largely with wave propagation in infinite uniform plasmas. Such waves are generally dispersive and their characteristics depend strongly on the collective properties of the plasma, i.e., those properties linked to the behavior of a large number of plasma particles. Collective phenomena are important when the plasma frequency ω_p is significant relative to the other characteristic frequencies involved, (the observation frequency ω and the electron cyclotron frequency ω_c) . Meanwhile, numerous experiments have been performed using relatively small, bounded laboratory plasmas which are rather nonuniform in the steady state. The experiments have produced not only dispersive effects, but resonant phenomena introduced by and intimately related to the existence of the boundaries and the nonuniform electron density profile. Subsequent theoretical investigations yielded new insight concerning the fundamental character of waves in bounded plasmas.

Most prominent in recent years are studies of resonances and wave propagation in plasmas whose electrons have a relatively high temperature on the order of tens of thousands of degrees. Typical experiments have involved microwave studies of the continuous wave scattering and noise emission from these hot plasmas. Particularly significant are the results of studies carried out near the harmonics

of the electron cyclotron frequency. Strong peaks in noise emission and scattering have been found when $\omega \simeq n\omega_c$ where n is an integer. The effects observed are related in an essential way to the thermal motions of the electrons and the finite size of their orbits relative to the wavelength of any propagating waves.

Investigation of magnetoplasmas with low electron temperatures has been much less thorough. Since extrapolation from hot to cold plasma is not generally straightforward, it is of interest to establish experimentally the microwave properties of cold plasmas. This has been done on a limited basis in the past. From a theoretical point of view, one would like to test the validity of some of the myriad approximations adopted by the plasma theorist trying to solve the complex equations which describe the dynamics of a cold plasma.

This thesis is a study of the high frequency properties of low temperature electron plasma columns in a longitudinal magnetic field. Emphasis is given the collective normal mode behavior for low electron densities $((\omega_p/\omega)^2 < 1)$ in the vicinity of electron cyclotron resonance $((\omega_c/\omega) \simeq 1)$. The study has been carried out with the dual goal of documenting some experimental phenomena and, by comparison, testing the applicability of a simplified zero temperature theoretical model. The experimental observations give a relatively complete picture of the microwave properties (extraordinary mode) of the plasmas studied, encompassing continuous wave scattering and noise emission measurements, as well as the demonstration of the occurrence of related two-pulse echo processes. All data show the presence of collective effects which

yield a normal mode spectrum strongly dependent on the electron density. The theoretical developments of this paper deal largely with a physical model consisting of a one-dimensional slab of cold (zero temperature) nonuniform plasma immersed in a magnetic field. The primary motivation of these calculations is a qualitative comparison with experimental data. Considering the nature of the theoretical model, the over-all success of the theory in predicting many of the important features of the observations is striking. The experimental and theoretical results suggest that the phenomena observed involve plasma oscillations at the upper hybrid frequencies ($\omega_h^2 = \omega_c^2 + \omega_p^2$) of the plasma. Of particular significance is the strong relation between the echo processes and these upper hybrid normal modes.

Data on continuous wave reflection from some afterglow rare gas discharges are given in Section II.A. The electron temperature in these plasmas is low, approaching room temperature. The reflection from the plasma is investigated as a function of frequency in the vicinity of electron cyclotron resonance ($\omega = \omega_c$) with electron density ($\propto \omega_p^2$) as a parameter. A broad peak in reflection is found in the region $(\omega_c/\omega) \leq 1$. This peak shifts to lower values of (ω_c/ω) and broadens as the electron density increases. For all values of electron density a sharp peak is observed very near $(\omega_c/\omega) = 1$, the cyclotron resonance condition.

Section II.B describes noise emission measurements made on the same plasmas described in Section II.A. The data show peaks and structure which are qualitatively the same as those observed in the reflection experiments. That is, one observes in both emission and

scattering experiments a cyclotron resonance peak and a subsidiary peak whose position depends strongly on the electron density. The simplicity and symmetry of the structure of both types of data are noteworthy and have not been previously observed.

A theoretical model involving a cold bounded magnetoplasma with a nonuniform electron density profile is described in Section II.C. Incorporating this plasma model with an appropriate transmission line structure reproduces qualitatively the conditions of the experiment. Calculations then indicate that the cold plasma model qualitatively predicts the resonance peak which shifts and broadens with increasing electron density. The experimental and theoretical results suggest that this peak involves resonance effects at the upper hybrid frequencies of the plasma. However, the theory cannot account consistently for the presence of the cyclotron resonance peak.

Section III.A gives data on a new two-pulse echo process which occurs in the same plasmas studied in Section II. The purpose of this section is to establish the intimate relation between the echoes and the upper hybrid normal modes studied in Section II, demonstrating the dominant role played by collective effects in the formation of this echo. The amplitude of the first echo was measured as a function of (ω_c/ω) . A direct comparison between this echo amplitude data and the CW reflection data is given for several gases. The echoes are found strongest in a narrow band of frequencies near the maximum upper hybrid frequency of the nonuniform plasma column. These facts unalterably distinguish the upper hybrid echoes from previously observed cyclotron echoes, which have been explained using independent electron theories.

The properties of echoes from a general collection of anharmonic oscillators are discussed in Section III.B. The theoretical calculations have a dual function. First, through emphasis of finite-pulse-width effects, the calculations show explicitly the role of the various characteristics of the oscillators in echo processes. The point is to further delineate the general features thought requisite of classical echo systems. Such finite-pulse-width effects have not been previously treated and are operative in the plasma echo experiments of the preceding section. Second, the calculations give general formulas and results which are used directly in computations involving the cold plasma model. The oscillators of this section are a general mathematical analog of the upper hybrid normal modes of a cold non-uniform plasma.

In Section III.C the Lagrangian description of the cold plasma slab is presented in a form exactly analogous to the system of oscillators treated in Section III.B. The results of Section III.B are then used to calculate in detail some of the important properties of echoes from upper hybrid oscillations. The limiting cases of low electron density and weak excitation are considered. However, considerable attention is given to echo properties under large signal conditions, that is, those conditions under which saturation of nonlinear effects becomes significant. In spite of the numerous approximations made, the resulting theory is notably successful in qualitatively accounting for several of the major features of the experimental results. For example, the theoretical echo is strongest in a narrow band of

frequencies near the maximum upper hybrid frequency of the plasma slab, in agreement with the experiments. Furthermore, the large signal computation of the dependence of the amplitude of the first echo on excitation pulse separation and amplitude yields a complex behavior in general agreement with experiment.

II. CONTINUOUS WAVE SCATTERING AND EMISSION

With due regard to the relation to the problem of thermonuclear fusion, much attention has been focussed in recent years on the microwave properties of bounded, hot electron plasmas in magnetic fields. For example, intense noise emission peaks have been observed near the harmonics of the electron cyclotron frequency for very high harmonic number (1). Subsequent scattering, emission and wave propagation experiments have given evidence (2) supporting a strong relation between the observations and the cyclotron harmonic waves first described by Bernstein (3). Also, subsidiary series of resonances found in small laboratory plasmas near the cyclotron harmonic frequencies were studied and described theoretically by Buchsbaum and Hasegawa (4). These resonances were attributed to standing wave effects created by the steady-state nonuniform electron density profile and boundaries of the plasma. All these effects are intimately related to the electron temperature (finite Larmor radius effects) and most experiments were carried out with high electron density ($(\omega_p/\omega) \gtrsim 1$) . In general, considerable understanding of the wave dispersion and resonance effects in bounded hot magnetoplasmas has been achieved, bringing theory and experiment closer together.

Meanwhile the microwave properties of magnetoplasmas with low electron temperatures and densities have received much less attention. A few studies have been made on effects such as noise emission (5) and echoes (6) from quiescent cesium plasmas. Also, the low density afterglow plasma has attracted increased attention in the past few years.

Following the discovery of cyclotron echoes (7), several experimental investigations of echo processes (8-10) and pulse effects (11) in afterglow discharges have been made. Bauer, Blum, and Gould (10) were the first to study the continuous wave (CW) properties of these afterglow plasmas and relate these properties to the echo phenomena. The purpose of this section is to present a study of the CW scattering and emission in the vicinity of cyclotron resonance from such afterglow rare gas discharges under low density conditions ($(\omega_p/\omega) \lesssim 1$).

Under low temperature and density conditions cyclotron harmonic effects are no longer significant. At first, one might expect to see only simple cyclotron resonance effects in a frequency range very near $\omega = \omega_c$. However, plasma wave theory (12) predicts wave dispersion, cutoffs and resonances which vary according to the polarization and direction of propagation of the wave, the magnetic field strength, the electron density, etc. As dictated by the experimental geometry, we will be concerned with the properties of the extraordinary mode which propagates and is elliptically polarized in the plane perpendicular to the static magnetic field. The extraordinary mode in an infinite uniform plasma has an electrostatic resonance at the upper hybrid frequency $\omega_h^2 = \omega_c^2 + \omega_p^2$. Some resonance effects observed in hot laboratory plasmas of finite extent have been attributed to the upper hybrid resonance of the inhomogeneous plasmas (5, 11, 13). The experimental results of this section show evidence of both a simple cyclotron resonance and upper hybrid resonance effects.

Section II.A of this paper gives the results of experiments measuring the CW reflection as a function of magnetic field (ω_c/ω) and electron density $(\omega_p/\omega)^2$. Data on the relative noise emission from the plasma are given in Section II.B. The emission data show the same qualitative features found in the reflection experiments, having both cyclotron and upper hybrid resonance effects. A simplified theoretical model involving a cold inhomogeneous plasma is described in Section II.C. Although the theoretical calculation predicts upper hybrid resonance effects, it fails to predict consistently the observed cyclotron resonance effects.

II.A. Reflection Experiments

The plasmas studied experimentally were rare gas, afterglow discharges created by a 21 MHz rf pulse of about 50μ sec in length. They were contained in a glass cylinder of 1.8 cm i.d. and about 1 m in length, aligned coaxially with the static magnetic field $\underline{B}_o$ of a solenoid formed by ten pancake type coils. The glass tube was inserted through and perpendicular to the narrow walls of a waveguide section (S and X bands) so that the configuration for the microwaves was $\underline{E} \perp \underline{k} \perp \underline{B}_o$ where $\underline{E}$ is the electric field and $\underline{k}$ is the propagation vector of the signal. The magnetic field B_o was homogeneous to one part in 10^4 over the volume of plasma within the waveguide. All data represent crystal rectifier detected signals which were plotted automatically on an X-Y recorder.

The glass cylinder was connected by flexible tubing to a conventional high-vacuum system. All of the high vacuum portion of the

system was baked at 400°C overnight in order to reduce the amount of impurities. A pressure of about 10^{-7} mm Hg was achieved in the empty plasma vessel. The gases used were Matheson research grade and were introduced to the system by a controlled leak valve.

The plasma was placed in one of the side arms of a balanced microwave bridge system formed by the use of a magic tee (see Fig. II.1). Both side arms were terminated in matched loads. A magic tee has the property (14) that if the H-arm (input) and E-arm (output) are terminated in matched loads and a signal E_{in} enters the input, the signal in the output arm E_{out} is given by

$$E_{out} = (\Gamma_1 - \Gamma_2) \frac{E_{in}}{2} \qquad (1)$$

where Γ_1 and Γ_2 are the reflection coefficients seen at the junction looking into side arms one and two, respectively. If we assume that the scattering from the waveguide holes and the glass are such that the scattered fields superpose, Γ_1 is the sum of the reflection coefficient from the plasma Γ_p and from the glass and holes Γ_g. Equation 1 becomes

$$E_{out} = (\Gamma_p + \Gamma_g - \Gamma_2) \frac{E_{in}}{2}$$

A slide screw tuner placed in arm 2 and adjusted to cancel reflections (in the absence of the plasma) from the glass tube and holes, giving $\Gamma_2 = \Gamma_g$, yields

$$E_{out} = \Gamma_p \frac{E_{in}}{2}$$

Thus a properly balanced microwave bridge apparatus yields directly the reflection coefficient of the plasma, eliminating the unwanted reflections due to undesirable experimental conditions such as holes in the waveguide walls. For the magic tees and frequencies used, the maximum VSWR measured when looking into any individual arm with the other three terminated was about 1.1 for both S-band and X-band. Therefore, any errors in the measured reflection coefficients should be less than a few percent.

Figure II.1 gives a block diagram of the instrumentation and shows the experimental geometry. The signal follows path A for the reflection experiments. Path B is used for the echo experiments of Section II. The 21 MHz 100W power oscillator is pulsed creating a plasma and turning off at time $t = 0$ (by definition). The oscillator is capacitively coupled to the plasma by means of a tuned, parallel L-C circuit. The signal generator produces a continuous wave signal which is pulse modulated (about 1 μsec width) by the PIN diode at the time $t = T_a$ (afterglow time). The master timing circuits repeat this sequence at 60 Hz. The plasma density decays with a time constant of typically between a few hundred microseconds and a few milliseconds, depending on the gas and the conditions. Thus, a reflection experiment using pulses short compared to the decay time is performed at constant plasma density for all practical purposes. Although such pulses are not CW, experiments using them yield results essentially identical to a CW measurement if the spectral width ($\sim$ 1 MHz) of the pulse is narrow compared to the normal mode spectrum width of the plasma. This

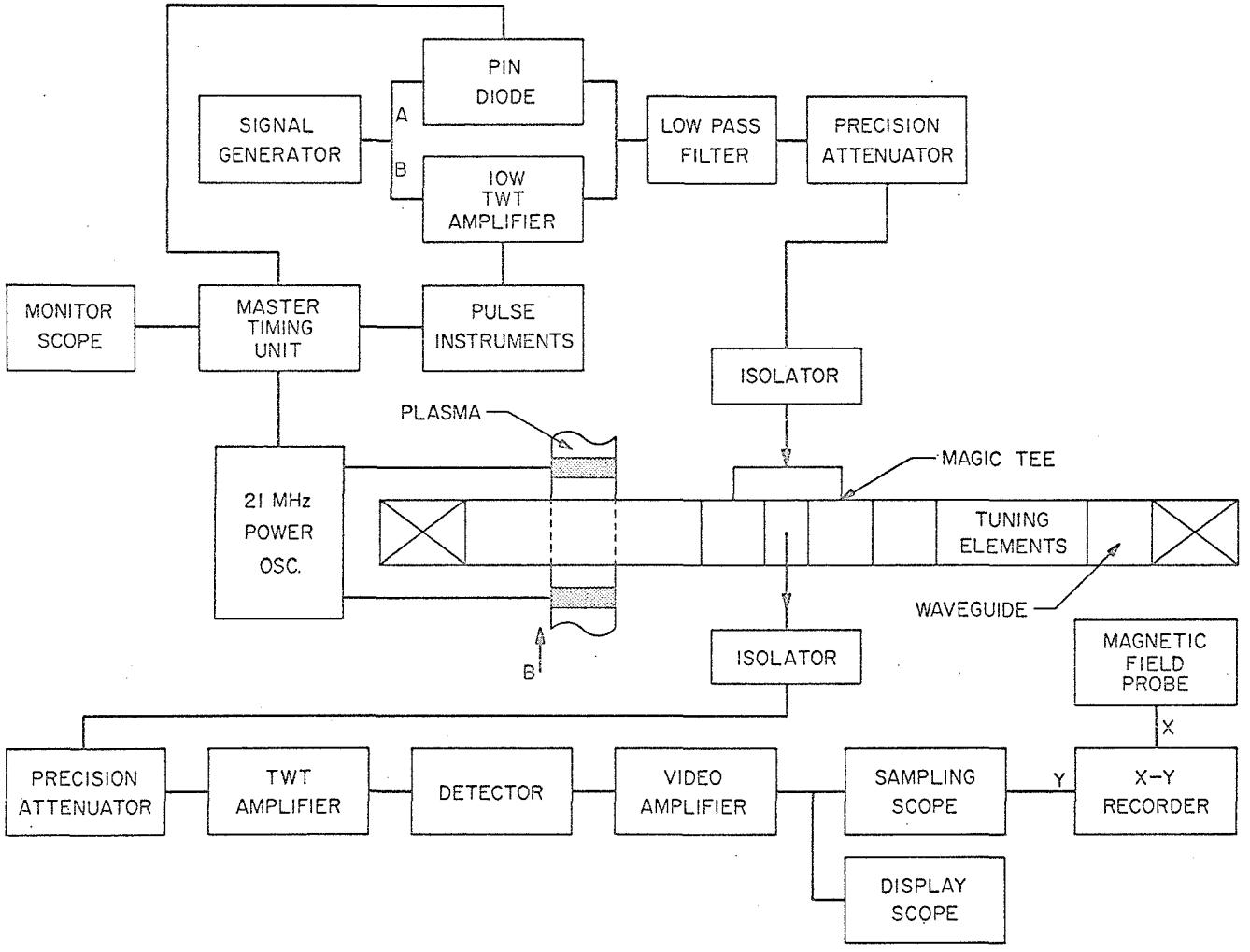

Fig. II.1 Block diagram of the experimental apparatus. The signal follows path A for the CW experiments, path B for the short-pulse and echo experiments.

inequality is maintained for all data shown. Also, true CW signals tend to modify the density decay apparently due to heating of the electrons. The pulsed incident signal helps minimize such effects. Following reflection from the plasma, the signal is amplified, crystal detected, and displayed on a sampling oscilloscope. Using the manual scan feature of the sampling oscilloscope, the detected signal is sampled at a fixed time. The sampling oscilloscope produces a DC voltage proportional to the reflected signal amplitude. This DC voltage is used to drive the y-axis of an X-Y recorder. The voltage drop across a resistor in series with the magnet coils is directly proportional to the magnetic field strength and is applied to the x-axis of the recorder. One can now easily measure the reflection from the plasma as a function of magnetic field and electron density.

The electron temperature of afterglow plasma such as that studied here is thought to decay very rapidly, with time constants as short as tens of microseconds. Electron neutral collisions cannot account for such fast energy relaxation and not much is understood about the actual processes. Little quantitative evidence is available. However, preliminary experiments in our laboratory (15) show radiation temperatures typically down to $\lesssim 2000^{\circ}K$ at $T_a = 100$ μsec for neon and argon. Since the temperature measurements show structure indicative of collective and/or nonequilibrium (in a thermodynamic sense) behavior, the temperature given represents an upper bound on that corresponding to the mean energy of the electrons. Therefore, it will be assumed that the electron temperature is constant and low (at most one or two thousand degrees) for all data taken in the late afterglow.

Basically, we would like to study the normal mode spectrum of the plasma by measuring the reflection from it as a function of frequency. However, since it is difficult to compensate consistently for the frequency dependence of all the microwave components used, the incident signal frequency ω was fixed, while the magnetic field was varied, with the electron density fixed. This procedure is theoretically entirely equivalent to frequency variation, since only the ratios (ω_c/ω) and (ω_p/ω) are relevant. As a practical matter we implicitly assume that the plasma conditions (peak density, density profile, decay time, etc.) do not change with magnetic field. Since the percentage changes in magnetic field are relatively modest, it is likely that this is a reasonable assumption. The values of (ω_c/ω) shown in the data are accurate to within $\pm$ 0.2%.

Setting a perspective on the type of plasmas we are studying, Fig. II.2 shows the reflection from a neon plasma as a function of (ω_c/ω) at early afterglow times, where the electron temperature is still relatively high, on the order of electron volts. As is the case for all figures in this paper, detailed experimental conditions (such as neutral gas pressure and microwave power) are given in Appendix C. Two classical hot plasma effects are exhibited: [1] cyclotron harmonic phenomena (2) near $(\omega_c/\omega) = 1/n$, $n=1,2,\cdots$, and [2] the so-called Buchsbaum-Hasegawa modes (4), just above $(\omega_c/\omega) = 1/2$. The cyclotron harmonic effects disappear virtually as soon as the experiment is performed in the afterglow rather than in the active discharge. The evidence of the Buchsbaum-Hasegawa modes also disappears rapidly. Thus we have another indication that the electron temperature decays very rapidly.

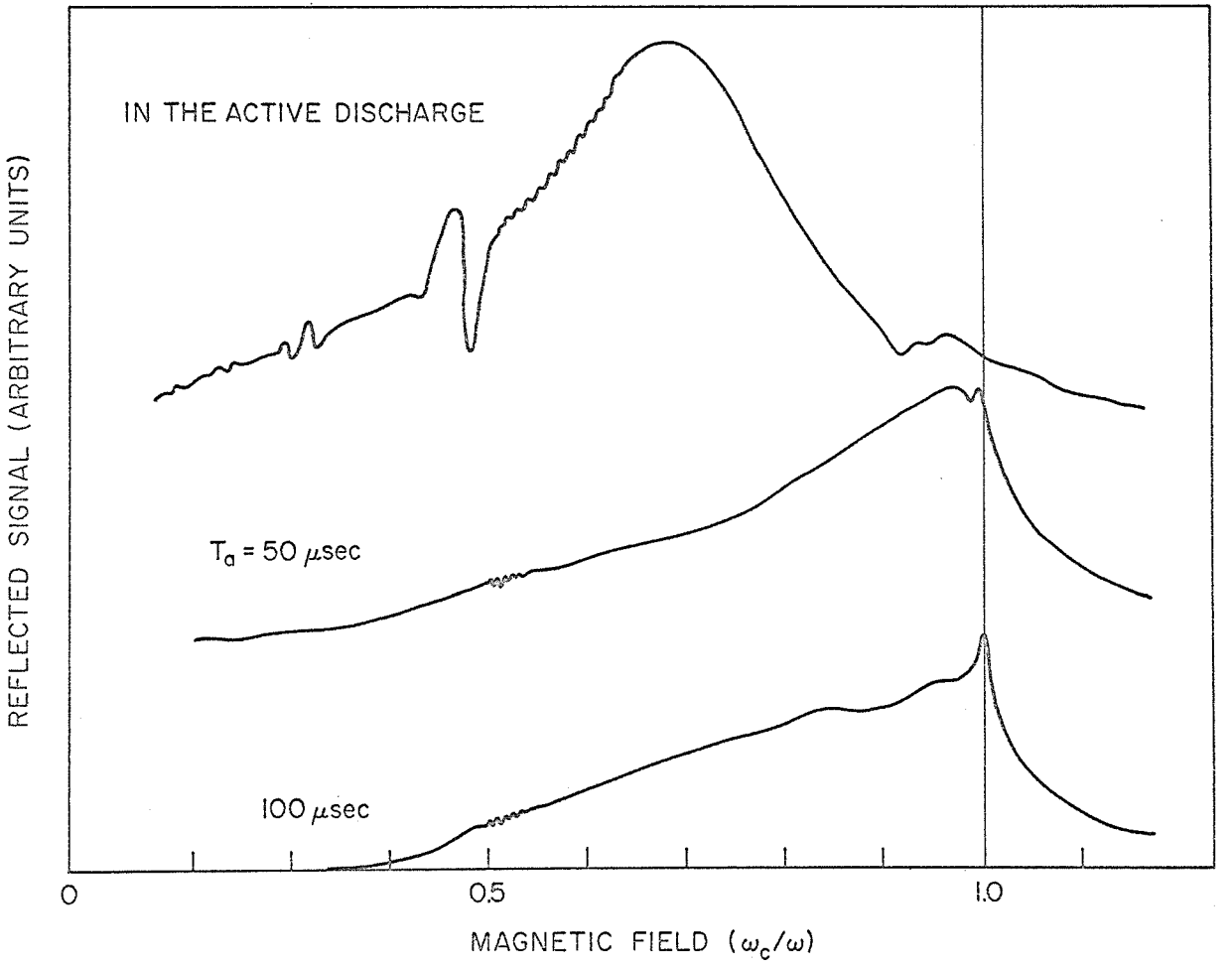

Fig. II.2 Reflection vs. magnetic field for neon in the active discharge and early afterglow (S-band).

Figures II.3,4 show the reflection from neon and argon afterglows at later T_a where the temperature is low. These data were taken in the S-band apparatus ($\omega/2\pi$ = 3.0 GHz) and show clearly the presence of collective behavior. As is the case for all data in this section, the receiver gain is the same for all curves in a given figure unless otherwise stated in the caption. The sharp peak in reflection near cyclotron resonance, $(\omega_c/\omega) = 1$ and the broad peak at lower values of (ω_c/ω) are very characteristic for both neon and argon. Note the consistent scaling of the general features of the data with T_a and, therefore electron density, since we assume that the electron temperature has already reached a constant level. The peak in the scattering which significantly shifts and broadens at high electron densities has the general appearance of a common feature of reflection, emission, and absorption spectra of cyclotron-resonance experiments reported by other observers (4,16,17). This feature is attributed to the upper hybrid resonance of a cold, inhomogeneous plasma (18). In fact, the onset of significant scattering at low values of (ω_c/ω) has proved to be a good measure of the maximum electron density of non-uniform plasma columns (17). Since small laboratory plasmas of the type used here are typically rather inhomogeneous in the steady state, the plasma possesses a whole range of upper hybrid frequencies $\omega_h^2 = \omega_c^2 + \omega_p^2$. Significant scattering apparently only takes place for $(\omega_c/\omega) > (\omega_c/\omega_{ho})$ where $\omega_{ho}^2 = \omega_c^2 + \omega_{po}^2$ is the maximum upper hybrid frequency and ω_{po} is the maximum local plasma frequency. Thus, the onset point on the (ω_c/ω) axis is taken to be such that the incident

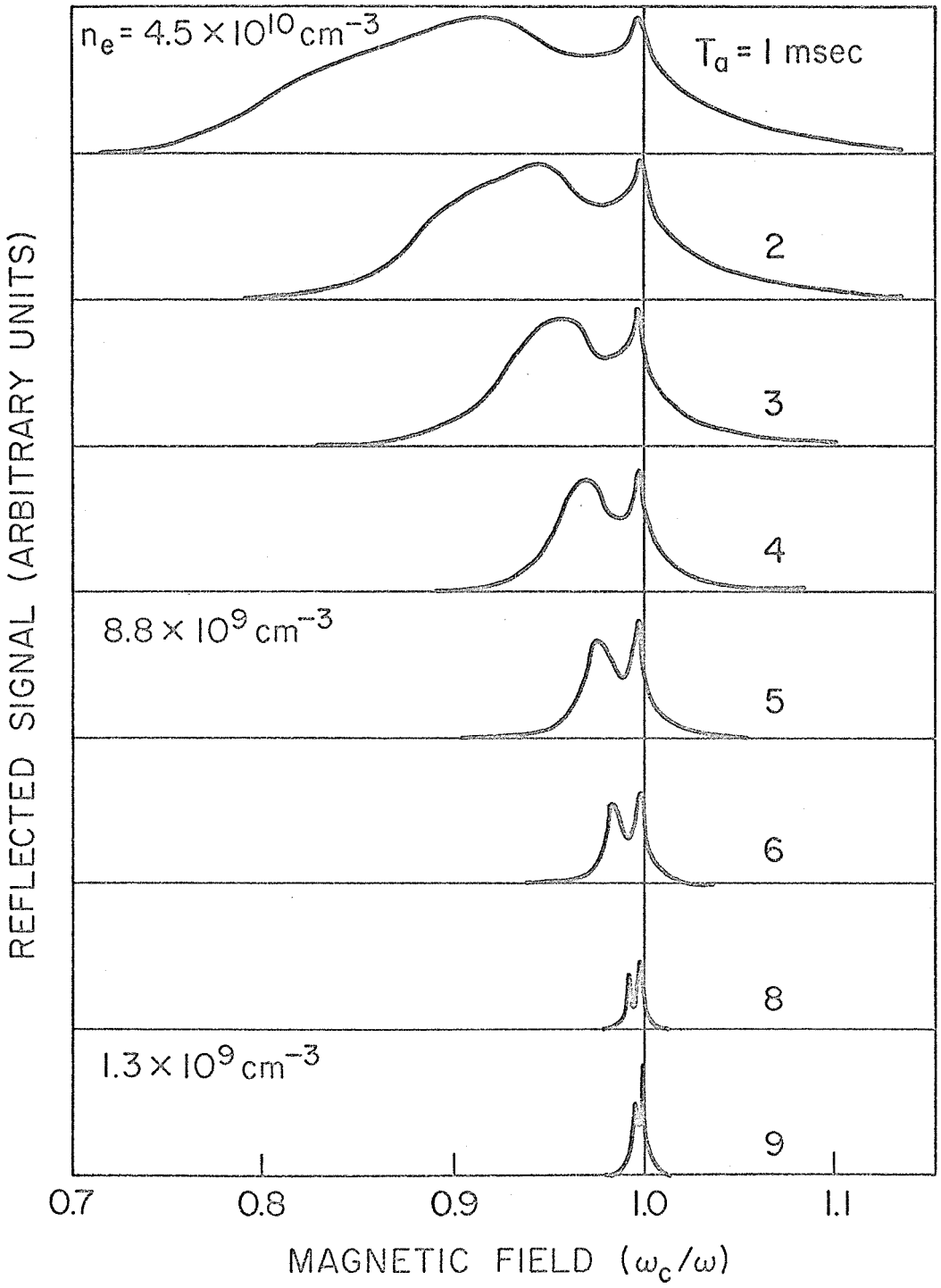

Fig. II.3 Reflection vs. magnetic field for a neon afterglow (S-band)

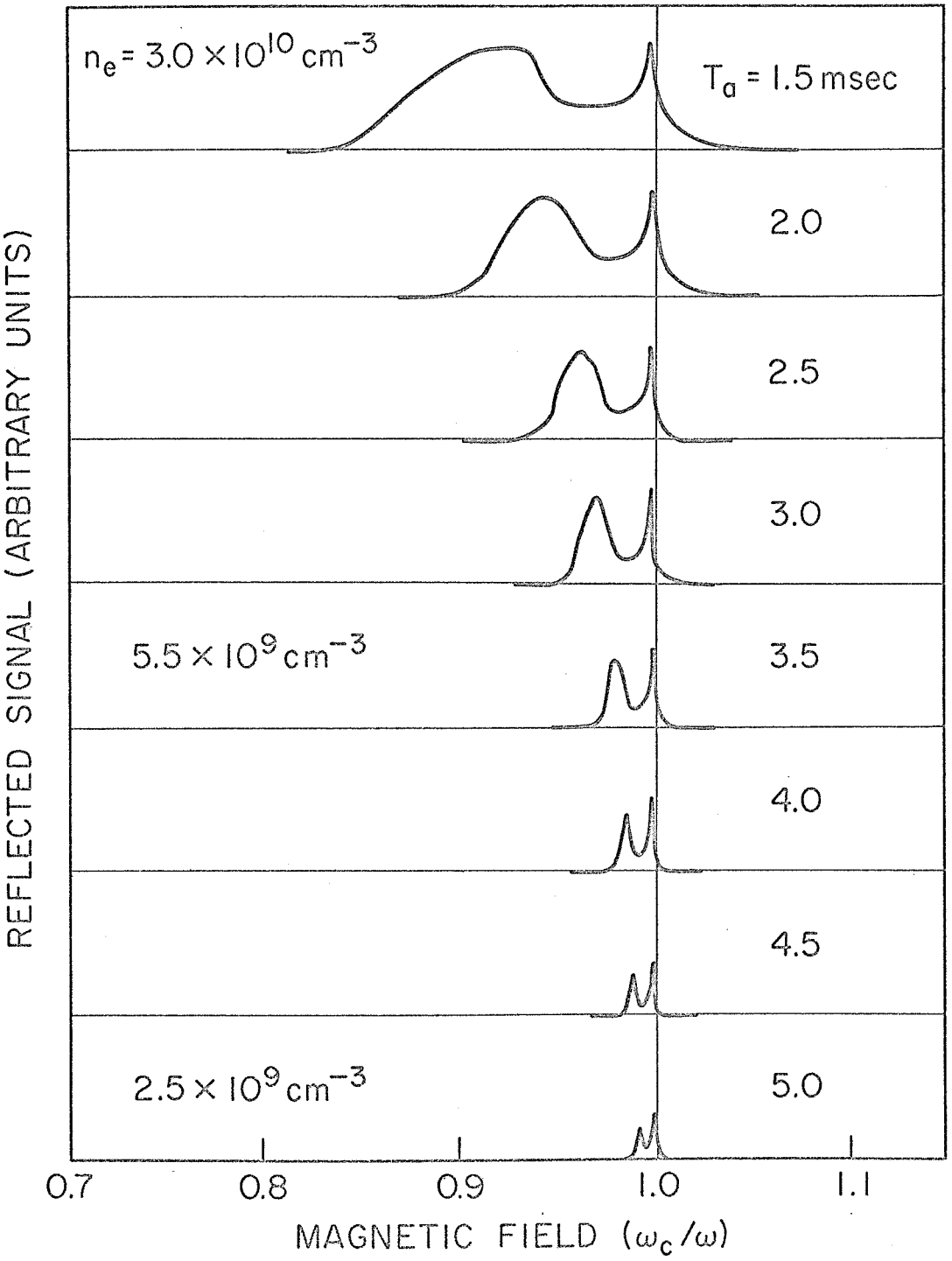

Fig. II.4 Reflection vs. magnetic field for an argon afterglow (S-band).

signal frequency is equal to the maximum upper hybrid frequency, i.e. $\omega = \omega_{ho}$. This interpretation is the source of the electron density n_e estimates given in Figs. II.3,4. Furthermore, these ideas are consistent with the interpretation of echo experiments performed on the same plasmas (see reference (10) and Section III of this paper). It is apparent from the data that the definition of the onset point is somewhat arbitrary. Some curves show a slight break in the slope on the rising side (as (ω_c/ω) is increased) of the broad peak. This break may be the mark of the location of the condition for maximum upper hybrid resonance. It is sometimes more pronounced than shown in Figs. II.3,4. However, it is not easily followed as T_a increases. As a matter of consistency, the onset point is taken to be that value of (ω_c/ω) such that the reflection is 20% of its peak value.

The narrow cyclotron resonance peak is an anomaly with respect to the cold plasma interpretation. Observations (16) in other plasmas in which the electron temperature is higher do not show such a strong cyclotron resonance effect. We also find that the cyclotron resonance peak tends to be washed out at high temperatures as one can see from the data of Fig. II.2. The relevance of these effects to appropriate theoretical models will be discussed below.

Although detailed studies of the reflection as a function background neutral pressure were not made, the data are qualitatively similar for pressures as high as 500μ Hg. Also, the power reflection is typically about 10% at the peaks of the curves for T_a one or two milliseconds and about 50% at the peak in the active discharge.

Reflection curves for helium are given in Fig. II.5. Again, the results scale consistently with electron density. The data are markedly different from that for neon and argon. The narrow reflection peak at cyclotron resonance is still present. However, the pronounced upper hybrid peak has been replaced by a sharp break in the slope of the curves. The natural association of this break with the maximum upper hybrid frequency is apparent. Lacking a quantitative theory, we have made this association in arriving at the electron densities given.

Figure II.6 displays the electron density vs. T_a as taken from the data of Figs. II.3-5. The data points for each gas are fit reasonably well by a simple exponential decay. The rapid decay of the helium afterglow is probably related to the fact that its low energy electron-neutral collision frequency is much higher than that of argon and neon (19). The usefulness of the reflection measurements as a density diagnostic technique is immediately apparent. In fact, a quantitative theory would facilitate relatively accurate density measurements. The technique becomes more inaccurate as the electron density decreases, since the location of the point $(\omega_c/\omega) = 1$ becomes crucial.

Reflection experiments were also performed at X-band, checking the generality of the results of the S-band investigation. The reflection vs. (ω_c/ω) at various afterglow times in argon is shown in Fig. II.7. The basic components used at X-band are functionally the same as those used at S-band. The incident signal frequency $\omega/2\pi$ was fixed at 9.0 GHz. The general features are quite similar to the S-band results. However, the peak at cyclotron resonance is now

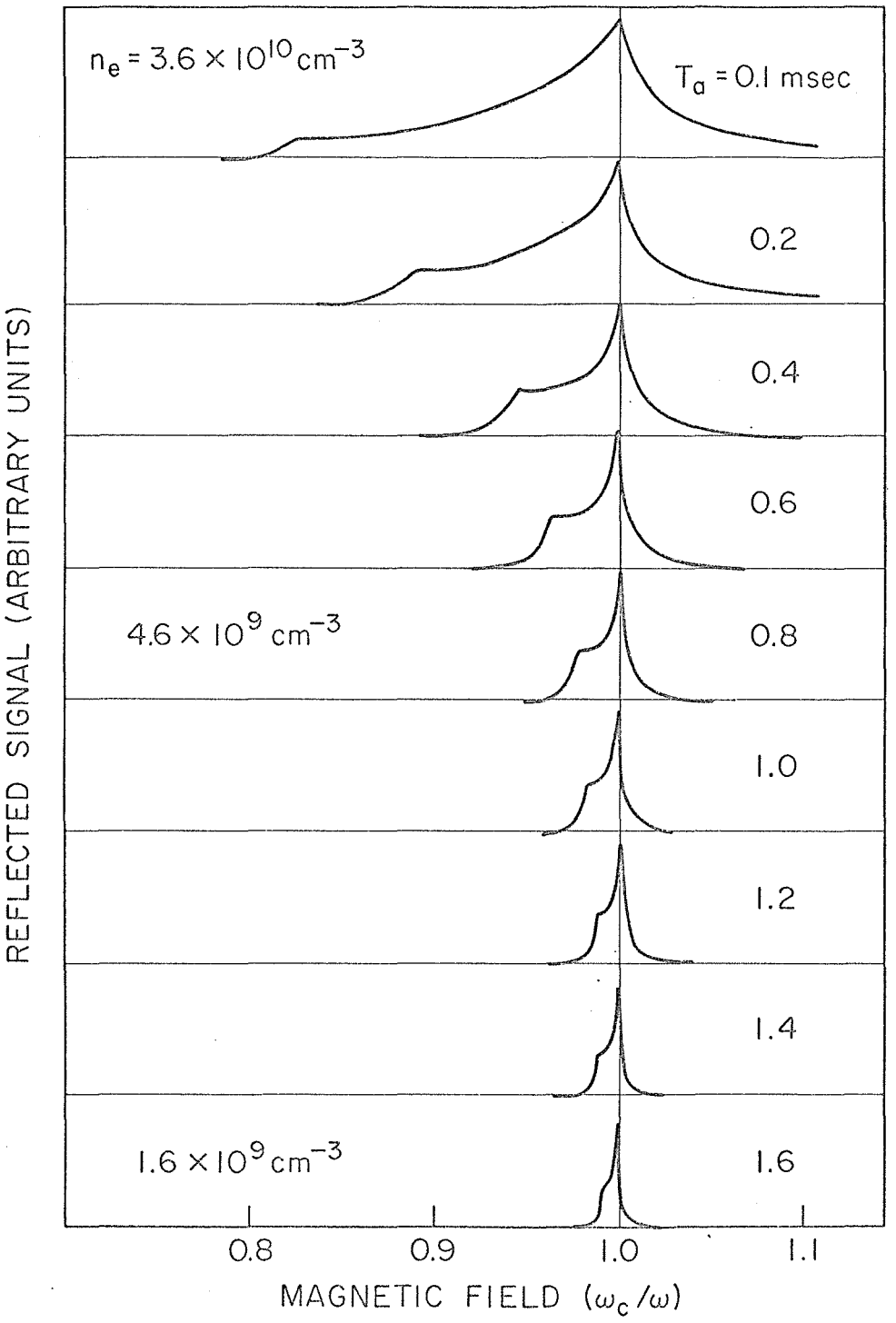

Fig. II.5 Reflection vs. magnetic field for a helium afterglow (S-band).

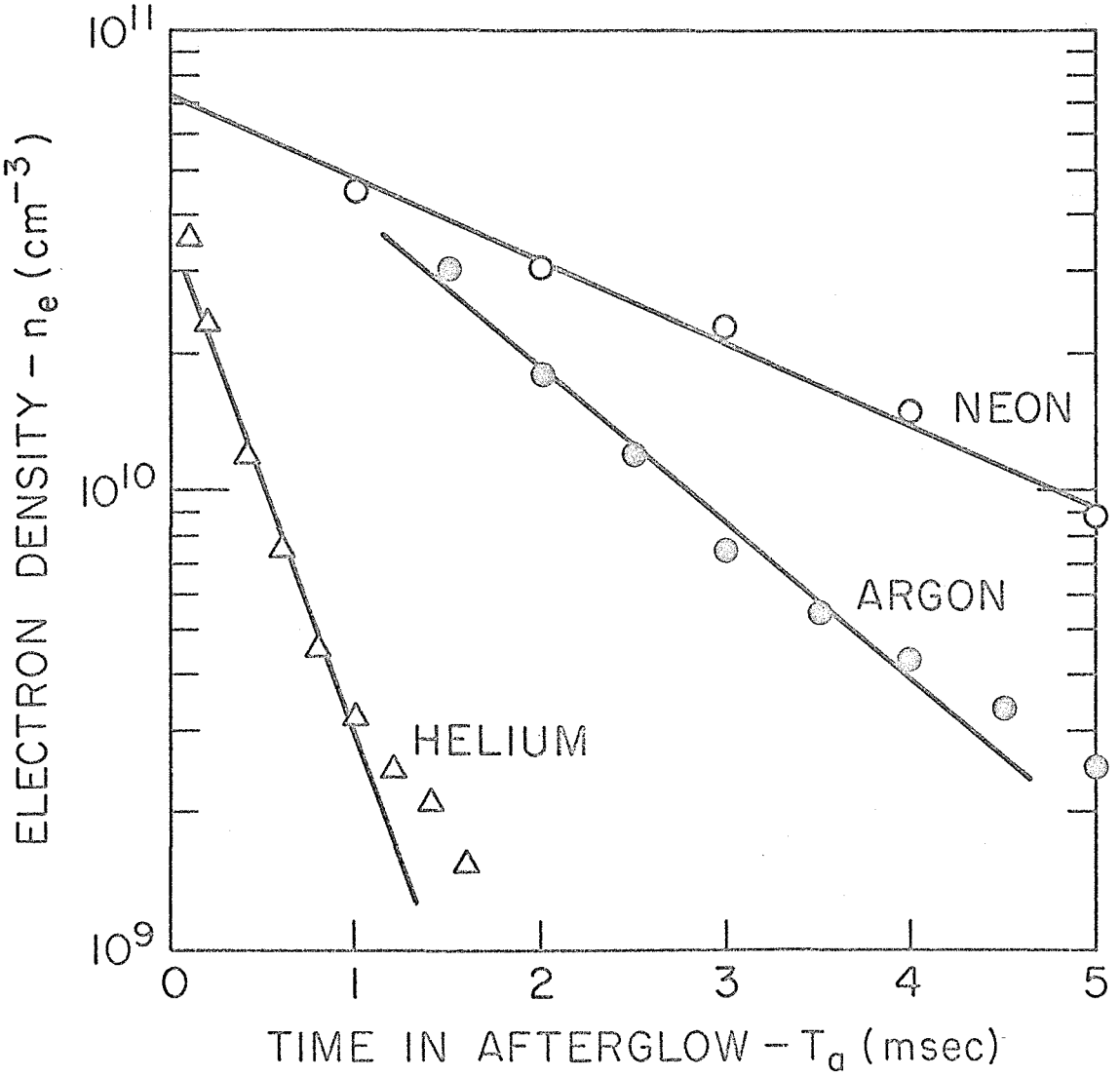

Fig. II.6 Electron density vs. time in the afterglow for Ne, A and He as deduced from the CW reflection data.

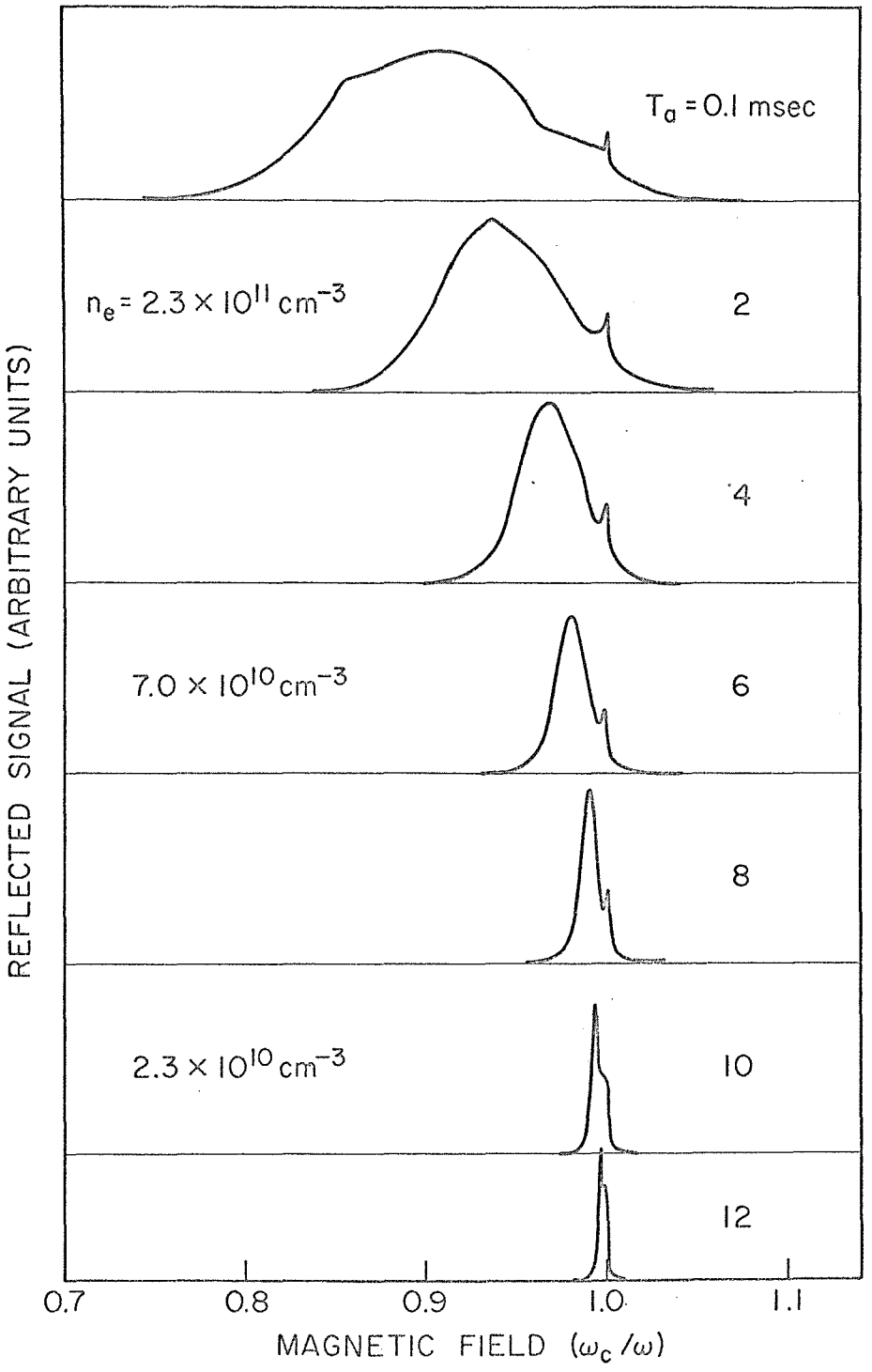

Fig. II.7 Reflection vs. magnetic field for an argon afterglow (X-band).

diminished relative to the upper hybrid peak. The electron densities were calculated using the same interpretation of the results given for the S-band data.

II.B Noise Emission Experiments

A time-gated microwave radiometer designed and built by R.Stenzel (15) was used to measure the noise emission from the plasmas as a function of magnetic field and electron density. Basically, the radiometer is a superheterodyne microwave receiver which is turned on for an interval of 1 μsec at the time T_a, in the afterglow. The local oscillator frequency is 3.0 GHz. The IF center frequency is 7 MHz with a half power bandwidth of 8 MHz. The image was not filtered. This presents no problem as long as the characteristic spectral widths of the plasma emission are greater than about 25 MHz, which is the case for all data shown. The receiver was gated at the last IF stage. The resulting pulses were synchronously detected at the frequency of repetition of the experiment, with a time constant of 1 sec. The output of the synchronous detector was used to drive an X-Y recorder. The overall noise figure of the system is about 5 db. The plasma was again placed in an S-band waveguide in such a manner that the configuration $\underline{E} \perp \underline{k} \perp \underline{B}$ is maintained. An isolator was placed between the plasma and the receiver, and a termination was placed behind the plasma as shown in Fig. II.8. Other plasma conditions were the same as those of the reflection experiments.

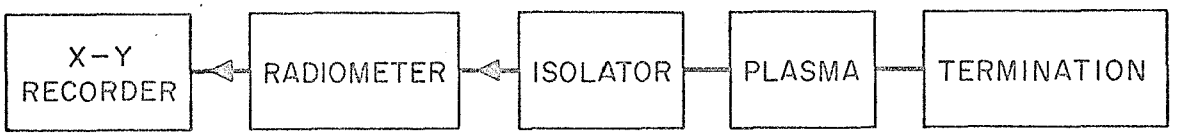

Fig. II.8 Block diagram of noise emission experimental apparatus

The relative noise emission from an argon afterglow similar to that used in obtaining the reflection data of Fig. II.4 is given in Fig. II.9. Again, the magnetic field was varied while the local oscillator frequency was held fixed. The most significant feature of these data is its strong qualitative relationship to the reflection data of Fig. II.4. The noise emission shows both the upper hybrid peak and the peak at cyclotron resonance. As T_a is increased, the noise power available becomes too small compared to the inherent system noise to allow meaningful measurements.

Figure II.10 gives the noise emission data for a helium afterglow. The plasma conditions are essentially the same as those used in obtaining the reflection data of Fig. II.5. Again the strong qualitative similarity between the reflection data and the noise emission data is apparent. One is thus led to conclude that, in general, for

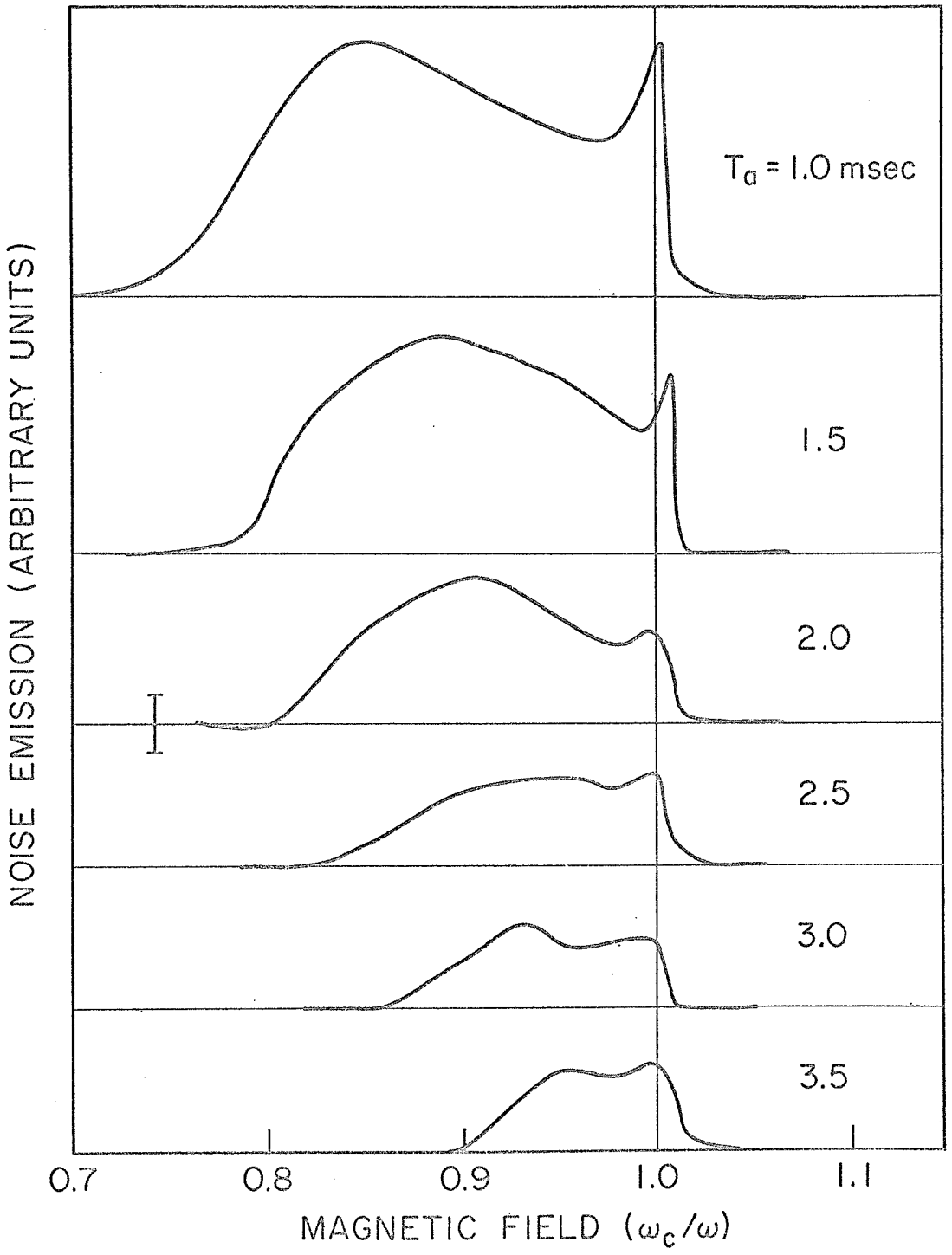

Fig. II.9 Noise emission vs. magnetic field for an argon afterglow. The data for T_a = 1.0 msec was taken with a receiver gain one-half that for other T_a. The vertical bar indicates the noise level.

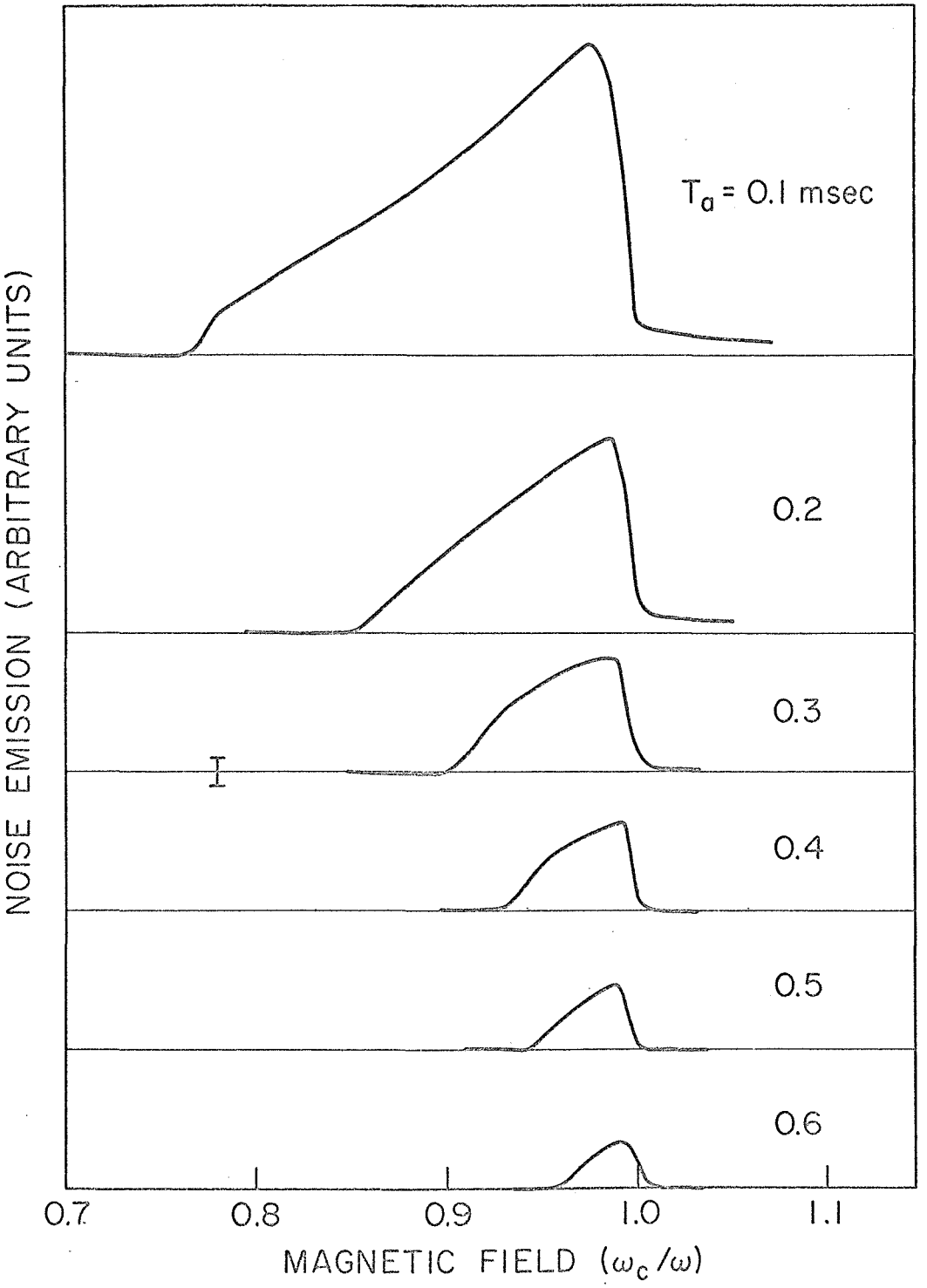

Fig. II.10. Noise emission vs. magnetic field for a helium afterglow. The vertical bar indicates the noise level.

the plasmas studied here, the reflection and noise emission show qualitatively the same relative behavior. That is, both types of experiment show the same peaks, valleys, etc. This experimental fact is an important one as we shall see in the theoretical discussion given in the next section.

II.C Cold Nonuniform Plasma Theory

Attempting to account qualitatively for the general features of the reflection and emission data, we consider a one-dimensional inhomogeneous cold plasma slab of thickness 2a situated in a uniform magnetic field $\underline{B}$ which is parallel to the slab faces [see Fig. II.11(a)]. The plasma is placed between two parallel conducting plates separated by a distance 2ℓ. The steady-state electron density is assumed to depend on x in such a manner that $\omega_p^2(x) = \omega_{po}^2(1 - x^2/a^2)$. Collisions are neglected. We consider the plasma to be charge neutralized in the steady state by a background of fixed, positive ions. Simulating the conditions of the experiment, we place a short section of this plasma slab in a parallel-plate transmission line which has a matched generator at one end and is terminated in its characteristic impedance Z_o at the other end as shown in Fig. II.11(a). In order to do this we must take the plasma to be bounded in the plane perpendicular to the x direction, in effect, removing the restriction to a one-dimensional problem. However, we will ignore this complication and assume that the plasma dimensions are such that the properties of the one-dimensional slab are a good approximation. That is, we neglect

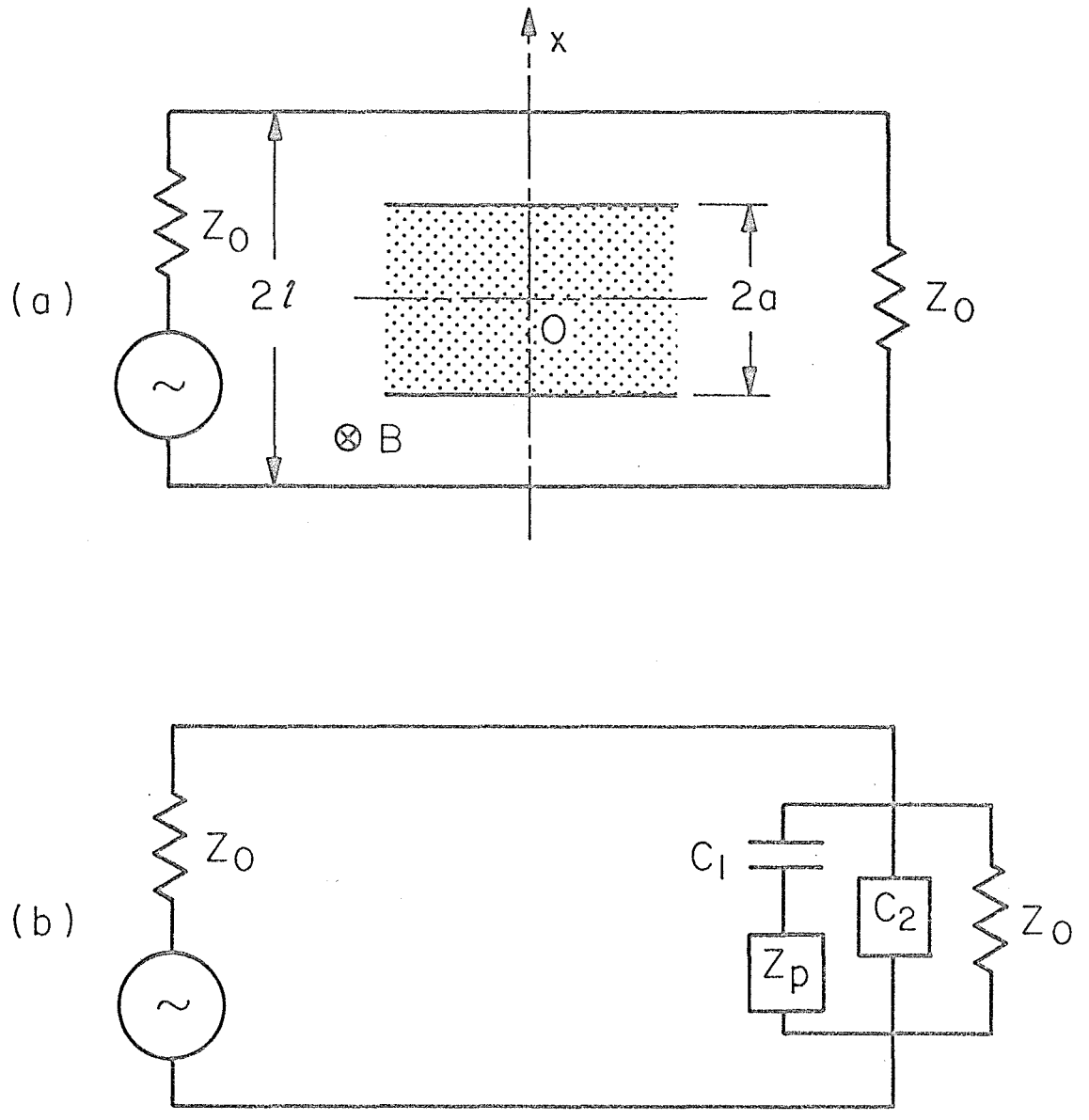

Fig. II.11 (a) Diagram showing geometry of the plasma slab and parallel-plate transmission line which comprise the theoretical model.

(b) Lumped-element equivalent circuit of the plasma-slab, transmission-line model.

fringing field effects. Since in the experiment the lateral dimensions of the plasma are small compared to the guide wavelength, we replace the plasma of Fig. II.11(a) which is distributed along the transmission line by a simple lumped-element equivalent circuit as shown in Fig. II.11(b). The circuit element C_1 is the capacitance of the vacuum between the plasma and the conducting plates, and is given by $C_1 = \varepsilon_o A/2(\ell-a)$, where ε_o is the permittivity of free space and A is the lateral area of the capacitor-slab system. The negative capacitance C_2 results from the equivalent circuit approximation and is equal to $-(\varepsilon_o A/2\ell)$.

The dependence on (ω_c/ω) of the reflection coefficient seen at the generator on the transmission line will yield the theoretical equivalent of the experimental reflection data. Removing the ideal generator from the circuit and placing an isolator between the impedance Z_o and the plasma yields the configurations of the noise emission experiments (see Fig. II.12). Use of the Nyquist theorem will permit one to compute the emission vs. (ω_c/ω). In either case one needs the expression for the plasma impedance which we will now derive.

We restrict our attention to electrostatic oscillations of the plasma so that we retain only Poisson's equation of Maxwell's equations. For such one-dimensional electrostatic systems, the total current density (particle or fluid current J_p plus displacement current) $J_o(t)$ in the x-direction is a spatial invariant,

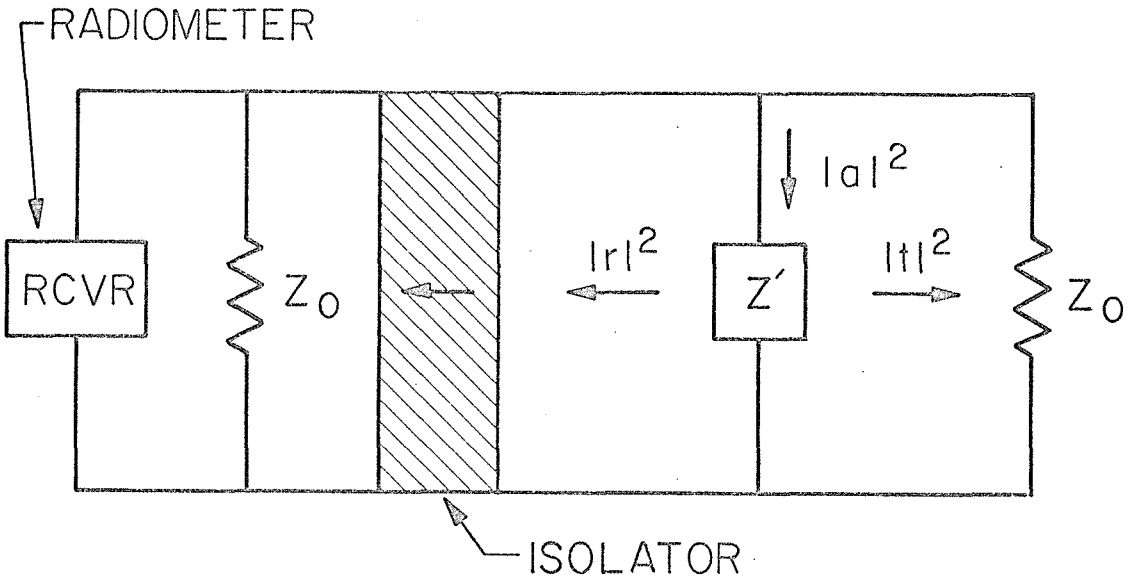

Fig. II.12 Schematic diagram of transmission line equivalent of noise emission experimental apparatus. Z' is the lumped impedance of the plasma and the capacitors C_1 and C_2 of Fig. II.11.

$$\frac{\partial}{\partial x}[J_o(t)] = \frac{\partial}{\partial x}[\varepsilon_o \frac{\partial E}{\partial t} + J_p] = 0$$

where E is the electric field. For a system of particles which can be described by a local relation between particle currents and the electric field, one can derive an equivalent permittivity ε so that,

$$J_o(t) = \varepsilon \frac{\partial E}{\partial t} = i\omega\varepsilon E \qquad (2)$$

where ω is the frequency of oscillation. For a cold uniform collisionless plasma (20),

$$(\varepsilon/\varepsilon_o) = 1 - \frac{\omega_p^2}{\omega^2 - \omega_c^2} \tag{3}$$

For an inhomogeneous cold plasma ε is a function of x and Eqs. 2 and 3 are valid locally. The plasma impedance is then given by

$$Z_p = -\frac{1}{A}\int_{-a}^{a} \frac{E}{J_o}\,dx = \frac{(\omega_c^2 - \omega^2)}{i\omega\varepsilon_o A}\int_{-a}^{a} \frac{dx}{\omega_c^2 + \omega_p^2(x) - \omega^2} \tag{4}$$

As the integrand in Eq. 4 stands it has simple poles at symmetrical values of x when ω lies in the band of upper hybrid frequencies, $\omega_c \leq \omega \leq \omega_{ho}$. Inclusion of electron-neutral collision effects removes this singularity from the path of integration. However, one can evaluate the integral in the limit of zero collision frequency using the Dirac formulation of such integrals. These steps are carried out in Appendix A, giving an exact closed form expression for Z_p over the entire real frequency domain. The impedance is found to have a real part only when ω is in the range of upper hybrid frequencies. The fact that there is a real part to the impedance in the absence of collisional processes is a property of the continuum nature of the normal modes of the cold inhomogeneous plasma. Basically, the plasma resonates with any applied field whose frequency ω is such that $\omega^2 = \omega_h^2(x) = \omega_c^2 + \omega_p^2(x)$ (21). The resonance is local and occurs at those points x where $\omega^2 = \omega_h^2(x)$, i.e. the condition of local upper hybrid resonance. In our collisionless model the electric field is infinite at the resonance points. However, this singularity in the normal mode field is integrable in the Dirac sense and one obtains a

finite slab impedance. Of course, in a real plasma the strength of the electric field at the resonance points is limited by the dissipation processes (collisions). Thus, the expression for Z_p given in Appendix A is the limiting case and is approximately valid for $(\nu/\omega) << 1$, where ν is collision frequency of electrons with other plasma species.

The complex reflection measured at the generator of Fig. II.11(b) is given by $r = Z_o/(2Z' + Z_o)$, where Z' is the combination impedance of the plasma, the capacitance C_1, and the negative capacitance C_2,

$$\frac{1}{Z'} = -\frac{i\omega\varepsilon_o A}{2\ell} + \frac{1}{Z_p + \frac{2a}{i\omega\varepsilon_o A}} \quad .$$

Experimentally, a square law detector would measure $|r|^2$ which has the form

$$|r|^2 = F[R, (\ell/a), (\omega_{po}/\omega), (\omega_c/\omega)]$$

where $R = (Z_o\omega\varepsilon_o A/2\ell)$. In Fig. II.13 we plot $|r|^2$ vs. (ω_c/ω) for several values of $(\omega_{po}/\omega)^2$. The parameters R and (ℓ/a) do not have exact experimental equivalents. We have taken $R = 5$ and $(\ell/a) = 2$ as reasonable estimates. The parameter R determines the relative size of the characteristic line impedance Z_o and the plasma impedance Z_p. Roughly, R sets the over-all scale of the amount of reflection, while (ℓ/a) controls the relative height of the two peaks. The values chosen yield results that compare favorably with the experimental data. The resemblance between the neon and argon

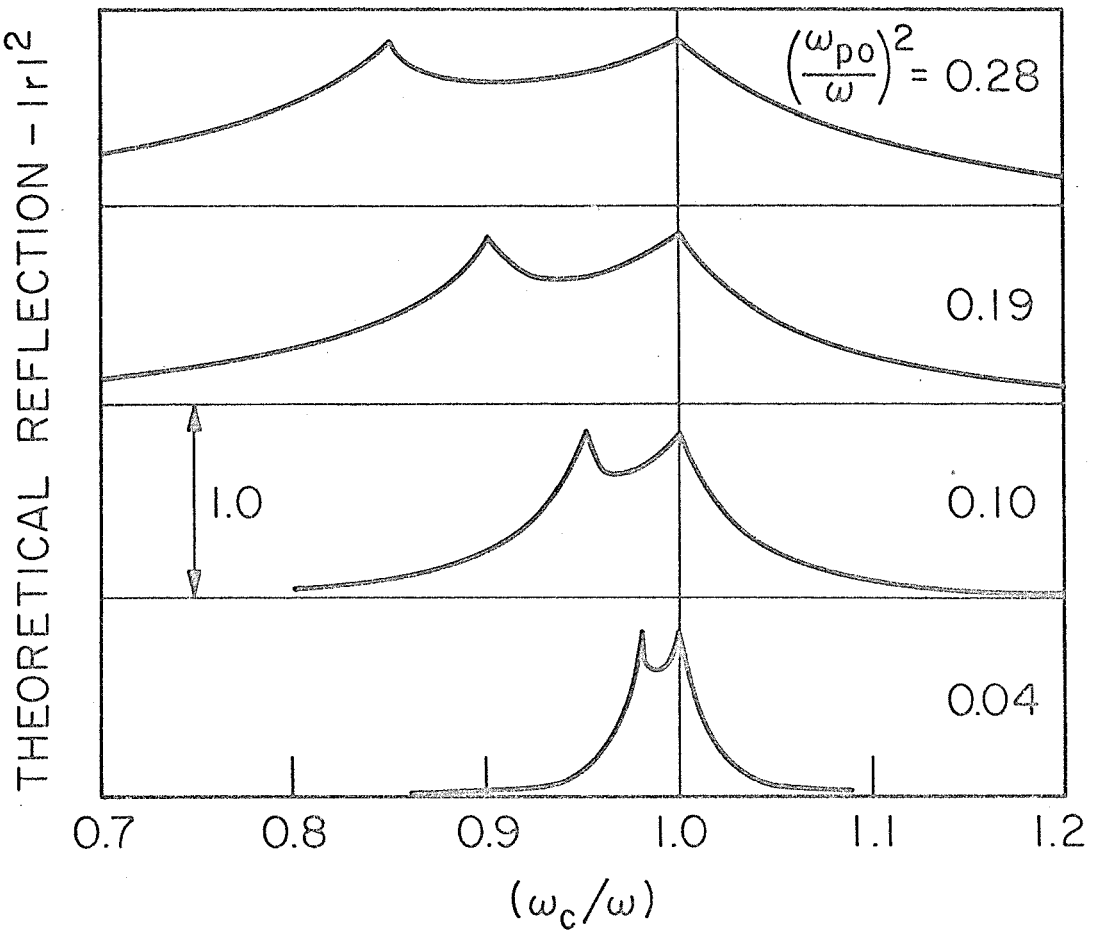

Fig. II.13 Theoretical reflection ($|r|^2$) vs. magnetic field (ω_c/ω) with electron density $(\omega_{po}/\omega)^2$ as a parameter.

experimental reflection curves and the theoretical ones is apparent. One peak in the theoretical reflection occurs at cyclotron resonance, $(\omega_c/\omega) = 1$, while a second peak occurs at the maximum upper hybrid frequency of the slab, $\omega_{ho}^2 = \omega_c^2 + \omega_p^2$. The two peaks are a manifestation of the fact that $|Z_p/Z_o|$ is very high near $\omega = \omega_{ho}$ and very low near $\omega = \omega_c$. Either condition yields a high reflection coefficient. The calculated peak values of $|r|^2$ are somewhat higher than those observed experimentally. Reduction in R would lower these values and change the shape of the curves somewhat. However, no new qualitative features appear and the two characteristic peaks are always present. The height of the two peaks is the same and is independent of electron density. The experimental peaks are also approximately equal and decrease only slowly with decreasing electron density. The quantitative difference between theory and experiment on the exact position of the upper hybrid peak is one shortcoming of the adopted model. Helium represents an anomaly with respect to the other gases and the calculated curves. However, it is possible to produce theoretical curves somewhat similar to the helium by adjusting R and (ℓ/a) .

Assuming thermodynamic equilibrium exists between the electron gas and the waveguide components, and the radiation field in the waveguide, the Nyquist theorem (22) can be used to calculate the noise emission of the plasma. The total noise power per unit bandwidth P_N passing through the isolator in Fig. II.12 is

$$P_N = kT_o|r|^2 + kT_o|t|^2 + kT_p|a|^2 \qquad (5)$$

where T_o is the temperature of the waveguide components, T_p is the plasma temperature, and k is the Boltzmann constant. The quantities $|r|^2$, $|t|^2$, and $|a|^2$ are the power reflection, transmission, and absorption coefficients of the junction created by the presence of the plasma in the waveguide circuit. Note that power conservation requires

$$|r|^2 + |t|^2 + |a|^2 = 1 \tag{6}$$

Using Eq. 6, the expression for the noise emission becomes

$$P_N = kT_o + k(T_p - T_o)\,|a|^2 \tag{7}$$

Since we are interested only in the relative noise emission, we need know only the properties of the absorption coefficient

$$|a|^2 = \frac{4Z_o\,\mathrm{Re}(Z')}{|2Z' + Z_o|^2} \tag{8}$$

Using the same values of parameters assumed in the reflection calculation $|a|^2$ was computed as a function of (ω_c/ω), resulting in the curves of Fig. II.14. Again, the plasma density is a parameter. The upper hybrid resonance emission effects are clearly present. However, there is no peak in emission near cyclotron resonance as is observed experimentally for all gases studied. This fact is a major failure of the cold plasma model, and results because $\mathrm{Re}(Z_p) = 0$ at $(\omega_c/\omega) = 1$. Changing the parameters R and (ℓ/a) cannot introduce the desired cyclotron resonance emission peaks.

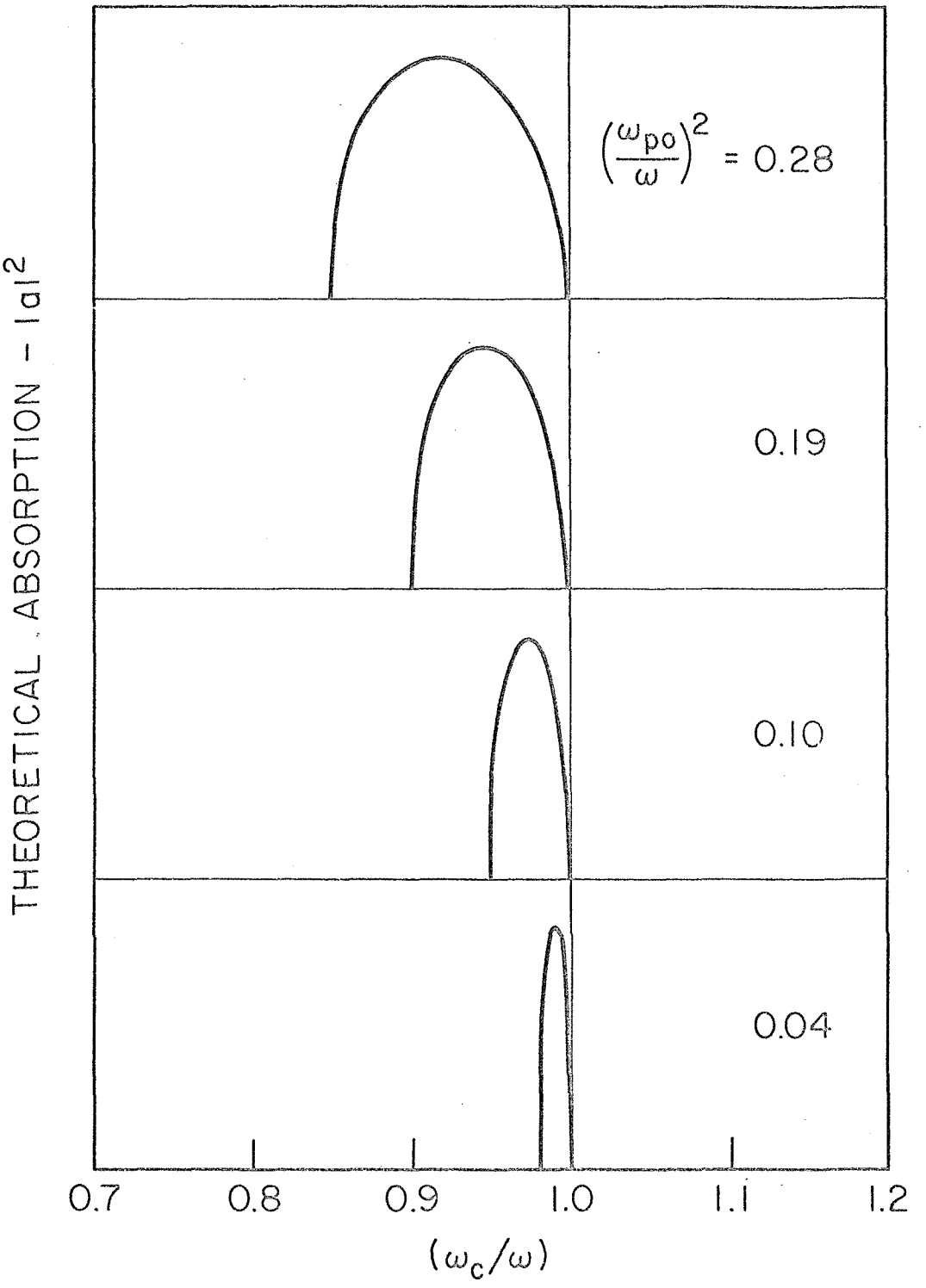

Fig. II.14 Theoretical absorption ($|a|^2$) vs. magnetic field with electron density as a parameter.

II.D. Discussion

The general simplicity and symmetry of the experimental reflection and noise emission data are striking. Both types of data show both cyclotron resonance effects and what have been interpreted as upper hybrid resonance effects. Furthermore, the reflection and emission data for a given gas show a very strong correlation. We were thus naturally led to the attempt of Section II.C to interpret the results with a simple cold plasma theory. However, the one-dimensional cold plasma theory cannot predict consistently the cyclotron resonance peaks or the position of the upper hybrid peaks. One might initially suspect the one-dimensional nature of the model as the source of the discrepancy. At the very least, a weakening of the effective space charge restoring force ($\propto \omega_p^2$) would be expected in a two-dimensional geometry. However, calculations of the scattering and absorption of a plane wave by an infinite, but nonuniform cold plasma cylinder also do not show a cyclotron resonance peak (23). In this particular calculation the electrostatic approximation for the fields inside the plasma was not made. Other calculations of absorption by cold plasmas of various geometries show only upper hybrid resonance effects (18,24). Kuckes and Wong (25) have presented a calculation of the absorption in a one-dimensional inhomogeneous cold plasma which shows one peak at cyclotron resonance and one at the cut-off frequency which is the solution of $(\omega_c/\omega) + (\omega_p/\omega)^2 = 1$. However, their calculation was made with parameters appropriate to their experiments which were considerably different from ours. In particular, their experiments were performed

with (ka) large (≈ 10) while (ka) is small (≈ 0.4) in our experiments. The more realistic calculation in cylindrical geometry carried out in our laboratory (23) does not show these effects when (ka) is small. Only the upper hybrid resonances are important. Tetenbaum and Bailey (26) have found evidence of the peaks of Kuckes and Wong in noise emission experiments. However, their measurements were carried out in a stimulated hot afterglow, and in a geometry such that (ka) is large, ≈ 10. When (ka) is large, multiple wave resonances and high order multipole scattering terms become important. The absence of a cyclotron resonance peak in absorption thus appears to be an inherent property of the cold plasmas of the type considered here. A similar peak is observed at cyclotron resonance in the magnetic field spectra of echoes from these plasmas (see Section III).

Pulse-stimulated ringing experiments (11,27) in similar afterglow plasmas have shown that the long time response is strongest at the frequencies ω_c and ω_{ho}. These results are qualitatively consistent with the CW data presented here. That is, from the CW data one would expect pulse measurements to show a double peak in the frequency domain. In fact, we have carried out pulse reflection experiments (see Section III.A) and low density ringing experiments (28) which exhibit the same general behavior. However, there is some question as to whether the pulsed ringing occurs exactly at ω_{ho} or at some mean hybrid frequency as one would expect on the basis of the CW data. At very low electron densities such as those used in some of the ringing experiments (11,27), it is difficult to distinguish such differences

quantitatively.

One further fact supporting the upper hybrid resonance interpretation of the data is the existence of echoes observed in experiments with these same plasmas (10). An inhomogeneous cold plasma theory successfully predicts some of the salient features of these echoes which are thought to involve directly upper hybrid plasma oscillations. This subject is treated in Section III.

Of course, cold plasma models are only approximate in the final analysis. The theory of electrostatic oscillations in inhomogeneous, hot plasmas yields standing wave normal modes whose oscillation frequencies are intimately related to the nonuniform electron density profile and the associated upper hybrid frequencies (4,29). As is the case with the cold plasma modes, the hot plasma modes are distributed in the band $[\omega_c, \omega_{ho}]$. At low temperatures and densities like those of our experiments, these modes are very closely spaced, approaching a continuum. Thus the frequency domain distribution of modes for the hot and cold plasmas are very similar. However, examination of the general properties of these modes shows that one would expect a very high number of modes per given frequency range in the vicinity of cyclotron resonance. One might speculate that the cyclotron resonance effects observed arise because of this high density of modes, and that the basic disagreement between cold plasma theory and the experimental data exists because the plasmas studied are not cold enough to make the true cold plasma theory valid, particularly when (ω_c/ω) is near one.

Finally, some remarks concerning the effect of geometry on calculated resonance frequencies are appropriate. For the one-dimensional electrostatic problems the hybrid frequencies $\omega_h^2 = \omega_c^2 + \omega_p^2$ are the relevant ones. In two-dimensional cylindrical geometry numerical factors may be introduced, yielding modified hybrid frequencies. For example, a uniform cold plasma cylinder exhibits a dipole resonance (30) at the frequency ω which is a solution of $\omega_p^2 = 2\omega\ (\omega - \omega_c)$. For low electron densities this formula gives a condition identical with the upper hybrid formula. However, at high electron densities, the two formulas differ quantitatively. Our experiments and interpretation do not exclude the presence of such unaccounted for numerical factors. However, none of the qualitative features of the phenomena are affected.

References: Section II

1. G. Landauer, J. Nucl. Energy, Pt. C 4, 395 (1962).
2. For a review of these phenomena, see F. W. Crawford, Nucl. Fusion 5, 73 (1965).
3. I. B. Bernstein, Phys. Rev. 109, 10 (1958).
4. S. J. Buchsbaum and A. Hasegawa, Phys. Rev. 143, 303 (1966).
5. A. F. Kuckes and A. Y. Wong, Phys. Rev. Letters 13, 306 (1964); Phys. Fluids 8, 1161 (1965).
6. D. E. Kaplan, R. M. Hill and A. Y. Wong, Phys. Letters 22, 585 (1965).
7. R. M. Hill and D. E. Kaplan, Phys. Rev. Letters 14, 1062 (1965).
8. G. F. Herrmann, R. M. Hill and D. E. Kaplan, Phys. Rev. 156, 118 (1967).
9. R. S. Harp, R. L. Bruce and F. W. Crawford, J. Appl. Phys. 38, 3385 (1967).
10. L. O. Bauer, F. A. Blum and R. W. Gould, Phys. Rev. Letters 20, 435 (1968).
11. R. M. Hill, D. E. Kaplan and S. K. Ichiki, Phys. Rev. Letters 19, 154 (1967).
12. T. H. Stix, The Theory of Plasma Waves (McGraw-Hill Book Company, New York, 1962).
13. G. Bekefi, J. D. Coccoli, E. B. Hooper and S. J. Buchsbaum, Phys. Rev. Letters 9, 6 (1962); K. Mitani, H. Kubo and S. Tanaka, J. Phys. Soc. Japan 19, 211 (1964).
14. C. G. Montgomery, Ed., Techniques of Microwave Measurements, MIT Radiation Laboratory Series (McGraw-Hill Book Company, New York, 1948), p. 515.
15. R. Stenzel (private communication).

References: Section II (Continued)

16. G. Bekefi, J. D. Coccoli, E. B. Hooper and S. J. Buchsbaum, Phys. Rev. Letters 9, 6 (1962); S. Tanaka, H. Kubo and K. Mitani, J. Phys. Soc. Japan 20, 462 (1965).

17. H. J. Schmitt, G. Meltz and P. J. Freyheit, Phys. Rev. 139, A1432 (1965); C. D. Lustig, Phys. Rev. 139, A63 (1965); S. Tanaka, J. Phys. Soc. Japan 21, 1804 (1966).

18. S. J. Buchsbaum, Bull. Am. Phys. Soc. 7, 151 (1962); S. J. Buchsbaum, L. Mower and S. C. Brown, Phys. Fluids 3, 806 (1960).

19. S. C. Brown, Basic Data of Plasma Physics (M.I.T. Press, Cambridge, Massachusetts, 1967).

20. W. P. Allis, S. J. Buchsbaum and A. Bers, Waves in Anisotropic Plasmas (M.I.T. Press, Cambridge, Massachusetts 1963), p. 23.

21. For a discussion of this phenomenon for a plasma in the absence of a magnetic field, see: E. M. Barston, Annals. Phys. 29, 282 (1964); see also, R. W. Gould and F. A. Blum, Eighth International Conference on Phenomena in Ionized Gases (Springer-Verlag, Vienna 1967), p. 405.

22. J. L. Lawson and G. E. Uhlenbeck, Ed., Threshold Signals, M.I.T. Radiation Laboratory Series (McGraw-Hill, New York 1950), p. 64.

23. R. H. Ault and R. W. Gould (private communication)

24. J. L. Hirshfield and S. C. Brown, Phys. Rev. 122, 719 (1961).

25. A. F. Kuckes and A. Y. Wong, Phys. Fluids 8, 1161 (1965).

26. S. J. Tetenbaum and H. N. Bailey, Phys. Rev. Letters 19, 12 (1967).

27. D. E. Baldwin, D. M. Henderson and J. L. Hirshfield, Phys. Rev. Letters 20, 314 (1968).

28. L. O. Bauer, Ph.D. Thesis, California Institute of Technology (May, 1968).

References: Section II (Continued)

29. G. A. Pearson, Phys. Fluids 9, 2454 (1966); H. L. Frisch and G. A. Pearson, Phys. Fluids 9, 2464 (1966).

30. F. W. Crawford, G. S. Kino and A. B. Cannara, J. Appl. Phys. 34, 3168 (1963).

III. ECHOES

Echoes from a plasma stimulated by multiple excitation pulses were first reported by Hill and Kaplan (1) in 1965. Their experiments involved excitation of a plasma in a strong, inhomogeneous magnetic field by pulses whose center frequency was near the electron cyclotron frequency. This plasma echo has come to be called the cyclotron echo. A theoretical model consisting of a collection of independent electrons gyrating in a nonuniform magnetic field and subject to energy-dependent collisions is believed to describe the effect adequately (2) if the plasma density is low enough (3). Other nonlinear mechanisms such as energy-dependent gyrofrequency (4,5) and nonlinear driving force effects (6) have been discussed but are too weak in relation to the energy-dependent collisions to be considered significant. More recently, Gould, et al. (7), have published theoretical and experimental descriptions of echoes from electron plasma waves in a hot, collisionless plasma. This plasma wave echo is intimately related to the collisionless damping of plasma waves as first described by Landau. The same phenomenon has been observed in ion plasma wave experiments (8). Furthermore, Bauer, Blum and Gould (3) have reported the most recent addition to the family of plasma echoes, two pulse echoes at electron upper hybrid resonance. Although studied under conditions similar to those of cyclotron echo experiments, the upper hybrid echo is observed when the plasma is in a very uniform magnetic field and is strongest near the maximum upper hybrid frequency ω_{ho} of the inhomogeneous plasma column, rather than near the cyclotron frequency. This

plasma echo is associated with the macroscopic modes of the plasma as described by Gould and Blum (9). Consequently, collective phenomena play a paramount role in the formation of this echo and independent particle theories are inadequate.

The plasma echoes discussed above have some general features in common. In each case, the macroscopic response of the particular system to a single pulse decays due to a phase mixing process that represents a loss of coherence rather than a true dissipation. Also, in each case, when a second pulse is applied to the plasma at a time τ following the first pulse, a reversal of the phase mixing is stimulated so that at times $t = n\tau$ a state of relative coherence exists. These states of relative coherence are manifested as relative maxima in the system response. Thus the application of two pulses to the plasma produces time-delayed multiple pulse responses which we call echoes. Figure III.1 shows a photograph of an oscilloscope display of such two-pulse echoes observed at upper hybrid resonance in argon. Note that although the time scale shown is short compared to a mean electron-neutral collision time, the response to each of the exciting pulses decays very rapidly due to phase mixing. Removal of either of the applied pulses causes the echoes to disappear. Since superposition applies to linear systems (no echoes from one pulse implies no echoes from two pulses), the echo process must be nonlinear.

Two-pulse echoes of the type shown in Fig. III.1 are the subject of this section. Some experimental properties of the upper hybrid echo will be documented in Section III.A, with particular emphasis on the relation to the scattering experiments described in

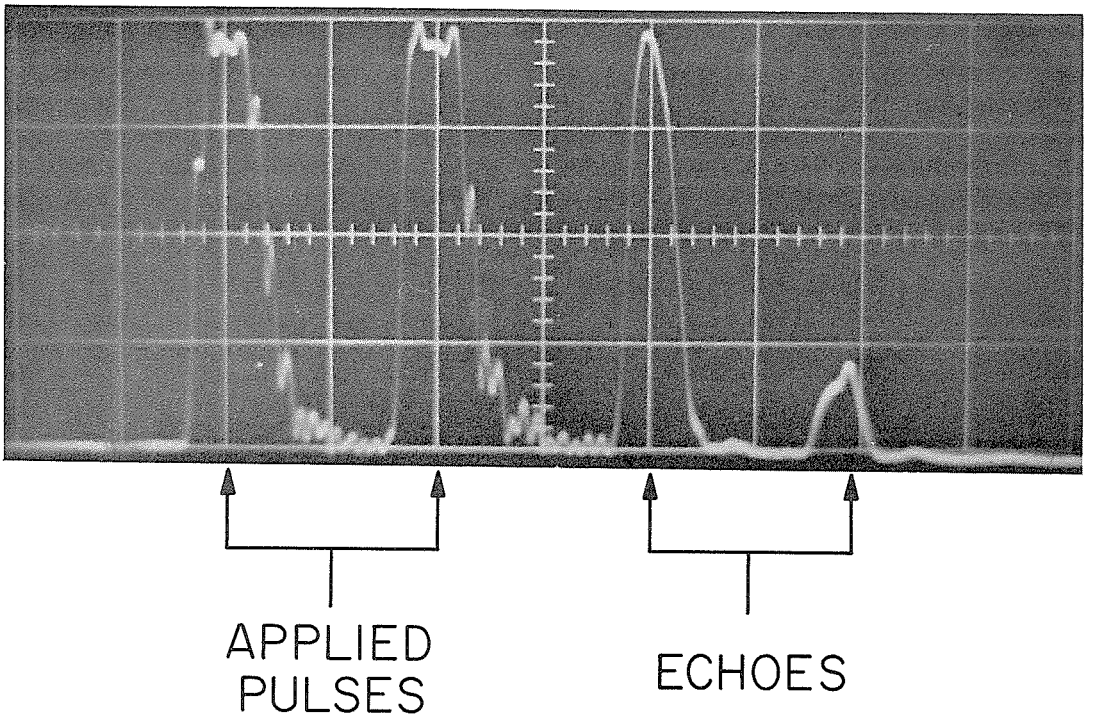

Fig. III.1 Oscilloscope display of two-pulse upper hybrid echoes in argon. Each major horizontal division is 50 nsec.

Section II. It is shown experimentally that in the S-band experiments the echo is strongest near the maximum upper hybrid frequency of the plasma as indicated by the CW data. Direct comparison between the CW reflection and echo amplitude data is made for several gases. The properties of echoes from a cold nonuniform magnetoplasma slab are calculated in Section III.C. The theory predicts the echoes to be strongest near the maximum upper hybrid frequency of the plasma slab, in agreement with experiment. Furthermore, computation of the detailed properties of these echoes yields results in qualitative agreement with most of the corresponding experimental measurements made by Bauer (10). Section III.B discusses the properties of echoes from a general collection of nonlinear oscillators. The purpose of this section is to treat

the case in which the finite spectral width of the excitation pulses is important. This problem has not been previously solved and the analysis gives results essential to the calculations of Section III.C. The reader somewhat familiar with the plasma echoes may choose to note only the main points of Section B and then go on to Section C.

III.A. Echo Experiments

The plasmas studied were the same afterglow, rare gas discharges described in Section II. The experimental apparatus is also basically the same. The only changes were in the form of the addition of the electronic equipment necessary for the generation of short microwave pulses (11). The signal follows path B of Fig. II.1. The magic tee arrangement serves no direct function in echo experiments, but plays an invaluable role since it permits companion reflection experiments of the type given in Section II. The microwave pulses were obtained by pulsing the grid of 10W Litton traveling wave tubes (X and S band) which were fed by a CW signal generator. With commercially available pulse generators and pulse transformers, microwave pulses with half-widths as short as 15-20 nsec can be formed. Shorter pulses were made by using the pulse generators to drive a blocking oscillator whose output was applied to the traveling wave tube grid. With this technique pulse half-widths of about 5 nsec can be achieved. The pulse widths quoted in the text are the approximate half-width of the crystal detected microwave pulses. The concomitant bandwidth of such short pulses require relatively wide bandwidth video amplifiers and

oscilloscopes. A Tektronix 585A was used for visual displays such as that shown in Fig. 1. However, most of the data presented here are studies of detected echo amplitude versus some external parameter. These data were taken by using a Hewlett-Packard 185B sampling oscilloscope and a fixed time sampling technique (described in Section II) in conjunction with an X-Y recorder. It should be emphasized that the CW scattering configuration of $\underline{E} \perp \underline{k} \perp \underline{B}$ is preserved and that the magnetic field is again homogeneous to one part in 10^4 over the volume of plasma excited by the microwaves.

One major point of the experimental results presented here concerns the relation of the observed echoes to the CW scattering results of Section II. The echo experiments employ high power, very short microwave pulses, while the scattering experiments were performed using low power, wide pulses. One naturally questions the relation of the two experiments. If the plasma responds in a linear fashion, the relation between a CW and a short pulse reflection experiment can be easily understood. Let $C(\omega)$ be the CW frequency response of the plasma as given by the data of Section II, and $P(\omega)$ be the Fourier transform of a short pulse $P(t)$ centered at t_o. If $P(t)$ is symmetric about t_o, the plasma response $R(t)$ at $t = t_o$ is

$$|R(t_o)|^2 = \left| \int_{-\infty}^{\infty} d\omega \; C(\omega) \; |P(\omega)| \right|^2$$

Thus, the reflection from the plasma at the time corresponding to the center of the applied pulse (t_o) is related to the area of the product of $C(\omega)$ and $P(\omega)$ (the convolution).

As $P(\omega)$ approaches a delta function $\delta(\omega - \omega_o)$ (CW signal) $R(t_o)$ approaches $C(\omega_o)$ as it should. When $P(t)$ is a short, but finite pulse, such that the width of $P(\omega)$ is less than the width of $C(\omega)$, $R(t_o)$ is expected to show the general features of the CW response curves with detailed and sharp features smeared out. The data of Fig. III.2 show that this is indeed the case experimentally. The dashed curves are displays of the maximum amplitude of the reflection from a neon afterglow of a 20 nsec microwave pulse of 0.5W peak power as a function of (ω_c/ω) with $\omega/2\pi = 3.0$ GHz (all data at S-band were taken at this frequency). The solid lines are CW reflection measurements taken under identical conditions. The CW data are that of Fig. II.3. Since there are no striking differences between the two sets of data, it is concluded that the high power, very short pulses couple to the same plasma normal modes which are observed in low power CW measurements. This observed relation between CW and short pulse experiments was found characteristic of all plasmas studied. Therefore, this problem will not be considered further and we will assume that there are no fundamental differences between the two types of experiments.

Having established that the high power, short pulses such as that used in echo experiments couple to the same collective normal modes observed in CW experiments, one's curiosity arises immediately concerning echoes from such plasmas. The independent particle theories (2,4,5) which were used to explain the occurrence of cyclotron echoes are no longer valid. Indeed, would one expect to observe echoes at all in these relatively high density plasmas in very uniform

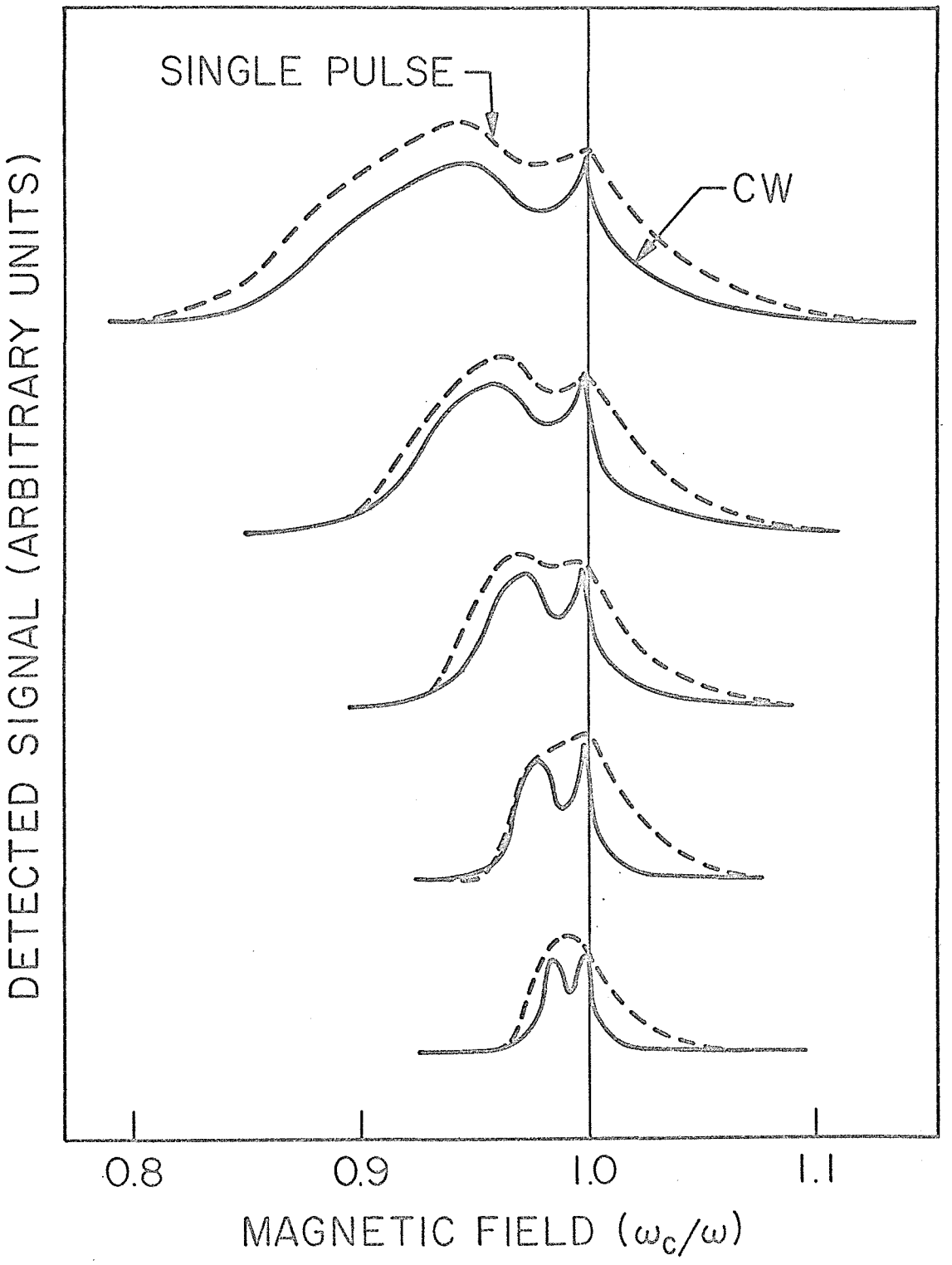

Fig. III.2 Comparison of CW and single-pulse reflection for neon.

magnetic fields? Of course, echoes are observed; they are the upper hybrid echoes (3) mentioned above. The echoes were stimulated by two microwave pulses of frequency ω separated by a time τ. The echoes consist of short bursts of radiation emitted by the plasma near times $t = n\tau$, $n = 1,2,\cdots$ after the second applied pulse (recall Fig. III.1). Since τ is typically on the order of hundreds of nanoseconds, while the characteristic time for the afterglow decay is on the order of a few milliseconds, an echo experiment can be performed at essentially constant plasma conditions (density and temperature). One of the most useful displays of information about the upper hybrid echo will prove to be what we shall call the echo magnetic field spectrum, i.e. a curve showing the dependence of the echo amplitude on (ω_c/ω). These echo spectra lend themselves naturally to comparison with the CW scattering results since both are easily measured as the magnetic field is varied and the density is held constant. Figure III.3 is a composite diagram of the CW, single-pulse, and echo spectra for neon. The experimental conditions are the same as those for the data of Fig. III.2, the two pulses stimulating the echo each being identical to the one used in the single-pulse reflection experiment, and separated by 100 nsec. The estimates of $(\omega_{po}/\omega)^2$ shown are based on the interpretation given in Section II for the CW response. These echo spectra have one striking feature that unalterably distinguishes the upper hybrid echo from the previously studied cyclotron echo. The upper hybrid echo is strongest at a point that is shifted by a large amount (several times the spectral half-widths) from the condition for free electron cyclotron

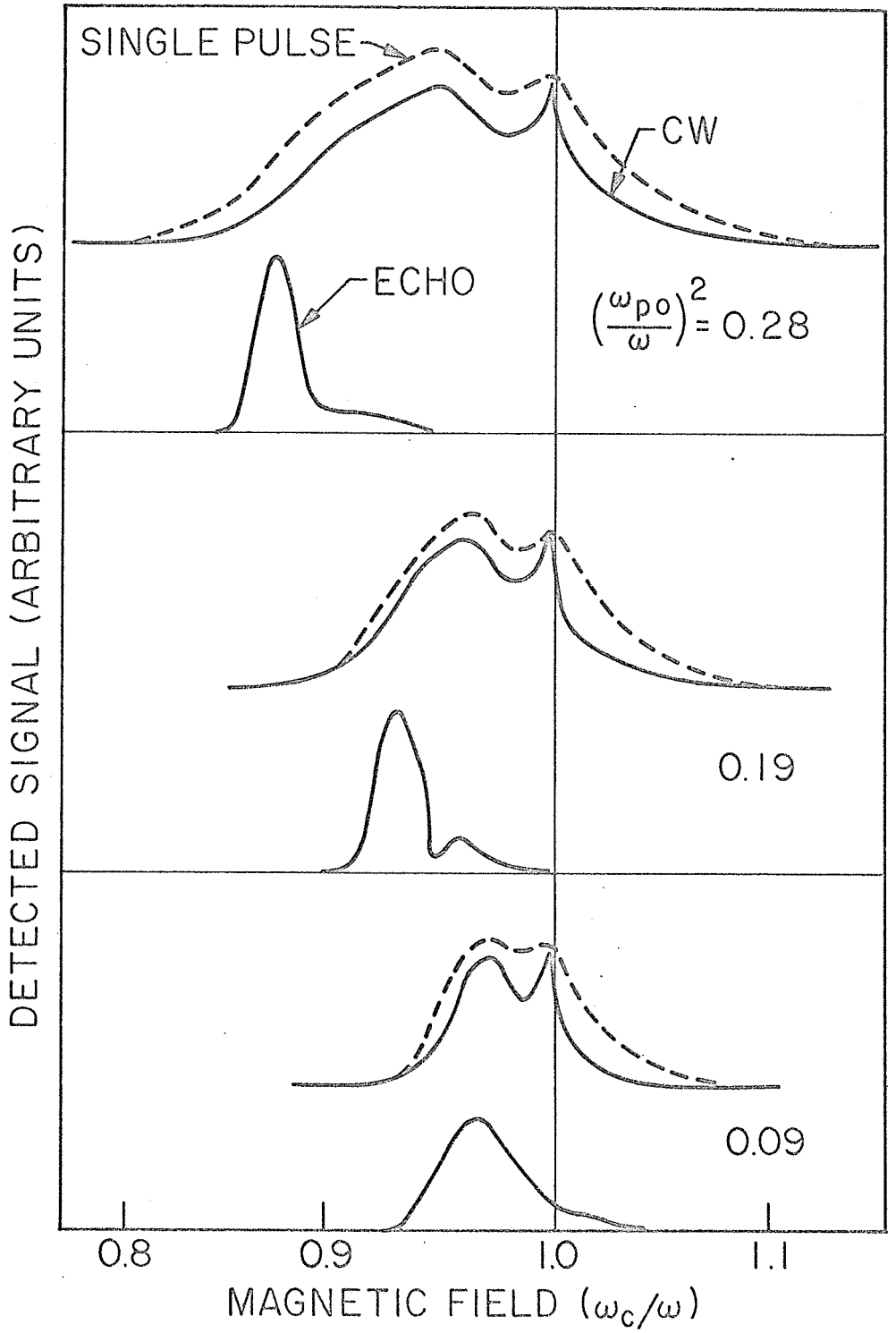

Fig. III.3 Composite diagram of experimental data on CW reflection, single-pulse reflection, and echo spectra for neon.

resonance, but it occurs near what the CW experiments mark as the maximum upper hybrid frequency of the plasma. As the upper hybrid frequency varies with the plasma density, the position of the peaks in the echo spectra follow, always occurring near the plasma's maximum upper hybrid frequency. This strong relation is the source of the name "upper hybrid echoes".

Figures III.4,5 show further data on the relation between the echo and the CW scattering for the gases argon and helium. As one might expect from the results of Section II, the data for argon are quite similar to those for neon, while the data for helium are somewhat different. Although in both cases the echo is strongest near the maximum upper hybrid frequency, the echo spectra for helium are very wide; in this gas the echo is weaker only by a factor of about two at cyclotron resonance than at the maximum upper hybrid frequency. But in argon and neon under the conditions given, the echo is much weaker near cyclotron resonance and the echo spectra are relatively narrow. Under appropriate conditions (lower power pulses and/or lower densities), a subsidiary relative maximum in the echo spectra occurs (10) near cyclotron resonance in argon and neon. This peak is apparently related to the peak near cyclotron resonance observed in the CW reflection and emission experiments. Considering cold plasma theory, this effect will prove to be an anomaly in echo properties as it was in CW properties of the plasma.

Some further anomalies in the helium echo experiments are worth noting. The long time macroscopic response to the individual applied

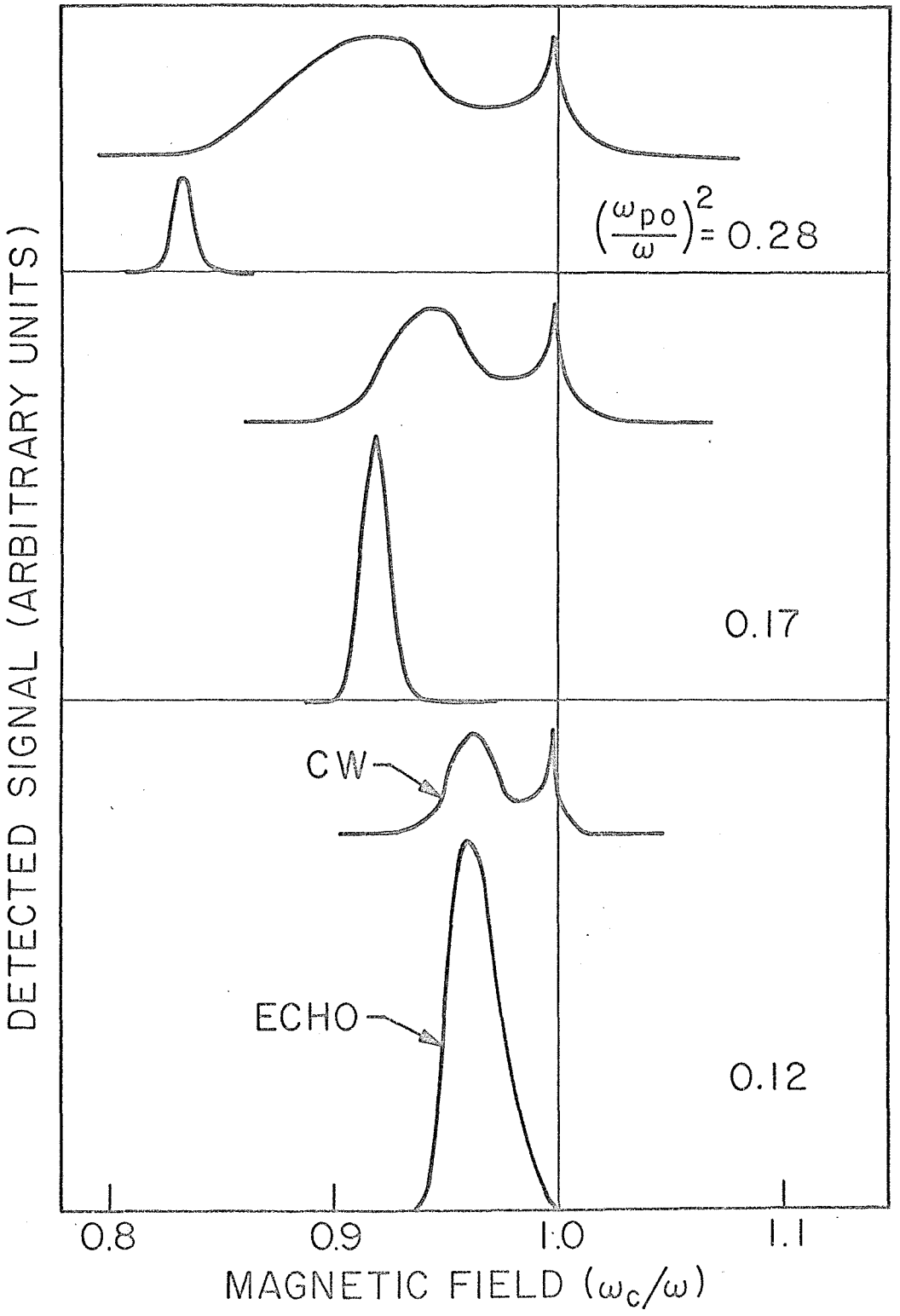

Fig. III.4 Comparison of CW reflection and echo spectra for argon.

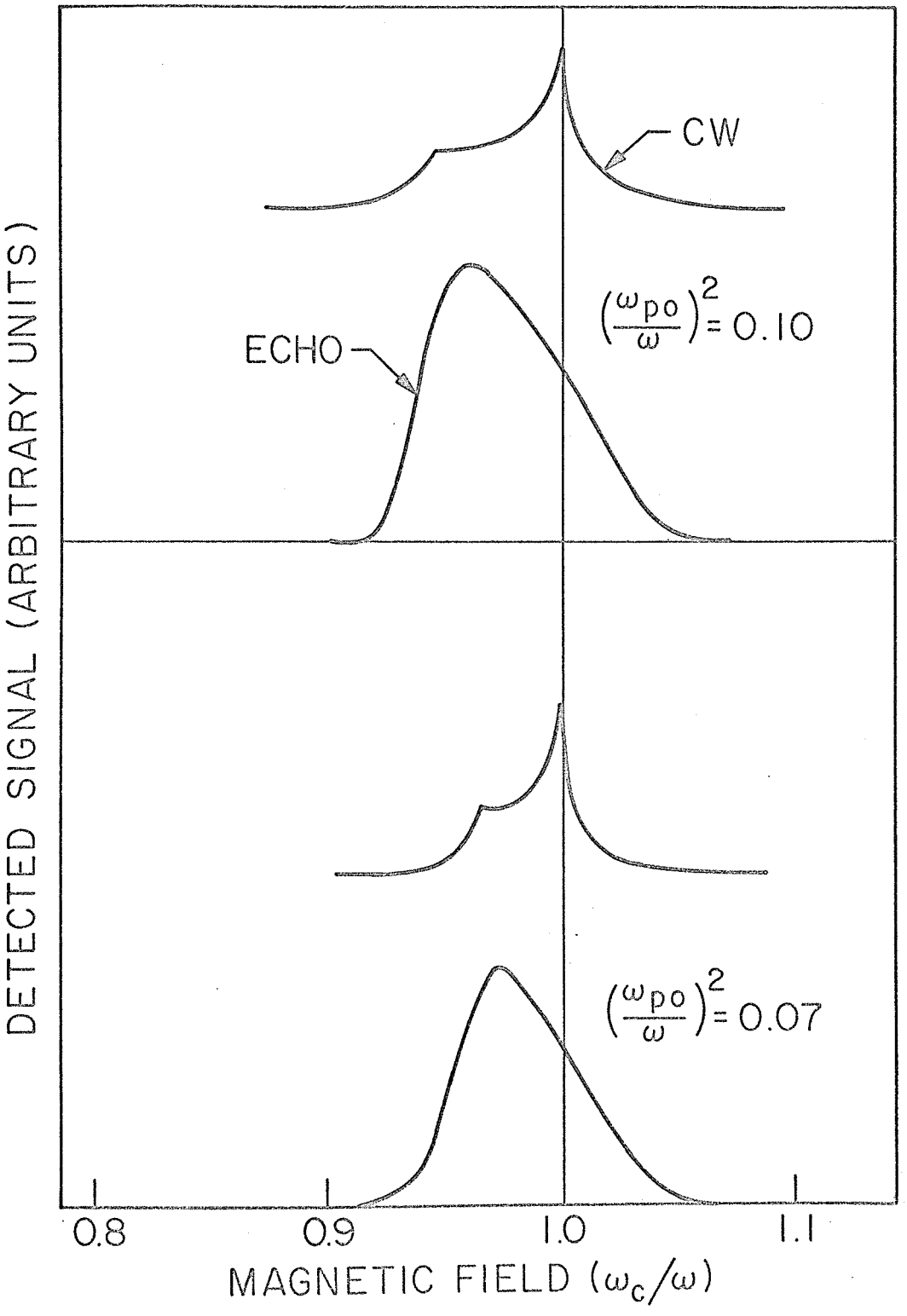

Fig. III.5 Comparison of CW reflection and echo spectra for helium.

pulses (single pulse response) tends to be of the order of the echo strength. When it is necessary to reduce τ so that the echo and this response are comparable, strong interaction between the two occur. For example, a strong beating occurs as one changes the magnetic field or the pulse spacing. Such effects occur in neon and argon, but are of small significance at high power and electron density. The echo amplitude data of Fig. III.5 have been averaged over this beating. In some cases it is not clear that an echo even occurs. When the echo is weak relative to the single-pulse response, this interaction which modulates rapidly with changing magnetic field can be used as a signature of the existence of an echo process. Also, relative to argon and neon, it proved difficult to obtain echoes in helium at very low densities ($\lesssim 10^9 cm^{-3}$) high pressure ($\gtrsim$ 15μ Hg). The problem with pressure is understandable since the elastic collision cross section of electrons with neutral atoms is larger for helium than either neon or argon at low electron energies. Such collision processes tend to destroy the echo (see Section III.B). In addition, if the pulse power is decreased by 10 db, the echo spectra of Fig. III.5 becomes symmetrical and peaked near the center of the CW curves rather than near ω_{ho}. Similar, but less drastic effects occur in neon and argon (see discussion below).

In the low density limit ω_{ho} and ω_c become virtually indistinguishable and the echo spectra are peaked near $(\omega_c/\omega) = 1$, as is the case for cyclotron echoes. Unfortunately, several unwanted complications are found under these conditions, particularly in neon and argon. First, the beating effect discussed above generally becomes stronger, tending to make measurements of echo properties difficult.

Second, the two peaks observed in CW reflection and emission experiments begin to contribute in equal strength to the echo process. Because these two contributions are at different frequencies, the detected signal presents a very strong beat pattern both in the single-pulse response and the echo. Other properties of the upper hybrid echo such as variation with input power and pulse separation are equally complicated. All of these characteristics have been studied experimentally in detail by Bauer (10) and will be compared with theoretical calculations to be given below.

Echo experiments were also performed at X-band with the same basic apparatus used in the S-band experiments described above. The data of Fig. III.6 show the comparison between the echo and CW spectra for argon with $\omega/2\pi = 9.0$ GHz. The remarkable feature of this data is that the echo is strongest at a value of (ω_c/ω) which is shifted by only a few percent from cyclotron resonance, even at very high densities. The echo is not strong near the maximum upper hybrid frequency. This fact is rather surprising when one considers the qualitative similarity between the X-band and S-band CW reflection data. Furthermore, experiments carried out at $\omega = 8.0$ Gc/sec indicate that the echo is strongest at a frequency approximately half-way between cyclotron resonance and the maximum upper hybrid frequency. Thus, as the signal frequency is increased, the position of the maximum echo moves closer and closer to $(\omega_c/\omega) = 1$. It should be emphasized that the experiments at the various frequencies are as identical as is practicable. Although the magnetic field and signal frequency are both changed, their ratio

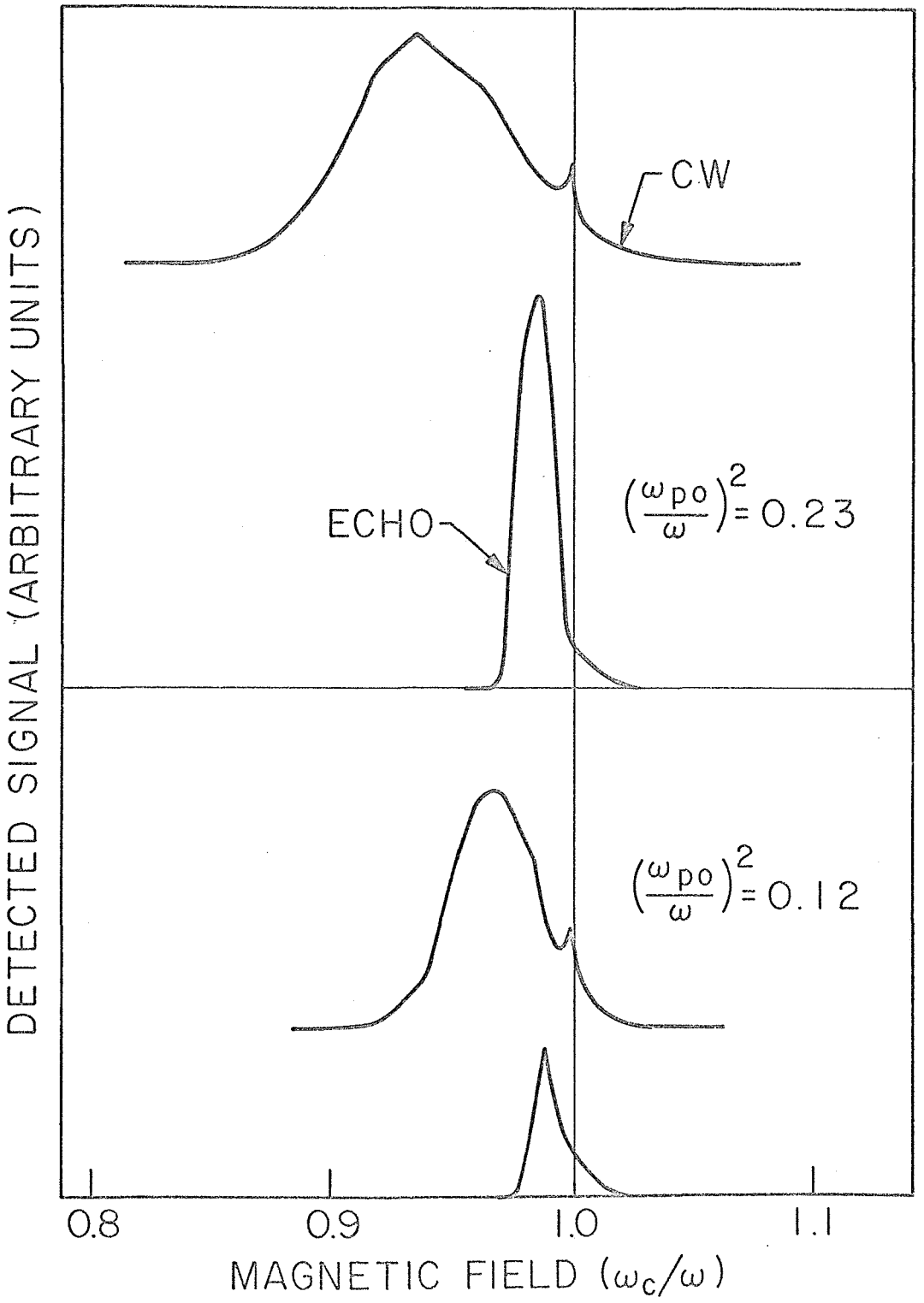

Fig. III.6 Comparison of CW reflection and echo spectra for argon at X-band.

remains constant. The electron densities are also comparable. Experiments at X-band with the plasma contained in a tube of short axial length (≈ 6 cm) have also produced echoes shifted only a few percent from cyclotron resonance (12). Although this geometry introduces peculiar scattering resonances both above and below $(\omega_c/\omega) = 1$, the echo is apparently associated only with the plasma modes in the region $(\omega_c/\omega) \leq 1$, i.e., the upper hybrid type modes. The peak in the echo spectrum was always such that $(\omega_c/\omega) \leq 1$. Experiments in other geometries (rare gas afterglows in rectangular bottles) at X-band give strongest echoes in between $(\omega_c/\omega) = 1$ and the maximum upper hybrid frequency (13). Furthermore, Kaplan, Hill and Wong (14) failed to find echoes at the maximum upper hybrid frequency in high density cesium plasmas.

An understanding of this puzzling phenomenon may lie in one's ability to couple energy to the upper hybrid modes of oscillation (14). According to cold plasma theory (15) there exists an evanescent layer through which the wave must tunnel when it is in the extraordinary polarization and is propagating through a region of inhomogeneous electron density which is such that the upper hybrid resonance condition is satisfied somewhere in the density profile. The efficiency of tunneling through this barrier is expected to decrease with decreasing wavelength (increasing frequency) as compared to the characteristic scale length of density gradient in the plasma. Thus, one would expect the point of maximum echo to move to high (ω_c/ω) as ω increases, exactly as is observed experimentally. However, the experiments

present some perplexing facts which do not appear to be consistent with this interpretation. First, the echo is not significantly weaker at X-band than at S-band as one might expect. Second, the CW and single-pulse reflection curves at X-band show substantially the same behavior as those at S-band. That is, the interaction (as measured by reflection) of these signals with the modes near the maximum upper hybrid frequency does not appear to be much affected.

Summarizing, experimental data has been shown demonstrating the existence of echoes in experiments performed with the same afterglow plasmas studied in Section II. Most striking is the relation between the echo spectra and the CW reflection data of Section II. Comparison shows that the echoes (at S-band) are strongest near the maximum upper hybrid frequency of the plasma. Measurements at X-band show a markedly different character, the echo being strongest at points between the cyclotron frequency and the maximum upper hybrid frequency, but still apparently associated with upper hybrid phenomena. Approaching further understanding of this plasma echo process, the remainder of this paper will deal with the development of a theory which exhibits qualitatively many of the salient features of the experimental results.

III.B. Theory of Echoes from a System of Nonlinear Oscillators

Since the original discovery of multiple pulse echo phenomena in nuclear spin resonance experiments (16), the generality of the basic characteristics of these processes has become increasingly apparent. Although the original descriptions of spin echoes were based primarily on the Bloch equation which treats the spin in a classical manner (as a precessing top), an analogous equation of motion has been shown to be valid for any two-level quantum system (17). The discovery of multiple pulse plasma echoes (1), which can be described in a strictly classical manner, triggered new discussions (4,6) of the fundamental properties of classical echo systems and emphasized the generality of these echo phenomena. Indeed, multiple pulse echoes have been observed in all states of matter (18) (solid, liquid, gas and plasma) involving physical phenomena as diverse as photons (19) and standing spin waves (20). Gould (4) has outlined three basic characteristics which link to some degree these various echo systems and establish a basis for judging classical physical systems capable of exhibiting echo phenomena:

(1) The system should consist of a nondegenerate collection of oscillators which can be excited externally;

(2) Some nonlinear effect must be operative either during the excitation or evolution of the system; and

(3) The relaxation of the oscillators must be slow enough to allow observation of the echoes.

It is the intent of this section to consider the pulse response of a collection of dissipationless harmonic oscillators with weakly

nonlinear restoring forces, showing explicitly the role of the above criteria in the formation of echoes, and deriving some fundamental characteristics of these echoes. The treatment of the initial value problem (delta function excitation pulse) involving one such oscillator is the subject of standard texts (21) on nonlinear mechanics. We will describe the essential features of two-pulse echo processes for a collection of such oscillators, particularly in the case where the excitation occurs in the form of pulses of finite width (rather than delta functions). This problem has not been previously treated. The results of this section will prove invaluable in the discussion of a cold plasma physical model to be discussed in Section III.C.

Consider an ensemble of undamped harmonic oscillators of number density per unit frequency range $n(\omega_o)$ whose amplitude y obeys the equation

$$\frac{d^2y}{dt^2} + \omega_o^2 y\,(1 + \alpha y + \beta y^2 + \cdots) = F(t) \qquad (1)$$

where $\alpha, \beta, \cdots$ are small constants, ω_o is the characteristic frequency of a particular oscillator in the linear approximation, t is time, and $F(t)$ is an externally applied force. The external force F is assumed to be zero in the distant past and the distant future (i.e., a pulse). We assume that the oscillators constitute a physical system which has a macroscopic observable $Y(t)$ which is the superposition of all oscillator amplitudes weighted by their number density:

$$Y(t) = \int d\omega_o n(\omega_o)\, y(\omega_o, t) \qquad (2)$$

The exact nature of $n(\omega_o)$ will depend on the particular physical system being considered.

In the linear approximation $\alpha, \beta, \cdots = 0$, Eq. 1 is that of a simple harmonic oscillator driven by $F(t)$. The particular solution to this linear equation is

$$y(t) = \frac{1}{\omega_o} \int_{-\infty}^{t} \sin \omega_o(t - t') \, F(t') \, dt' \tag{3}$$

We would now like to derive the particular solution to the nonlinear Eq. 1. In analogy with the Lindstedt (21) method of treatment of the initial value problem, we use a perturbation analysis to seek solutions to Eq. 1 periodic in $\theta = \omega t$. Thus we look for solutions of the form

$$y = y_o + \varepsilon y_1 + \varepsilon^2 y_2 + \cdots$$

with

$$\omega = \omega_o + \varepsilon \omega_1 + \varepsilon^2 \omega_2 + \cdots$$

which satisfy (at long times)

$$y(\theta) = y(\theta + 2\pi)$$

The parameter ε has been introduced to aid in the perturbation scheme. Equation 1 can be written

$$\omega^2 \frac{d^2 y}{d\theta^2} + \omega_o^2 \, y[1 + \alpha y + \beta y^3 + \cdots] = F(t)$$

To zero order (ε^o), we have

$$\frac{d^2 y_o}{d\theta^2} + y_o = \frac{1}{\omega_o^2} F(t) \tag{4}$$

While to first order (ε^1), the equation

$$\frac{d^2y_1}{d\theta^2} + y_1 = -\alpha y_o^2 - \beta y_o^3 - \frac{2\omega_1}{\omega_o}\frac{d^2y_o}{d\theta^2} \tag{5}$$

results. The terms involving y_o on the RHS of Eq. 5 serve as driving terms for the first order solution y_1. Equation 4 is that of a simple harmonic (linear) oscillator driven by F and has the particular solution

$$y_o(\theta) = \frac{1}{\omega_o^2}\int_{-\infty}^{\theta} \sin(\theta - \theta')\, F(\frac{\theta'}{\omega})\, d\theta' \tag{6}$$

As a boundary condition we take y_o to be zero in the distant past; thus, the solution to the homogeneous form of Eq. 4 is zero.

Consider now the long time (large θ) behavior of y_o. Since F is at most a series of pulses, we define long times to be those such that

$$\int_{-\infty}^{t} e^{i\omega t'}\, F(t')\, dt' \simeq \int_{-\infty}^{\infty} e^{i\omega t'}\, F(t')\, dt' \equiv f(\omega) \tag{7}$$

where $f(\omega)$ is the Fourier transform of $F(t)$. Therefore, for long times

$$y_o(\theta) \simeq \frac{\omega}{\omega_o^2}\left[f_r(\omega)\sin\theta - f_i(\omega)\cos\theta\right] \tag{8}$$

where f_r and f_i are the real and imaginary parts of f. Upon inserting the solution for y_o given in Eq. 6 into the RHS of Eq. 5, it is clear that at very late times the RHS will contain terms

proportional to $\sin\theta$ and $\cos\theta$. Terms of this form are in resonance with the undamped oscillator described by the LHS of Eq. 5, i.e. these terms are secular. Thus as $t \to \infty$, $y_1 \to \infty$ and the perturbation scheme is violated. Fortunately, we can eliminate these secular terms (in the limit $t \to \infty$) by requiring the first order correction to the frequency ω_1 to take on a certain value. Keeping only the secular part of the RHS of Eq. 5 yields (for long times)

$$\frac{d^2 y_1}{d\theta^2} + y_1 = \left[2\frac{\omega_1}{\omega_o} - \frac{3}{4}\frac{\omega^2}{\omega_o^4}\beta(f_r^2 + f_i^2)\right] y_o$$

To eliminate the secularity, the bracketed expression must be zero, giving

$$\omega_1 = \frac{3}{8}\beta\frac{\omega^2}{\omega_o^3}|f|^2$$

To first order, the frequency is

$$\omega = \omega_o + \frac{3}{8}\frac{\beta}{\omega_o}|f(\omega_o)|^2 \qquad (9)$$

In order to arrive at a complete solution for y to order ε, we should now solve for y_1. This would be cumbersome; we will therefore restrict ourselves to be concerned only with the changes in frequency of the oscillator in question, presuming this to be the physically interesting and significant quantity. In doing this, nonlinear effects occurring during the application of the pulse are ignored. Herrmann and Whitmer (6) give a formal description of echoes arising from these effects. We will show below that the frequency

shift nonlinear terms are enhanced by the evolution of time. Basically, we are assuming that the excitation pulse width is short compared to the time after the pulse at which we make any observations, i.e., the times for which we apply the approximate solution. For the two-pulse echo process described below, this implies that the half-widths of the two excitation pulses is small compared to the time separation of the two pulses. This assumption is consistent with the entire scheme of solution and will prove to be quite fruitful, yielding the essential ideas concerning echoes. To second order, one can show that Eq. 9 becomes

$$\omega = \omega_o + \frac{1}{\omega_o}\left[\frac{3}{8}\beta - \frac{5}{12}\alpha^2\right] |f(\omega_o)|^2 \qquad (10$$

The solution for y is approximately $(t \to \infty)$

$$y(t) \simeq \frac{1}{\omega_o} \int_{-\infty}^{t} \sin \omega(t-t') F(t')\, dt' \qquad (11)$$

with ω given by Eq. 10.

Equation 11 is the desired result, giving the approximate nonlinear solution for y valid at long times. Note the similarity between this nonlinear solution and the linear solution given in Eq. 3. The solutions are of exactly the same form. However, as $t \to \infty$, the nonlinear oscillator evolves in a sinusoidal manner with a frequency slightly shifted from ω_o by an amount which depends on the level of excitation supplied by the external force. Roughly, the oscillator frequency is amplitude dependent. We now have the essential results necessary to describe the response of the oscillator system to any

sequence of pulses.

First, consider the linear response of one oscillator to a single pulse $F(t)$ at long times,

$$y_o(t) \simeq \frac{1}{\omega_o} [f_r(\omega_o) \sin \omega_o t - f_i(\omega_o) \cos \omega_o t] \tag{12}$$

which is an undamped sinusoid.

Combining Eqs. 2 and 12, we obtain the macroscopic response

$$Y(t) = \int d\omega_o \frac{n(\omega_o)}{\omega_o} f_r(\omega_o) \sin \omega_o t - \int d\omega_o \frac{n(\omega_o)}{\omega_o} f_i(\omega_o) \cos \omega_o t \tag{13}$$

Both terms on the RHS of Eq. 13 are of the form

$$g(t) = \int d\omega\, g(\omega) \begin{matrix} \sin \\ \cos \end{matrix} \{\omega t\} \tag{14}$$

By the Riemann-Lebesque lemma

$$\lim_{t \to \infty} g(t) = 0$$

if $g(\omega)$ is absolutely integrable (22). The function $g(t)$ approaches zero on a time scale of the order of $(1/\Delta\omega)$ where $\Delta\omega$ is the half-width of $g(\omega)$. Thus the macroscopic response $Y(t)$ goes to zero as $t \to \infty$, even though each individual oscillator evolves to a state of sinusoidal oscillation with constant amplitude (see Fig. III.7). This phenomenon can be understood as a process of "phase mixing". Many of the individual oscillators have different frequencies (required by assumption of nondegeneracy). When the oscillators are excited by a short pulse, those significantly affected are approximately in phase at

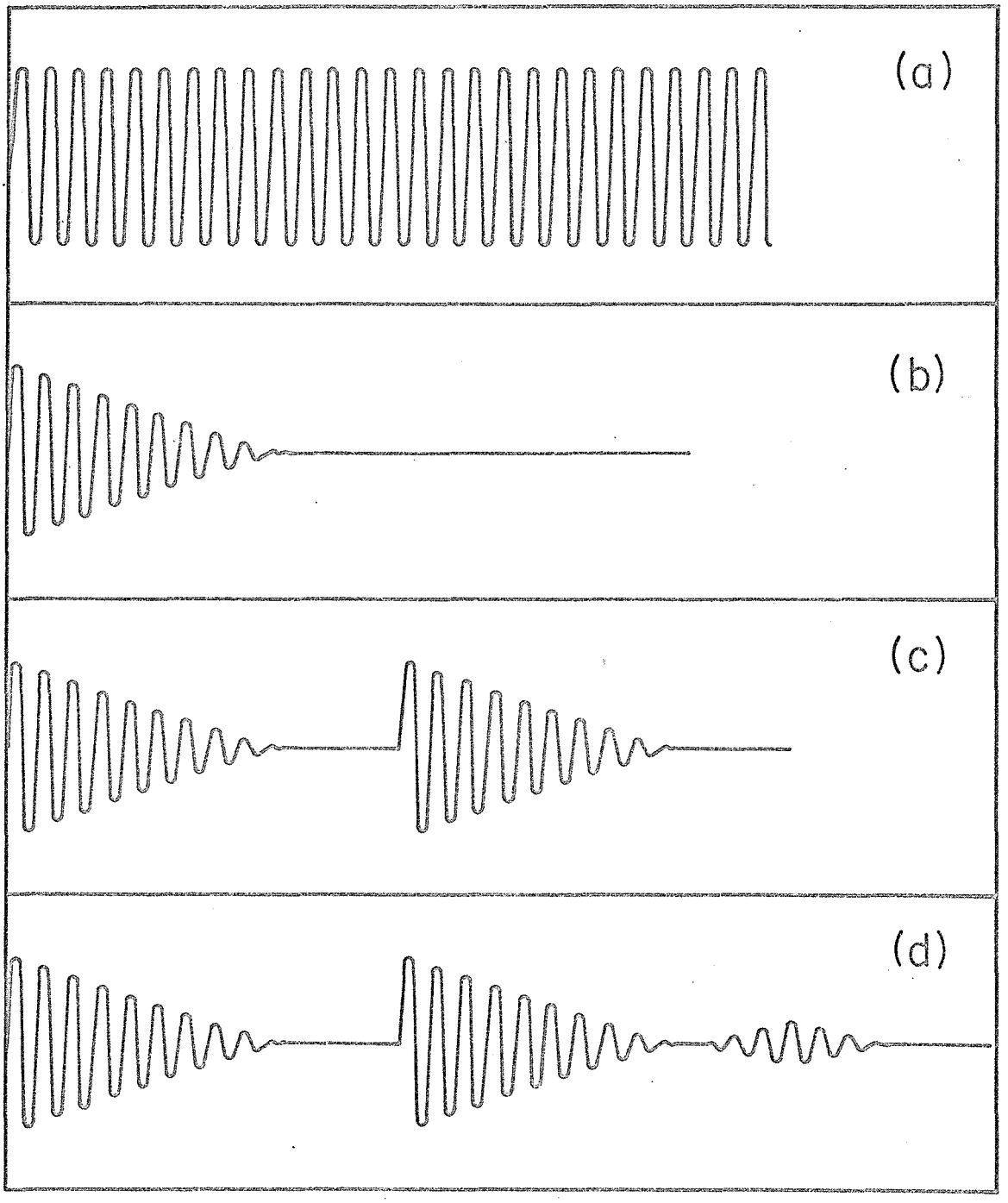

Fig. III.7 Oscillator response vs. time:
(a) Response of one oscillator to one pulse, linear or nonlinear;
(b) Response of a collection of oscillators to one pulse, linear or nonlinear;
(c) Response of a collection of linear oscillators to two pulses;
(d) Response of a collection of nonlinear oscillators to two pulses.

early times (just after the application of the pulse). As time progresses, since their frequencies are different, the oscillators become less and less phase coherent. In fact, without knowledge of the exact nature of the oscillators and the external force, for long times the most reasonable assumption is that the oscillators' phases are random. What is the total signal (macroscopic response) received from this system of randomly phased oscillators? This problem is much like Lord Rayleigh's example of the difference in intensity of a sound from N (a large number) musical instruments in phase and randomly phased. The well-known result is that the randomly phased set of instruments yields an intensity that is a factor of $(1/N)$ smaller than that for a set of instruments with coherent phases. Thus as $t \to \infty$ our set of oscillators would also be expected to yield a signal which "phase mixes" to zero. The weakly nonlinear response, which we have derived for one oscillator, gives for the system of oscillators

$$Y(t) = \int d\omega_o \frac{n(\omega_o)}{\omega_o} f_r(\omega_o) \sin \omega t - \int d\omega_o \frac{n(\omega_o)}{\omega_o} f_i(\omega_o) \cos \omega t$$

where ω is given by Eq. 10. The arguments about phase mixing do not change and the nonlinear solution $Y(t) \to 0$ as $t \to \infty$ also. So far, nothing of unusual significance has appeared in the formulation of the response to a single pulse.

Second, consider the application of two pulses $F_1(t)$ and $F_2(t)$ centered at the times $t = -\tau$ and $t = 0$. We assume that F_1 and F_2 are symmetric about their centers. This assumption is not crucial or necessary, but serves as a very reasonable simplification

giving $f_{1i}(\omega) = 0 = f_{2i}(\omega)$. In the linear approximation superposition applies and the response to two pulses is just the sum of the separate responses to the two individual pulses (see Fig. III.7). On the contrary, the nonlinear solution does not follow a superposition principle. Indeed, the nonlinear response depends on the number and sequencing of applied pulses. Using the weakly nonlinear solution given above, the response of a single oscillator to the two pulses is approximately

$$y(t) = \frac{Im}{\omega_o} \left\{ [f_{1r}(\omega_o)\, e^{i(\omega_o + \Delta\omega_1)\tau} + f_{2r}(\omega_o)]\, e^{i(\omega_o + \Delta\omega_2)t} \right\} \qquad (15)$$

where (to first order)

$$\Delta\omega_1 = \frac{3}{8} \frac{\beta}{\omega_o} |f_{1r}|^2 \qquad (16)$$

and

$$\Delta\omega_2 = \frac{3}{8} \frac{\beta}{\omega_o} |f_{1r}\, e^{i\omega_o t} + f_{2r}|^2$$

$$= \frac{3}{8} \frac{\beta}{\omega_o} [f_{1r}^2 + f_{2r}^2 + 2f_{1r}f_{2r}\cos\, \omega_o\tau] \qquad (17)$$

In arriving at Eq. 15 the factor $\exp[i\Delta\omega_1\tau]$ is used in an approximate manner consistent with the assumption of short pulse width compared to separation. Combining Eqs. 15 and 17, a multiplicative factor appears within the curly brackets of Eq. 15 and has the form

$$\exp[i\, \frac{3}{4} \frac{\beta t}{\omega_o} f_{1r}\, f_{2r}\, \cos\, \omega_o\tau]$$

This factor is periodic in $(\omega_o\tau)$ and can be expanded in a Fourier

series (23)

$$e^{ix \cos \theta} = \sum_{n=-\infty}^{\infty} i^n J_n(x) e^{in\theta}$$

Resuming one of the series formed by inserting this result into Eq. 15 yields (24)

$$y(t) = \frac{Im}{\omega_o} \left\{ \sum_n i^n \left[i f_{1r}(\omega_o) J_{n+1}(zt) e^{i\Delta\omega_1 \tau} + f_{2r}(\omega_o) J_n(zt) \right] e^{i[\omega_o(t-n\tau) + \theta t]} \right\} \quad (18)$$

where

$$z = \frac{3}{4} \frac{\beta}{\omega_o} f_{1r} f_{2r} \quad (19)$$

and

$$\theta = \frac{3}{8} \frac{\beta}{\omega_o} [f_{1r}^2 + f_{2r}^2] \quad (20)$$

have been defined. The response of the whole system of oscillators is

$$Y(t) = Im \int d\omega_o \frac{n(\omega_o)}{\omega_o} \left\{ \sum_n i^n \left[i f_{1r} J_{n+1} e^{i\Delta\omega_1 \tau} + f_{2r} J_n \right] e^{i[\omega_o(t-n\tau) + \theta t]} \right\} \quad (21)$$

We now have a remarkable new feature in this solution which does not appear in the linear solution or in the nonlinear response to one pulse. There exist times $t = n\tau$ which are greater than $-\tau$ for which the integral of Eq. 21 does not phase mix to zero, since the

coefficient of ω_o in the exponential is zero at these times. Thus, we no longer have a monotonic decrease (phase mixing to zero) in the system response. In fact, it appears that $Y(t)$ will have relative maxima at the times $t = n\tau$, $n = 1,2,3,\cdots$. These relative maxima are the echoes we were seeking (see Fig. III.7). Note that if the applied pulses are rectangular in form, long times become all times after the trailing edge of the pulses. For such cases, the analysis of this section can be applied directly for all τ greater than the pulse widths.

We can now give a qualitative description of this two-pulse echo process and begin to establish the three basic characteristics of echo systems as given at the beginning of this section. The response due to the first pulse decays monotonically due to phase mixing. The second pulse effects a reversal of this phase mixing, causing a stimulated phase coherence, and a concomitant peak in response, to occur at times $t = n\tau$. This is possible, since the phase mixing process does not represent a loss in physical information; each individual oscillator continues to oscillate at constant amplitude. Of course, all real physical systems have dissipative effects (relaxation). Such relaxation processes cause a decay in the amplitude of the individual oscillators and thus represent a loss in information (energy). It is therefore clear that $n\tau$ must be less than a few relaxation times in order for the nth echo to be observable. The amplitude of the nth echo would be expected to decrease as $\exp[-n\tau/T]$, if T is the relaxation time.

Taking the imaginary part expressed in Eq. 21 gives

$$Y(t) = \int d\omega_o \frac{n(\omega_o)}{\omega_o} \left\{ \sum_{\substack{n \\ \text{even}}} (-1)^{n/2} \left[f_{1r} J_{n+1} \cos[\omega(t-n\tau) + \theta t + \Delta\omega_1 \tau] + f_{2r} J_n \sin[\omega(t-n\tau) + \theta t] \right] \right.$$

$$\left. + \sum_{\substack{n \\ \text{odd}}} (-1)^{\frac{n-1}{2}} \left[-f_{1r} J_{n+1} \sin[\omega(t-n\tau) + \theta t + \Delta\omega_1 \tau] + f_{2r} J_n \cos[\omega(t-n\tau) + \theta t] \right] \right\} \qquad (22)$$

Equation 22 is rather complicated, in general. To simplify the matter, consider the limit of very weak excitation (f_1, f_2 and t such that $zt, \theta t << 1$). Using the small argument approximation for the Bessel functions in Eq. 21 results in

$$Y(t) \simeq \sum_n \text{Im} \int d\omega_o \frac{n(\omega_o)}{\omega_o} \left\{ f_{2r} \left[\frac{3}{8} \frac{\beta}{\omega_o} f_{1r} f_{2r} t \right]^n e^{i[\omega_o(t-n\tau) + \theta t]} \right\} \qquad (23)$$

Furthermore, let τ be large compared to the characteristic time for phase mixing. Then, near $t = n\tau$, only the nth term in Eq. 23 need be kept (all terms are phase mixed to zero except the nth term for which $\omega(t-n\tau) \simeq 0$.) Thus the nth echo will be given approximately by

$$Y_n(t) \simeq \text{Im} \int d\omega_o \frac{n(\omega_o)}{\omega_o} f_{1r}^n(\omega_o) f_{2r}^{n+1}(\omega_o) \left[i \frac{3}{8} \frac{\beta t}{\omega_o} \right]^n e^{i[\omega_o(t-n\tau) + \theta t]} \qquad (24)$$

Given the above approximations, what properties of $n(\omega_o)$, $F_1(t)$, and $F_2(t)$ are required to yield an echo? Roughly, for the nth echo to be a pulse in time and distinguishable from the tail of the response to the excitation pulses, the product $nf_{1r}^{n} f_{2r}^{n+1}$ must have a finite half-width in the frequency (ω_o) domain. Since the three functions n, f_{1r}, f_{2r} appear in a product, this can be accomplished by making any <u>one</u> of the three restricted in bandwidth. The physical situation is often one such that the distribution of oscillators $n(\omega_o)$ is effectively restricted to a narrow band (for example, electrons in a slightly inhomogeneous magnetic field). In these cases, the excitation pulses can be very narrow in time (approximated by delta functions) and the echo shape is related to the Fourier transform of the distribution of oscillators

$$\text{Echo Shape} \sim \int d\omega_o \, e^{i\omega_o t} \, n(\omega_o) \qquad (25)$$

If $n(\omega_o)$ is very broad (such that the reciprocal half-width is greater than τ), F_1 and F_2 must be such that $f_{1r}^{n} \cdot f_{2r}^{n+1}$ is narrow. Although in principle one can overcome this difficulty by increasing τ, in practice, one is limited by the relaxation time of the oscillators (present in all physical systems) since relaxation destroys the information available at the time of the application of the second pulse which is necessary for the generation of echoes. Thus, in the case of broad $n(\omega_o)$ the echo shape is of the form

$$\text{Echo Shape} \sim \int d\omega_o \, e^{i\omega_o t} \, f_{1r}^{n}(\omega_o) \, f_{2r}^{n+1}(\omega_o) \, ,$$

given primarily by the shape of the exciting pulses. It is now clear that although the formation of echoes requires $n(\omega_o)$ to be nondegenerate, it need not be particularly narrow band. There is one more point of interest concerning Eq. 24. If the excitation pulses $F_1(t)$ and $F_2(t)$ have peak amplitudes A_1 and A_2, the nth echo has an amplitude

$$\text{Echo Amplitude} \sim A_1^n A_2^{n+1} \tau^n \tag{26}$$

Therefore, the first echo is a third order process, the second echo a fifth order process, etc. Furthermore, the echo amplitude goes to zero as τ goes to zero (the two pulses become one). This fact demonstrates that a finite pulse separation is necessary for the observation of an echo. Of course, the derived solution is valid only for sufficiently large τ. When τ is sufficiently small, nonlinear effects occurring during the application of the pulses become important. In any case, when the response to a single pulse is of finite time duration, the entire echo process becomes obscured at very small τ. This small τ domain is not of particular interest. The strength of the nonlinear effect, and therefore the echo, grows with increasing τ. Of course there are limits on this growth which we will now discuss.

We now return to the general formulas, Eqs. 21 and 22, and consider another limiting case. Suppose $n(\omega_o)$ is restricted to a narrow range of frequencies (narrow when compared with the spectra of the exciting pulses) and centered at a high frequency ω_o' ($1/\omega_o' \ll \tau$ and $(\Delta\omega_o)_{1/2} \ll \omega_o'$). Then we can rewrite Eq. 21 in the form

$$Y(t) = \mathrm{Im}\left\{ \sum_n \frac{i^n}{\omega_o'} \left[f_{1r}' J_{n+1}(z't)\, e^{i\Delta\omega_1'\tau} + f_{2r} J_n(z't) \right] e^{i\theta' t} \right.$$

$$\left. \times \int d\omega_o n(\omega_o)\, e^{i\omega_o(t-n\tau)} \right\} \qquad (27)$$

where the prime denotes that the variable is to be evaluated at ω_o'. Equation 27 has the general form

$$Y(t) = \mathrm{Im} \sum_n A_n(t)\, g(t - n\tau) \qquad (28)$$

Since z', $\Delta\omega_1'$, $\theta' \ll \omega_o'$, $A(t)$ is slowly varying compared to $g(t)$. Again, presuming ω_o' to be large compared to the reciprocal width of $n(\omega_o)$, Eq. 28 represents a series of pulses (echoes) at times $t = n\tau$ all with the same shape related to the Fourier transform of the oscillator distribution $g(t)$ (see Eq. 25) and with an amplitude related to $A_n(\tau)$ (24)

$$A_n(\tau) = \frac{i^n}{\omega_o'} \left[i f_{1r}' J_{n+1}(z'\tau)\, e^{i\Delta\omega_1'\tau} + f_{2r}' J_n(z'\tau) \right] e^{i\theta'\tau} \qquad (29)$$

It is important to notice that whatever the relation between $A_n(\tau)$ and the echo amplitude, the echo strength does not increase monotonically with excitation f and pulse separation τ as it did in the weak excitation limit. In fact, as $f,\tau \to \infty$, $A_n(\tau) \sim (1/\sqrt{\tau})$. Thus above a certain level, increasing the pulse separation decreases the echo strength. Furthermore, in changing both the excitation level and τ one expects modulating oscillations in the echo strength due to the oscillations in the Bessel functions. As $f,\tau \to \infty$, we have

$$A_n(\tau) \rightarrow \sqrt{\frac{2}{\pi z'\tau}}\,\frac{i^n}{\omega_o'}\left[-f_{1r}\,e^{i\Delta\omega_1\tau}\sin(z'\tau - \frac{n\pi}{2} - \frac{\pi}{4})\right.$$

$$\left. + f_{1r}\cos(z'\tau - \frac{n\pi}{2} - \frac{\pi}{4})\right]$$

The appropriate relation between the echo amplitude and $A_n(\tau)$ will depend on the physics of the system actually being considered and the nature of the detected signal. This relation is complicated by the fact that one must take the imaginary part in Eq. 28. Doing this yields a result of the form

$$Y_n(t) = \mathcal{A}_n(t)\int d\omega_o\, n(\omega_o)\sin\omega_o(t - n\tau) + \mathcal{B}_n(t)\int d\omega_o\, n(\omega_o)\cos\omega_o(t - n\tau) \qquad (30)$$

Since ω_o' is large, both terms in Eq. 30 are oscillating rapidly with relative maxima in amplitude near $t = n\tau$. Thus, both $\mathcal{A}_n$ and $\mathcal{B}_n$ contribute to the envelope of the echo and therefore to the echo amplitude, even though the coefficient of $\mathcal{A}_n(t)$ is zero at $t = n\tau$. Suppose in our experiment we detect the DC part of $|Y|^2$, then a reasonable estimate of the echo amplitude (peak of the echo envelope) is $(\mathcal{A}_n^2 + \mathcal{B}_n^2)$. This result is exact for $n(\omega_o)$ that are symmetric about ω_o'. The echo amplitude thus defined is

$$\text{Echo Amplitude} = \mathcal{A}_n^2 + \mathcal{B}_n^2 = \frac{1}{\omega_o^2}\left[f_{1r}^2 J_{n+1}^2(zn\tau) + f_{2r}^2 J_n^2(zn\tau) - 2f_{1r}f_{2r}J_n(zn\tau)J_{n+1}(zn\tau)\sin(\Delta\omega_1\tau)\right] \qquad (31)$$

As τ increases from zero, the echo amplitude at first increases very rapidly, but then begins to saturate and eventually goes to zero as $\tau \to \infty$. Figure III.8 shows the amplitude of the first echo ($n = 1$) as given by Eq. 31 for the case $f_{1r} = f_{2r}$, so that $\Delta\omega_1 = (z/2)$ and Eq. 31 can be written

$$\text{Relative Echo Amplitude} = z[J_2^2(z\tau) + J_1^2(z\tau) - 2J_2(z\tau)\, J_1(z\tau)\sin(\tfrac{z\tau}{2})] \tag{32}$$

Equation 31 is very similar to a result derived in the independent particle theories of cyclotron echoes (4,5). It would be indentical to the previous result if we had neglected the nonlinear response to the first pulse as was done in the previous calculations (4,5). In this case $\Delta\omega_1\tau = z\tau/2 \to 0$ and Eq. 32 becomes:

$$\text{Relative Echo Amplitude} = z[J_2^2(z\tau) + J_1^2(z\tau)] \ ,$$

the independent particle theories' result. Clearly, this approximation discards a term of the same order as those kept unless $(z\tau) \lesssim 1$. Therefore, we keep the terms involving $(\Delta\omega_1\tau)$ with the knowledge that a better approximation is achieved. This will prove particularly important in the studies of the large signal properties of the cold plasma echoes discussed in the next section.

In summary, it has been shown that a collection of nondegenerate harmonic oscillators with weakly nonlinear restoring forces subject to two excitation pulses has the following response. After the first pulse at $t = -\tau$, the macroscopic signal decays monotonically, due to

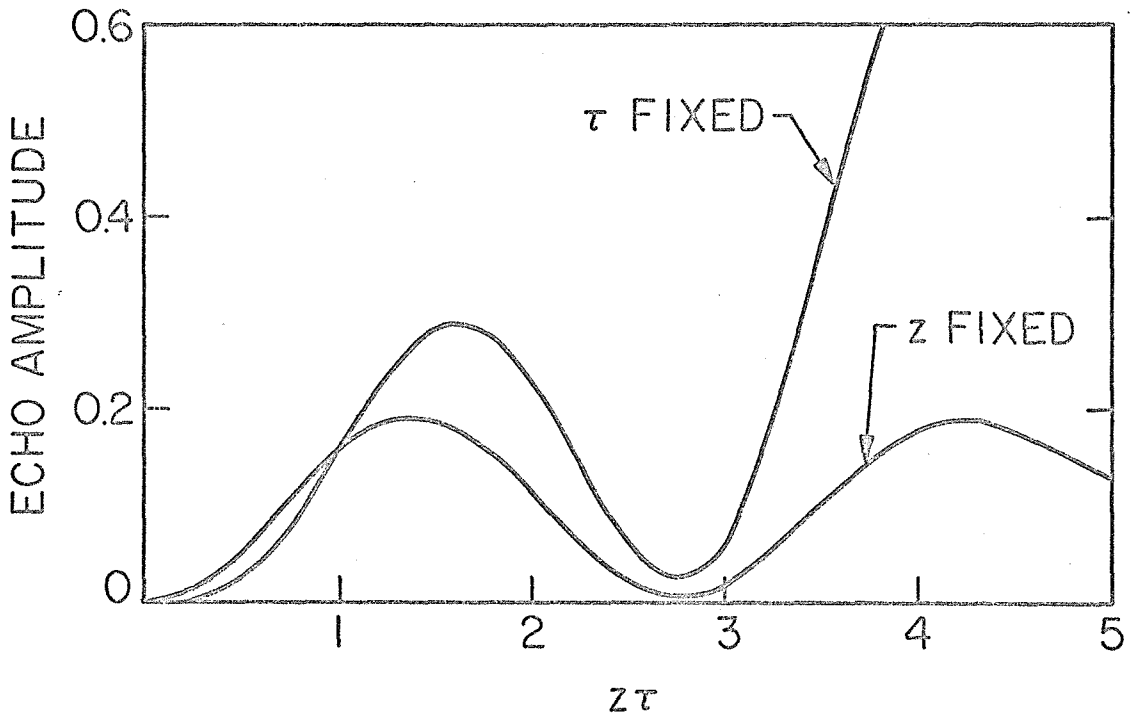

Fig. III.8 Relative echo amplitude vs. power (τ fixed) and vs. τ (z fixed), for the case of narrow oscillator spectrum or wide excitation pulse spectrum (see Eq. 32).

phase mixing. The rate of this decay is determined by the narrower of $n(\omega_o)$ and $f_{lr}(\omega_o)$. Following the second pulse at $t = 0$ the signal begins to decay, but exhibits a new non-monotonic behavior, i.e. relative maxima which we call echoes, occurring at $t = n\tau$, $n=1,2,\cdots$. In this manner, the second pulse has stimulated a reversal of the phase mixing processes effecting a relative coherence of the oscillators at the times $t = n\tau$. The theory developed applies to the case of arbitrary width of the two excitation pulses, demonstrating that echoes can be achieved even in systems with very wide (in principle, even infinite) oscillator distributions, simply by using excitation pulses of a narrow frequency width. The discussion in this section shows explicitly the role and importance of the three properties of classical multiple-pulse echo systems which were outlined previously: (a) collection of non-degenerate oscillators (supplies phase mixing); (b) nonlinear effects (enables second pulse to reverse the phase mixing, stimulating a relative coherence); and (c) small dissipation (keeps echo from being destroyed by loss of information.)

III.C. Theory of Echoes from a Cold Nonuniform Plasma

Immediately following the initial discovery of echoes in magnetoplasmas (1) numerous theoretical papers appeared (2,4,5,6) generally treating the plasma as a collection of independent particles. Collective plasma oscillation effects were ignored. The approximation of neglecting collective phenomena is expected to be valid only if the plasma density is low enough (3). However, it is clear from the data of Section III.A that the echoes we observe are intimately related to the upper hybrid collective modes of the plasma. The possibility of the existence of plasma echoes due to upper hybrid resonance effects was first suggested by Herrmann and Whitmer (6) although numerous other references to this idea can be found in the early cyclotron echo literature (2). Wong and Judd (25) attempted to explain their observations of echoes in a cesium plasma by means of a phenomenological collective model which includes radiation damping effects. Furthermore, Gould and Blum (9) have analyzed a physical model consisting of a cold nonuniform plasma which exhibits collective effects (upper hybrid oscillations) and is capable of producing echoes. In this section we will discuss this plasma model in detail and extend the analysis to conditions appropriate to the experimental ones given in Section III.A.

Some properties of a cold nonuniform plasma in a magnetic field have already been discussed in connection with the CW data of Section II. Although the theory of the cold plasma failed to predict consistently the peaks near cyclotron resonance, it does yield effects corresponding to upper hybrid resonance. One therefore might expect

this model to help develop an understanding of the upper hybrid echo which is observed experimentally. In fact, this model has been shown (9) to have the basic qualitative features, which were discussed in Section III.B, requisite of a two-pulse echo system: the collection of normal modes is the continuum of local upper hybrid oscillations and the nonlinearity is furnished by the spatial gradients in density. Considering its limitations, the theory will prove surprisingly successful in predicting qualitatively some important properties of this echo.

From Section III.B we know that in order to achieve echoes from a plasma, a nonlinear theory must be formulated. The linear theory of uniform, cold plasmas using the Eulerian equations of motion is the subject of standard texts on plasma waves. Using the Lagrangian description of the cold plasma, Dawson (26) has derived and discussed the appropriate nonlinear equations for longitudinal plasma oscillations in an infinite plasma without a magnetic field. For a uniform plasma he derived an exact equation which, in principle, is applicable in any number of spatial dimensions. Since our physical system must have a nondegenerate ensemble of normal modes in order to exhibit echoes, we must fix our attention on the nonuniform plasma. This is clear from a consideration of the normal modes in the linear approximation. In the linear, electrostatic approximation a uniform cold plasma supports oscillation only at one frequency, while a nonuniform cold plasma supports oscillation over a continuous band of frequencies. Barston (27) has considered such matters in detail, showing that a finite cold plasma with a continuous density profile resonates with applied fields for all

frequencies ω such that $\omega = \omega_p(x)$ (without a magnetic field). Upon adding an external magnetic field the resonance condition becomes $\omega^2 = \omega_p^2(x) + \omega_c^2$. Thus, an inhomogeneous cold plasma appears at the onset to have properties like those of the general echo system discussed in Section III.B.

The remainder of this section will treat just such a plasma, demonstrating the existence of echo processes and comparing the results in some detail with experimental observations. Maintaining simplicity, our attention will be restricted to one dimension. However, Appendix B derives Dawson's general uniform plasma equation of motion (good in any number of dimensions) for the case of an inhomogeneous plasma, emphasizing that the general ideas are valid in any number of dimensions.

III.C.1. General Formulation

We consider a one-dimensional inhomogeneous cold plasma slab of thickness $2a$ situated in a uniform magnetic field $\underline{B}$ which is parallel to the slab faces (see Fig. III.9) and constant in time (28). The steady state electron density is assumed to depend on x in a manner such that $\omega_p^2(x) = \omega_{po}^2 H(x)$, where $H(0) = 1$ and H falls monotonically to some value (≥ 0) at $|x| = a$, as shown in Fig. III.9. In addition, collisions are neglected and the steady state plasma is taken to be charge neutralized by a background of fixed positive ions.

Adopting the Lagrangian point of view, we consider the displacement δx of an electron fluid element (a macroscopic charge sheet)

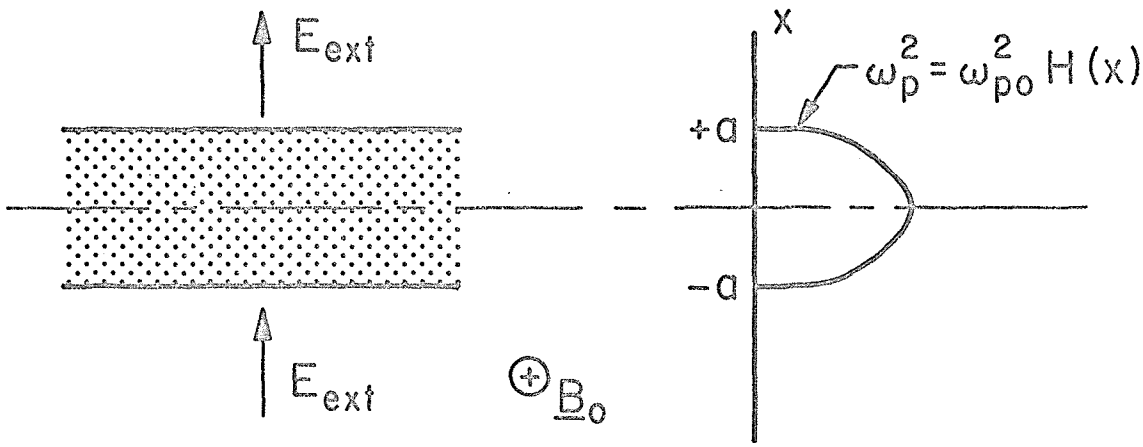

Fig. III.9. The plasma slab model

from its equilibrium position x_o (29)

$$x = x_o + \delta x \tag{33}$$

Conservation of charge requires

$$n_e(x)\, dx = n_i(x_o) dx_o \tag{34}$$

where n_e is the electron density and n_i is the ion density. If the transformation given by Eq. 33 is single-valued (one-to-one mapping) then $dx_o = (\partial x/\partial x_o)dx$ and

$$n_e(x) = n_i(x_o) \frac{\partial x_o}{\partial x} \tag{35}$$

In the longitudinal approximation we keep only the Poisson equation of Maxwell's equations. Then the equation of motion of one fluid element is given by

$$\frac{d^2(\delta x)}{dt^2} + \omega_c^2\ \delta x = -\frac{e}{m} E \tag{36}$$

where

$$\frac{\partial E}{\partial x} = \frac{e}{\varepsilon_o}[n_i(x) - n_e(x)] \tag{37}$$

Integrating Eq. 37 gives

$$E(x) = E_{ext} + \frac{e}{\varepsilon_o}\int_{x_o}^{x} n_i(y)\ dy \tag{38}$$

where E_{ext} is the externally applied field which is taken to be one or a series of pulses. The equation of motion (Eq. 36) becomes

$$\frac{d^2(\delta x)}{dt^2} + \omega_c^2\ \delta x + \int_{x_o}^{x_o+\delta x} \omega_p^2(y)\ dy = -\frac{e}{m} E_{ext} \tag{39}$$

For δx small, the integrand ω_p^2 of the integral in Eq. 39 can be expanded in a Taylor series about the point x_o

$$\omega_p^2(x) = \omega_p^2(x_o) + \omega_p^{2'}(x_o)[x-x_o] + \frac{\omega_p^{2''}}{2}[x-x_o]^2+\cdots$$

where a prime denotes a derivative with respect to x_o. The integral can now be easily carried out, giving

$$\frac{d^2(\delta x)}{dt^2} + \omega_h^2(x_o)\ \delta x\left[1+\frac{1}{2}\frac{\omega_n^{2'}(x_o)}{\omega_h^2(x_o)}\ \delta x+\frac{1}{6}\frac{\omega_h^{2''}(x_o)}{\omega_h^2(x_o)}\ (\delta x)^2+\cdots\right]$$

$$= -\frac{e}{m} E_{ext} \tag{40}$$

where $\omega_h^2 = \omega_p^2 + \omega_c^2$ is the upper hybrid frequency. Given E_{ext} we must now solve Eq. 40 for the motion of each fluid element. The value of any macroscopic variable at any particular time is then given by the superposition (the field equations are linear) of the corresponding microscopic variables of the individual elements of the plasma. Experimentally, a convenient quantity to measure is the voltage across the slab. From Eq. 37 the voltage response of the plasma to E_{ext} is given by

$$V = \frac{e}{\varepsilon_o} \int_{-a}^{a} dx_o \int_{x_o}^{x} dy\ n_i(y) \tag{41}$$

Expanding $n_i(y)$ in a Taylor series about $y = x_o$ and performing the first integral term by term, we obtain

$$V(t) = \frac{e}{\varepsilon_o} \int_{-a}^{a} dx_o \left[n_i(x_o)\delta x + n_i'(x_o) \frac{(\delta x)^2}{2} + n_i''(x_o) \frac{(\delta x)^3}{6} + \cdots \right] \tag{42}$$

Since we are primarily concerned with small perturbations, we keep only the leading term in Eq. 41. We have

$$V(t) = \frac{e}{\varepsilon_o} \int_{-a}^{a} dx_o\ n_i(x_o)\ \delta x(x_o,t) \tag{43}$$

where $\delta x(x_o,t)$ is the solution of Eq. 40. Thus, given E_{ext}, we can solve Eq. 40 and use the solution in Eq. 43 to compute the voltage response of the slab.

Equations 40 and 43 are the main results of the above discussion. It is particularly significant that these equations are of exactly the same form as Eqs. 1 and 13 which are the basic equations of Section III.B. Our immediate conclusion is that the voltage response of the inhomogeneous cold plasma to applied pulses in the voltage $V_{ext} = 2a\, E_{ext}$ can exhibit echo phenomena and has all the fundamental attributes of the general echo system discussed in the previous section. In this case an oscillator is a fluid element with a natural frequency equal to the upper hybrid frequency at the equilibrium location of that element $\omega_h(x_o)$. The oscillators are nondegenerate since ω_p^2 is a function of x . The oscillator density is related to the equilibrium particle density. The equation of motion of the oscillators is nonlinear since the spatial gradients of ω_p are nonzero. The calculation of the properties of these echoes as they vary with the magnetic field and the plasma density serves as the primary goal of the remainder of this section.

Unfortunately, there is a limitation on the conditions under which Eq. 40 is valid. The source of the limitation is a breakdown in the single-valued nature of the transformation given in Eq. 33. Rewriting Eq. 34 demonstrates the physical nature of the problem:

$$n_e(x) = \frac{n_i(x_o)}{1 + \frac{\partial(\delta x)}{\partial x_o}} \tag{44}$$

For any values of x_o and t such that

$$\frac{\partial}{\partial x_o}(\delta x) \rightarrow -1 \tag{45}$$

$n_e(x)$ increases without bound and the whole solution procedure is incorrect. Avoiding the condition of Eq. 45 is equivalent to requiring that the initial ordering (before the applied pulses) of the fluid elements with respect to x_o is maintained (26). Thus Eq. 41 is correct only under conditions such that

$$\frac{\partial}{\partial x_o}(\delta x) > -1 \tag{46}$$

Because violation of this condition (Eq. 46) implies that fluid elements begin to pass one another, it is sometimes called the "cross-over condition". As Dawson (26) points out, as violation of the cross-over condition is approached, electron thermal and viscous effects, which exist in a real plasma and have been ignored, will become important. We will return to this point later.

Let us now compute the voltage echoes which result from the application of two identical voltage pulses $V(t) = -(2ea/m)\, E_o F(t)$ at $t = -\tau$ and $t = 0$, where $F(t)$ is Gaussian in shape, $F(t) = \exp[-t^2/2(\Delta t)^2]$. The Fourier transform of $(e/2ma)\, V(t)$ is

$$f(\omega) = \frac{eV_o}{2ma}\frac{\Delta t}{\sqrt{2}} e^{-\frac{(\omega\Delta t)^2}{8}} \equiv \frac{V_o \Delta t e}{2\sqrt{2}\, ma}\, g(\omega) \tag{47}$$

Thus the long time total voltage response to these two pulses is given by (see Eqs. 15-17)

$$V(t) = \frac{m}{e}\int_{-a}^{a} \frac{\omega_p^2}{\omega_h} \operatorname{Im}\left\{ f(\omega_n)\, [e^{i(\omega_h+\Delta\omega_1)\tau} + 1]\, e^{i(\omega_h+\Delta\omega_2)t} \right\} dx_o \tag{48}$$

where ω_h is the local upper hybrid frequency at x_o and

$$\Delta\omega_1 = \frac{z}{2}$$

$$\Delta\omega_2 = z[1 + \cos\ \omega\tau]$$

with z given by the nonlinear terms of Eq. 40. By comparing with the results of Section III.B, we establish the following relation

$$z = [\frac{3}{4}\beta - \frac{5}{6}\alpha^2]\ \frac{f^2(\omega_h)}{\omega_h}$$

$$= [\omega_h^{2''} - \frac{20}{3}(\omega_h')^2]\ \frac{f^2(\omega_h)}{8\omega_h^3} \qquad (50)$$

which is correct to second order. Rewriting Eq. 48 separates the various echo contributions

$$V(t) = \frac{m}{e}\sum_{n=-\infty}^{\infty}\int_{-a}^{a}\frac{\omega_p^2}{\omega_h}\ \mathrm{Im}\left\{i^n\ f\left[J_{n+1}(zt)e^{\frac{iz\tau}{2}} + J_n(zt)\right]e^{i[\omega_h(t-n\tau)+\ zt]}\right\}dx_o \qquad (51)$$

We recall from the arguments in the previous section that $V(t)$ phase mixes to zero except at times $t = n\tau$. At these times relative maxima in $V(t)$ occur; these maxima are the echoes we are seeking. Assuming τ to be large compared to the characteristic time for phase mixing, near $t = n\tau$ only the nth term in the series of Eq. 51 is necessary to characterize the nth echo. Such conditions are prevalent in the experiments and will be assumed in the analysis. Also, most experimental measurements are restricted to the first echo, whose theoretical voltage is

$$V_1(t) = \frac{m}{e} \int_{-a}^{a} \frac{\omega_p^2}{\omega_h} \operatorname{Im} \left\{ i\, f[J_2(zt)\, e^{\frac{iz\tau}{2}} + J_1(zt)]\, e^{i[\omega_h(t-\tau) + zt]} \right\} dx_o \quad (52)$$

Of primary concern will be the echo strength as external parameters are varied. Since theoretically and experimentally the echo voltage is essentially an amplitude-modulated high frequency signal, we will define the theoretical echo amplitude (strength) to be the square of the peak voltage of the real time envelope of the echo signal. This definition is appropriate since the ideal experimental detector is a square-law rectifier.

Taking the imaginary part in Eq. 52 gives an equation of the form

$$V_1(t) = \int_{-a}^{a} dx_o\, \mathcal{A}_1(x_o,t) \sin \omega_h(t-n\tau) + \int_{-a}^{a} dx_o\, \mathcal{B}_1(x_o,t) \cos \omega_h(t-n\tau) \quad (53)$$

where

$$\mathcal{A}_1(x_o,t) = -\frac{m}{e} \frac{\omega_p^2}{\omega_h} f(\omega_h) \left[J_1(zt) \sin(zt) + J_2(zt) \cos\left(\frac{3}{2} zt\right)\right]$$

and (54)

$$\mathcal{B}_1(x_o,t) = -\frac{m}{e} \frac{\omega_p^2}{\omega_h} f(\omega_h) \left[J_1(zt) \cos(zt) - J_2(zt) \sin\left(\frac{3}{2} zt\right)\right] .$$

If $\mathcal{A}_1$ and $\mathcal{B}_1$ are symmetrical functions in the frequency domain centered at some high frequency ω_o', the echo amplitude E as defined above is

$$E_1 = A_1^2 + B_1^2 \quad (55)$$

where

$$A_1 = \int_{-a}^{a} dx_o \, \mathcal{A}_1(x_o,t)$$

and

$$B_1 = \int_{-a}^{a} dx_o \, \mathcal{B}_1(x_o t)$$

In general, $\mathcal{A}_1$ and $\mathcal{B}_1$ will not be exactly symmetrical, although they will be localized at a high frequency. The frequency domain asymmetry implies that the peak in the echo voltage envelope will not occur exactly at $t = n\tau$. Such effects are observed experimentally, but play a minor role relative to other echo characteristics. Furthermore, many of the experimental measurements were actually taken by sampling the strength of the response at a fixed time near $t = n\tau$. Therefore, we will confine our attention to studies of the echo amplitude and take the relations given in Eqs. 55 as reasonable estimates of the echo strength.

Before proceeding to calculate E_1, let us return to the troublesome matter of cross-over. The cross-over condition given in Eq. 46 places a limit on the validity of the solution for $V_1(t)$ given by Eqs. 53 and 54. Since $\delta x(x_o,t)$ has terms of the form $\cos[\omega_h(x_o)(t-\tau)]$ and $\sin[\omega_h(x_o)(t-\tau)]$, we need only the amplitude of such corresponding terms in an expression for $\partial(\delta x)/\partial x_o$. Furthermore, the localization of $\mathcal{A}_1$ and $\mathcal{B}_1$ in the frequency domain yields the inequality $zt \ll \omega_h t$. The cross-over condition becomes

$$\left|(\delta x)_{max} \frac{d\omega_h}{dx_o} t\right| < 1 \qquad (56)$$

where $(\delta x)_{max} = (f(\omega_h)/\omega_h)$.

In arriving at Eq. 56 only the leading term has been retained. This condition limits the maximum amplitude and/or the time for which the above solution is correct. For the assumed density profiles $d\omega_h/dx_o \to 0$ as $x_o \to 0$. Thus, the closer the equilibrium position of the fluid element is to the origin, the more easily the cross-over condition is obeyed. However, near $x_o = a$ a low excitation level and/or short times are required. Equation 56 can be rewritten in the following form:

$$\left| \frac{(zt)\ \omega_h}{[\frac{1}{8}(\omega_h^2)'' - \frac{5}{6}(\omega_h')^2]} \frac{\omega_h'}{\delta x_{max}} \right| < 1 \qquad (57)$$

For the assumed density profiles $\omega_h' < \omega_h''$, so that Eq. 57 reduces to

$$\left| \frac{4(zt)}{\delta x_{max}} \frac{(\omega_h^2)'}{(\omega_h^2)''} \right| < 1 \qquad (58)$$

For a given density profile, Eq. 58 places an upper limit on (zt) beyond which the derived solution is inapplicable. Near $x_o = a$, $[(\omega_h^2)'/(\omega_h^2)'']$ is of the order a. Thus for equilibrium positions near the plasma boundaries, one must require $(zt) \ll 1$, since the inequality $(\delta x)_{max} \ll a$ certainly must be maintained. Furthermore, for a general density profile of the form considered, $(\omega_h^2)' \to 0$ as $x_o \to 0$ faster than $(\omega_h^2)''$. Therefore, preventing cross-over does not limit the value of (zt) for $x_o = 0$, but requires $(zt) \ll 1$ for $x_o = a$. Since the echo amplitude E_1 is basically a function of $(z\tau)$, the cross-over condition limits the validity of the formula for E_1. We will return to this point below. However, in general, we will ignore the cross-over

problem.

Of course, there is another restriction on the above analysis which is imposed by the use of a perturbation technique. The nonlinear terms of Eq. 41 must remain small at all times.

$$\alpha(\delta x)_{max}, \quad \beta(\delta x)^2_{max} \ll 1 \tag{59}$$

III.C.2 Low Density Case: Cyclotron Echoes

The low density case represents one simplifying limit of the above analysis. Letting $\omega_p \to 0$, we define low density to be the density such that $\omega_{po} \ll \omega_c$ and the spread in upper hybrid frequencies $(\omega^2_{po}/2\omega_c)$ is small compared to the spectral width of the excitation pulses $(\Delta\omega)_{1/2} = 4/(\Delta t)_{1/2}$. Under these conditions all significant effects (scattering, echoes, etc) occur in the immediate vicinity of cyclotron resonance and the excitation pulses can be approximated by delta functions. Thus the conditions become very much like those of cyclotron echo studies. For this reason we call the echoes of this section "cyclotron echoes". However, the source of the oscillator nondegeneracy is completely different. In the cyclotron echo theories the oscillators were electrons in a nonuniform magnetic field, while we consider here nondegenerate upper hybrid oscillations in a uniform magnetic field.

The conditions prescribed above are equivalent to the approximation of a narrow distribution of oscillators applied at the end of

Section III.B. Also, if we take H to be parabolic in x so that $H(x) = 1 - x^2/a^2$ the leading term in Eq. 50 is independent of x. We ignore the problem of cross-over. (This matter will be given more attention below). With these approximations the analysis presented at the end of Section III.B is appropriate and the response is of the form

$$V_1(t) = \mathrm{Im}\left[A_1(t) \int_{-a}^{a} dx_o\, \omega_p^2\, e^{i\omega_h(t-\tau)}\right] \tag{60}$$

where

$$A_1(t) = \frac{m}{\omega_c e}\, i\left[J_2(zt)\, e^{\frac{iz\tau}{2}} + J_1(zt)\right]$$

is the echo amplitude factor which is slowly varying compared to the second factor in Eq. 60. A square law detector would measure $|A_1(\tau)|^2$ for the relative echo amplitude. This quantity was plotted as a function of input power and pulse separation in Fig. III.8. The second factor in Eq. 60 basically determines the echo shape:

$$\text{Echo Shape} \sim \int_{\omega_c}^{\omega_{ho}} d\omega_h \frac{\omega_h(\omega_h^2 - \omega_c^2)}{\sqrt{\omega_h^2 - \omega_{ho}^2}}\, e^{i\omega_h(t-\tau)} \tag{61}$$

From Eq. 61 we see that the echo real time width goes inversely as the plasma density. That is, as ω_p increases the spread in upper hybrid frequencies increases and its Fourier transform width decreases. Such effects are observed experimentally, although they are complicated by the second peak in the echo spectra found at cyclotron resonance.

III.C.3 High Density Case: Upper Hybrid Echoes

As the electron density increases, the spread in upper hybrid frequencies becomes larger than the spectral width of the excitation pulses. These conditions approach those of the experimental data presented in Section III.A and thus present one case we would like to analyze. First, the limit of very weak excitation pulses will be considered in order to illuminate some of the essential features of the theory. Then, arbitrary excitation level will be considered and the calculated results will be compared with the experimental data.

III.C.3a Weak echoes. Consider the results given in Eqs. 53, 54, 55 in the limit of very small excitation amplitude, $z\tau << 1$. We can then use the small argument expansion of the Bessel functions so that the relative peak voltage of the first echo is given by

$$V_1(\tau) \propto \int_{-a}^{a} dx_o \underbrace{\omega_p^2}_{N(\omega)} \underbrace{\left\{ \frac{\omega_h^{2''}}{\omega_h^2} - \frac{20}{3} \frac{(\omega_h')^2}{\omega_h^2} \right\} \frac{|f(\omega_h)|^3}{\omega_h^2} \tau}_{(\Delta\omega\tau)\left(\frac{|f|}{\omega_h}\right)} \qquad (62)$$

Again, we define the echo amplitude to be $E = V_1^2$. Thus we see that E grows as τ^2 and the cube of the input power. Also, the notation below Eq. 62 separates the various factors clearly. The density of oscillators $N(\omega)$ is basically ω_p^2 as was pointed out above. The second factor is the nonlinearity strength $(\Delta\omega\tau)$ times the Fourier transform of one of the excitation pulses $\frac{|f|}{\omega_h}$. As $\Delta\omega \to 0$, the echo amplitude goes to zero as it should, since a nonlinear response is

required. The importance of the spatial gradients in ω_p is now apparent. If they were zero, no echo could occur. The integral of the product $\omega_p^2|f|^3$ tends to be peaked at $\omega = \omega_{ho}$. This implies that the main contribution to the echo will come from those regions of the plasma near $x = 0$. This fact supports our neglect of the cross-over phenomena. However, for all functional forms of $H(x)$ fitting the description given above and falling off more rapidly than x^2, the term in curly brackets is zero at $x = 0$ and grows as x increases. This term will make the resulting echo amplitude peak at some value of ω slightly less than ω_{ho} and implies that the main contribution to the echo will come from those parts of the plasma with x slightly greater than zero. This feature of the echo process will prove to be a very important one, for the effect of the curly bracketed terms can be changed by increasing power, electron density, and/or pulse separation to a point such that the small argument expansion of the Bessel functions is no longer valid. Plotting V_1^2 as a function of (ω_c/ω) with electron density as a parameter will yield the theoretical equivalent of the echo spectra curves given earlier. Figure III.10 shows such curves as computed using Eq. 62 with $H(x) = 1 - x^2/a^2$ and $(\Delta\omega/\omega) = 0.04$. The resemblance to the experimental data is striking; at each density, the echo is strongest near the maximum upper hybrid frequency of the plasma. Note that the shape of curves are independent of power and pulse separation, since these factors appear only as a multiplier in Equation 62. However, as power and τ increase we must use the full expressions given in Equations 53, 54, 55 for the echo amplitude and we expect to see saturation effects as the arguments of the Bessel

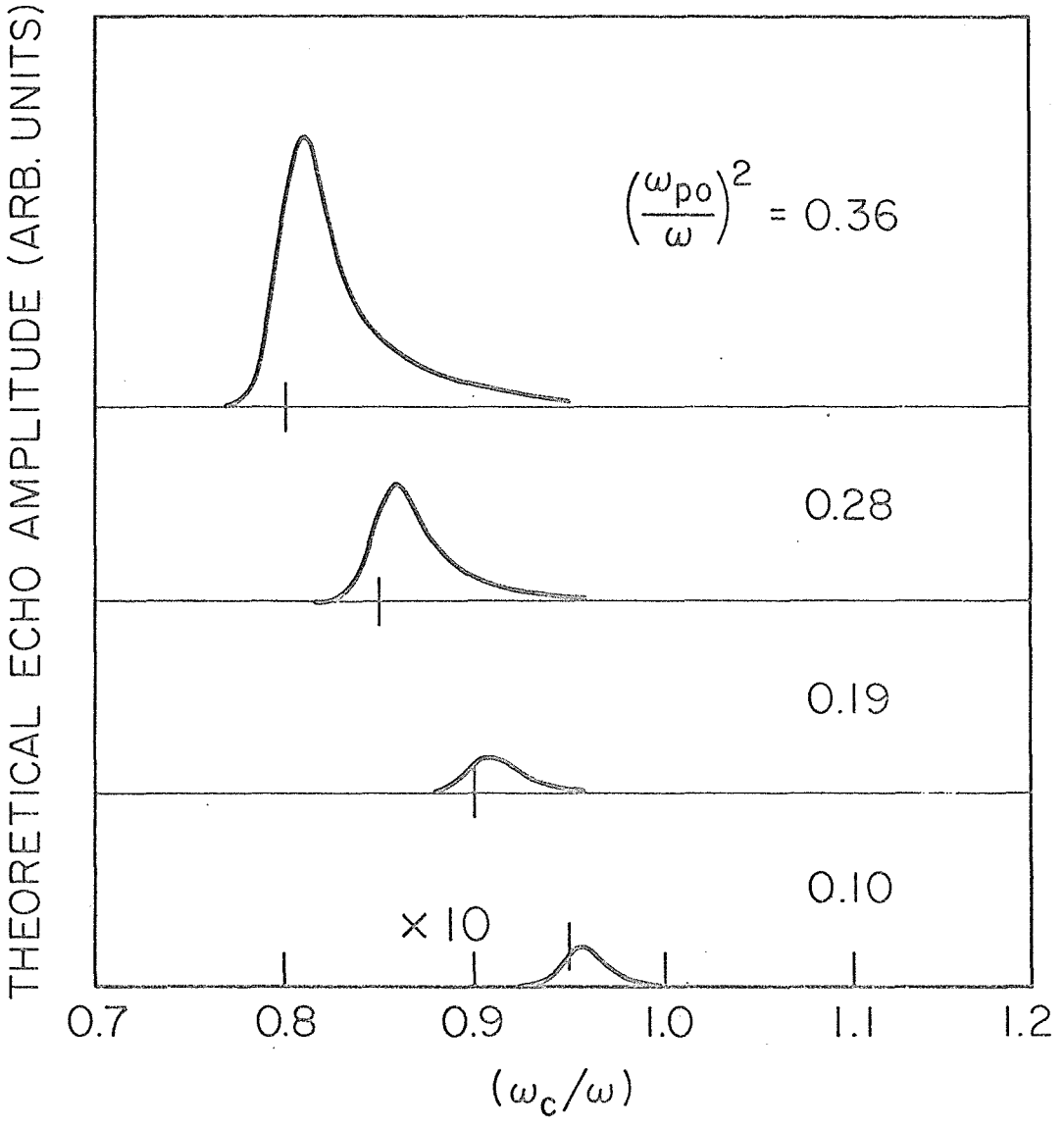

Fig. III.10 Theoretical echo spectra vs. electron density as given by weak excitation theory. The vertical bars locate maximum upper hybrid resonance $\omega = \omega_{ho}$.

functions exceed unity. These saturation processes are treated in the following section.

III.C.3b Large signal echoes. For high-density input pulse power, and/or τ the quantity $(z\tau)$ exceeds unity. The Bessel function terms then begin to decrease and oscillate with increasing $(z\tau)$. This effect represents saturation of the nonlinear processes and immensely complicates the echo properties. But it is under these conditions that much of the experimental data is taken. Therefore, we must now direct our attention to these saturation phenomena. Since we expect the echo amplitude itself to show a concomitant saturation, we refer to the echoes under these conditions as large signal echoes.

There are four basic independent variables which change the shape and amplitude of the echoes: (1) magnetic field (ω_c/ω), (2) electron density $(\omega_{po}/\omega)^2$; (3) separation of the two pulses (τ); and (4) input power of the pulses $(\propto V_o^2)$. The main objective here is to calculate the echo amplitude as these parameters are varied. The number of variables involved presents some difficulty. We need to calculate curves which give us the most information while requiring the least amount of work and generating the least amount of confusion. The most apparent family of curves which we need are the echo spectra, i.e., the echo amplitude vs. (ω_c/ω) with density power and pulse separation fixed. The experimental equivalents of these curves were given in Section III.A. In order to compute the echo amplitude E_1 the integrals of Eqs. 55 must be carried out. The integrands $\mathcal{A}_1$ and $\mathcal{B}_1$ are sufficiently complicated in general to warrant numerical treatment of

the integrals. Rewriting Eqs. 55 in a form convenient for numerical computation, we have

$$E_1 = A_1^2 + B_1^2$$

$$\begin{Bmatrix} A_1 \\ B_1 \end{Bmatrix} = \frac{V_o(\omega\Delta t)}{\sqrt{2}} \int_0^1 dy \, \frac{\omega_p^2}{\omega_h \omega} g(\omega_h) \begin{Bmatrix} a(z\tau) \\ b(z\tau) \end{Bmatrix} \tag{63}$$

where $y \equiv (x_o/a)$, $g(\omega)$ is the Gaussian given by Eq. 47 and

$$a(z\tau) = -\left[J_1(z\tau)\sin(z\tau) + J_2(z\tau)\cos(\tfrac{3}{2}z\tau)\right]$$

$$b(z\tau) = \left[J_1(z\tau)\cos(z\tau) - J_2(z\tau)\sin(\tfrac{3}{2}z\tau)\right] \tag{64}$$

with $z\tau$ given by Eq. 50. Using the fact that $\omega_p^2 = \omega_{po}^2 H(x)$, Eq. 50 can be written as

$$z = \left\{\frac{V_o^2 \Delta t^2}{64a^2}\left(\frac{e}{m}\right)^2 \left(\frac{\omega_{po}^2}{\omega^3}\right)\right\}\left\{g^2(\omega_h)\frac{\omega^3}{\omega_h^3}\right\}\left\{H'' - \frac{5}{3}\left(\frac{\omega_{po}^2}{\omega_h^2}\right)(H')^2\right\} \tag{65}$$

The first bracket in Eq. 65 is the term of most interest. For a given set of conditions it sets the scale of variation of $z\tau$. Note that it is directly proportional to the input power of the pulses ($\sim V_o^2 \Delta t^2$) , the electron density ($\sim \omega_{po}^2$), and the separation of the pulses (τ) . It is particularly significant that these factors appear in a mutual product. Because of this the change in certain properties of the echo depends roughly only on the percentage change in the

product $(z\tau)$. Also, we will be interested in the echo amplitude under saturation conditions, i.e. conditions such that the echo no longer grows rapidly with increasing excitation, but begins to level off or even decreases. As a result of the properties of Bessel functions, we know that saturation will begin to occur when $(z\tau)$ is of order one or greater. From the argument given above, increasing input power, electron density, and/or τ brings one closer to saturation. If we call the normalized input power P , the echo amplitude has the following functional form,

$$E_1 = P \times G[P\tau\ \omega_{po}^2, (\omega_{po}/\omega),\ (\omega_c/\omega)] \tag{66}$$

where the $(P\tau\omega_{po}^2)$ combination has been made explicit. It is helpful to keep in mind that as $P\tau \to \infty$, $G \sim (1/P\tau)$ (see Section III.B). Equation 66 is very useful for the purposes of qualitative understanding of some of the results to be given below.

At first sight the saturation condition $z\tau \sim 1$ may appear to violate both the perturbation condition (Eq. 59) and the cross-over condition (Eq. 58). However, since $z\tau \sim [\beta(\delta x)_{max}^2\ (\omega_h\tau)]$ and $(\omega_h\tau)$ is typically $\sim$2000, saturation does not imply a breakdown in the perturbation procedure. The $(\omega_h\tau)$ factor shows that the strength of the nonlinear effects is enhanced by the passage of time. Of course, as pointed out above, for x_o near a , the cross-over condition requires $(z\tau) << 1$ which implies no saturation. But for x_o near zero, the cross-over condition allows $(z\tau) >> 1$. This problem with the cross-

over condition will be ignored. This is not as bad as it seems. We will find that the primary contributions to the echo come from oscillations in the plasma near $x_o = 0$ where the cross-over restriction is not serious. Furthermore, under conditions where cross-over occurs the nonlinear effects may even be enhanced by viscous and temperature phenomena. In spite of all these approximations, the results will prove very enlightening.

Figures III.11-13 show plots of echo spectra with $(P\tau)$ and $(\omega_{po}/\omega)^2$ as parameters for the case of an x-4th density profile, $H(x) = 1 - (x/a)^4$ (30). The exciting pulses were taken to have spectral half widths $(\Delta\omega/\omega)$ of 0.04, a close approximation to the experimental conditions. The densities shown are comparable with the experimental ones of Section III.A. The vertical lines mark the value of (ω_c/ω) which corresponds to resonance at the maximum upper hybrid frequency ω_{ho} of the plasma. In these and other figures of this section both P and τ will be used as a shorthand notation for the same normalized variable

$$P\tau \quad \text{or} \quad P \quad \text{or} \quad \tau \Longrightarrow \frac{V_o^2 \, \Delta t^2}{8a^4} \left(\frac{\tau}{\omega}\right) \left(\frac{e}{m}\right)^2 \tag{67}$$

If P is written it is implied that when P is varied τ is held fixed and vice-versa. When the product $(P\tau)$ is written explicitly, it is implied that variation of either P or τ, or both applies to the case being considered. The echo amplitude is normalized to the value $E_o = 10^{-2} \left(\frac{m}{e}\right)^2 \frac{4a^4\omega^3}{\tau}$. Note that in all cases the echo is strongest near the maximum upper hybrid frequency of the plasma. The same

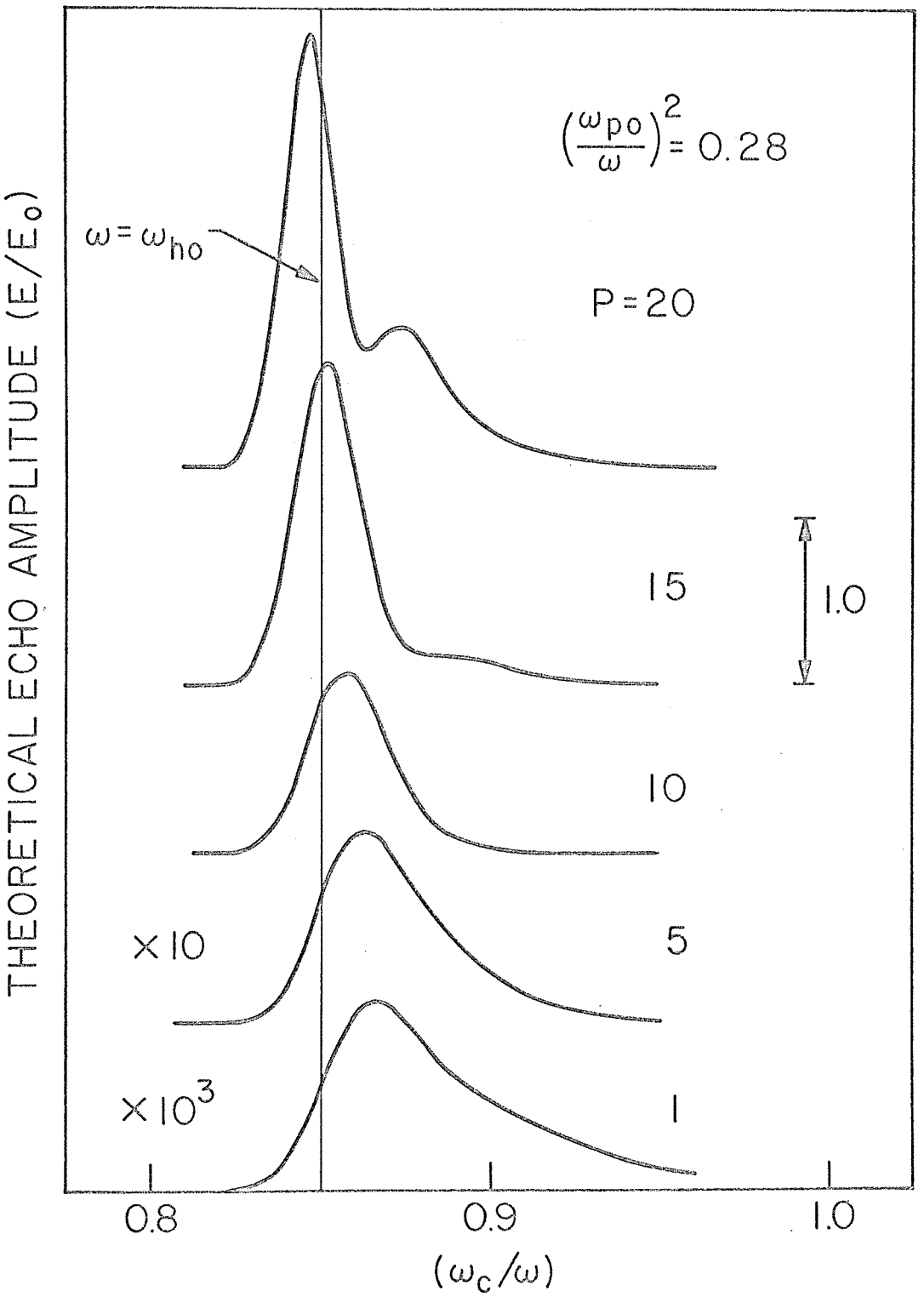

Fig. III.11 Theoretical echo spectra vs. power with $(\omega_{po}/\omega)^2 = 0.28$

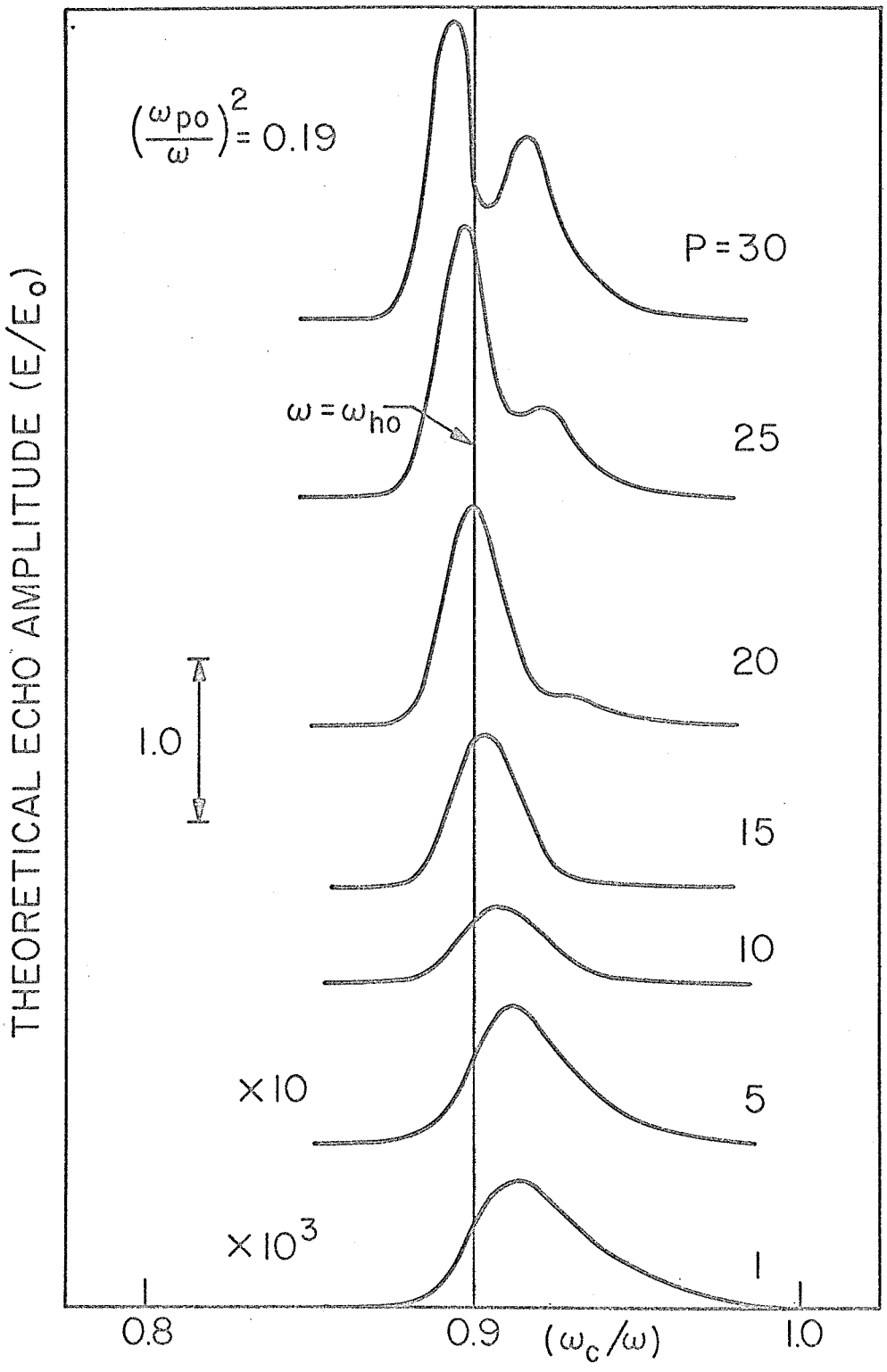

Fig. III.12 Theoretical echo spectra vs. power with $(\omega_{po}/\omega)^2 = 0.19$

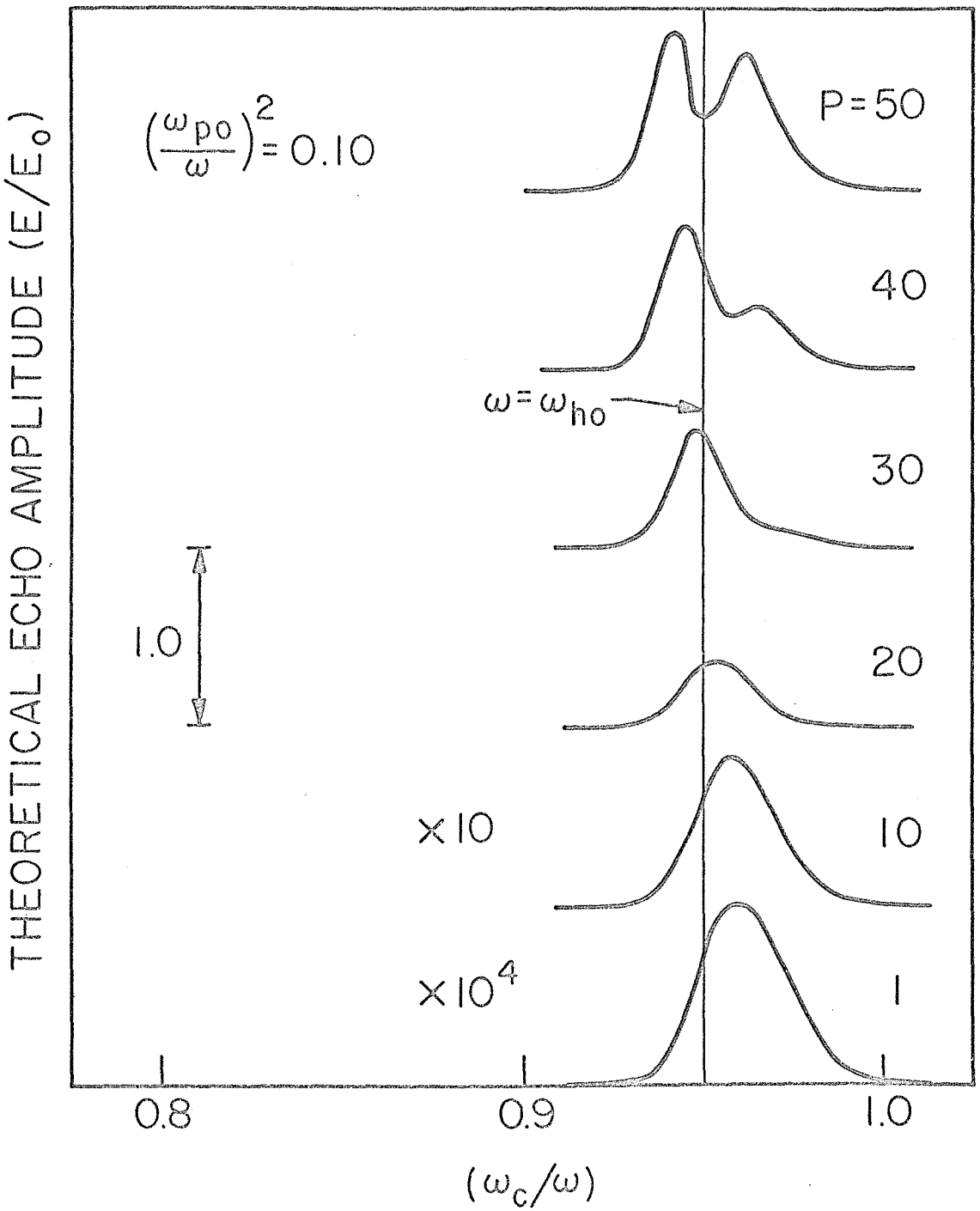

Fig. III.13 Theoretical echo spectra vs. power with $(\omega_{po}/\omega)^2 = 0.10$

phenomena was shown experimentally in Section III.A. Furthermore, the experimental and theoretical half widths are comparable. In fact, both the experimental and theoretical half widths decrease with increasing P. Since there is a rough inverse correlation between the real time echo half width and the echo spectrum half width, one would expect the echo to become wider in time as $(P\tau)$ increases. This is born out by experiments (10). The shift of the position, i.e. value of (ω_c/ω), of the maximum echo toward the maximum upper hybrid frequency as $(P\tau)$ is increased, is another characteristic feature of all the data (29). This shift is also observed experimentally (10); Fig. III.14 shows a typical set of Bauer's experimental curves. Inspection of Eq. 6b shows that changing either P or τ has <u>exactly the same effect</u> on the shape and position of the echo spectra. Another important result is that the shape and position of the low-$(P\tau)$ echo spectra become independent of $(P\tau)$. Thus the low-$(P\tau)$ echo spectra can serve as a convenient reference point for some measurements. The multiple peaks that develop at high values of $P\tau$ are evidence of strong saturation effects $(z\tau \gtrsim 1)$. As $(P\tau)$ is increased to even higher values than shown in the figures, the spectra exhibit numerous multiple peaks and a complex structure. As the density decreases, higher and higher values of $(P\tau)$ are required to see these saturation effects. Although experiments have shown mild (a small secondary peak) saturation effects in the echo spectra, strong double peaks were not found; this may be just a result of the limited power available in the experiments.

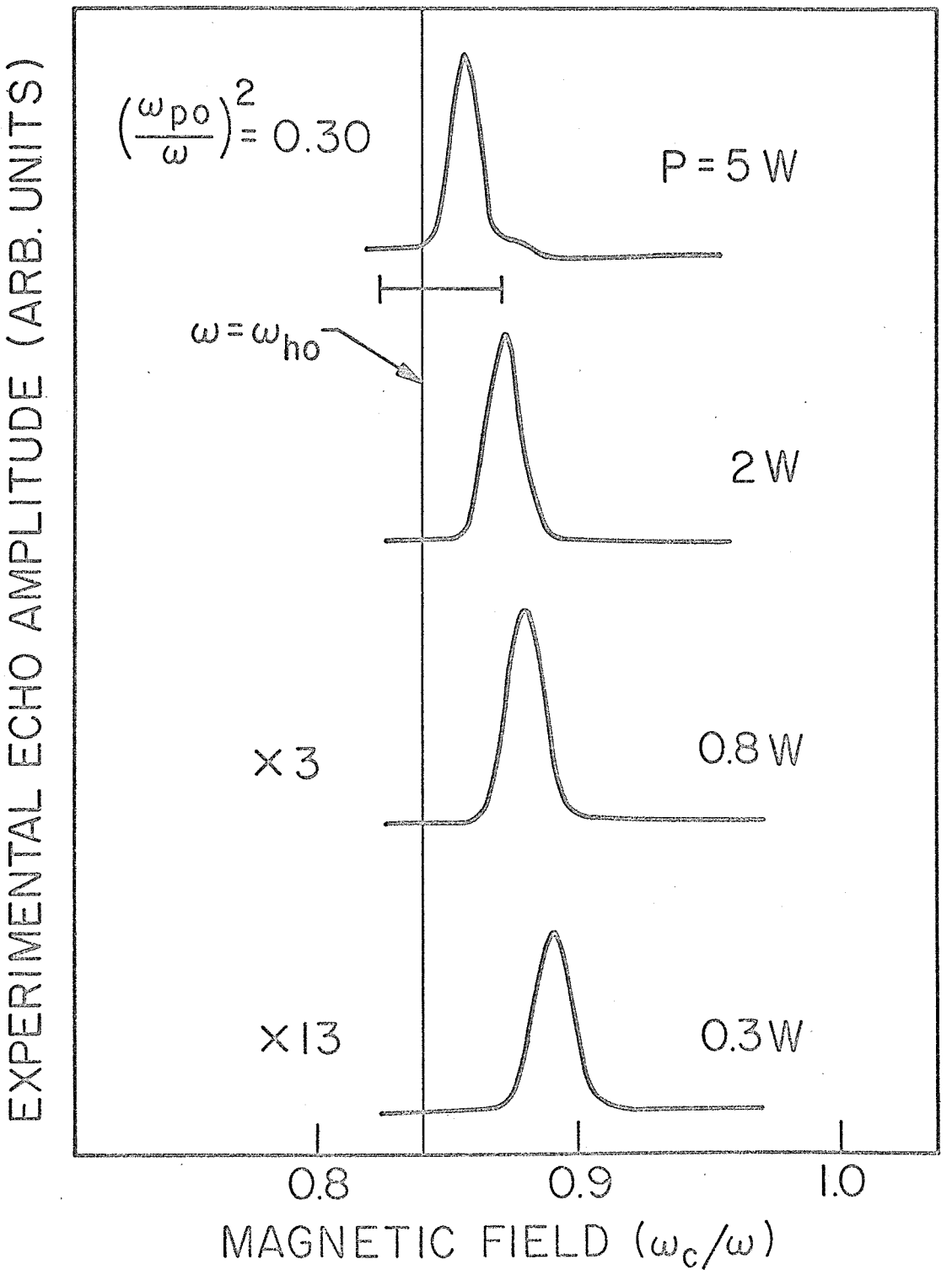

Fig. III.14 Experimental echo spectra vs. power (after Bauer). The horizontal bar indicates the approximate error in locating the line $\omega = \omega_{ho}$

Figure III.15a shows another useful characterization of the upper hybrid echoes in the form of the loci of points of maximum echo in the $[(\omega_c/\omega) - P\tau]$ plane. In the shaded region of the diagram saturation sets in and the spectra develop multiple peaks. The data of Fig. III.15a tell one how to choose the external parameters to achieve strong echoes. This diagram of peak echo loci is particularly interesting because the four major variables of the experiment are all varied. Moreover, the equivalence of the variation of P and τ becomes more apparent. Experimental equivalents of Fig. III.15a are easy to obtain and show qualitatively similar features (10). It is particularly significant that the equivalence of P and τ is born out by experiments. One further supplemental curve can be extracted from Figs. III.11-13. A plot of the peak echo amplitude versus density is shown in Fig. III.15b. The parameter is P and the echo is normalized to one at the highest density for each value of P. The echo amplitude falls off rapidly with decreasing electron density. Experimental data equivalent to that of Fig. III.15b show a more complex behavior and fall off more slowly, in general.

Despite all the approximations leading to the final echo amplitude formulas, the theoretical results of Figs. III.11-15 show a remarkable qualitative resemblance to the experimental data. No quantitative comparison between theory and experiment has been attempted due to the ideal nature of the theoretical model. Since all four independent variables (P,τ,(ω_{po}/ω), and (ω_c/ω)) are changed in Figs. III.11-15, the family of curves characterizes in principle most properties of the echo amplitude. As a practical matter it is

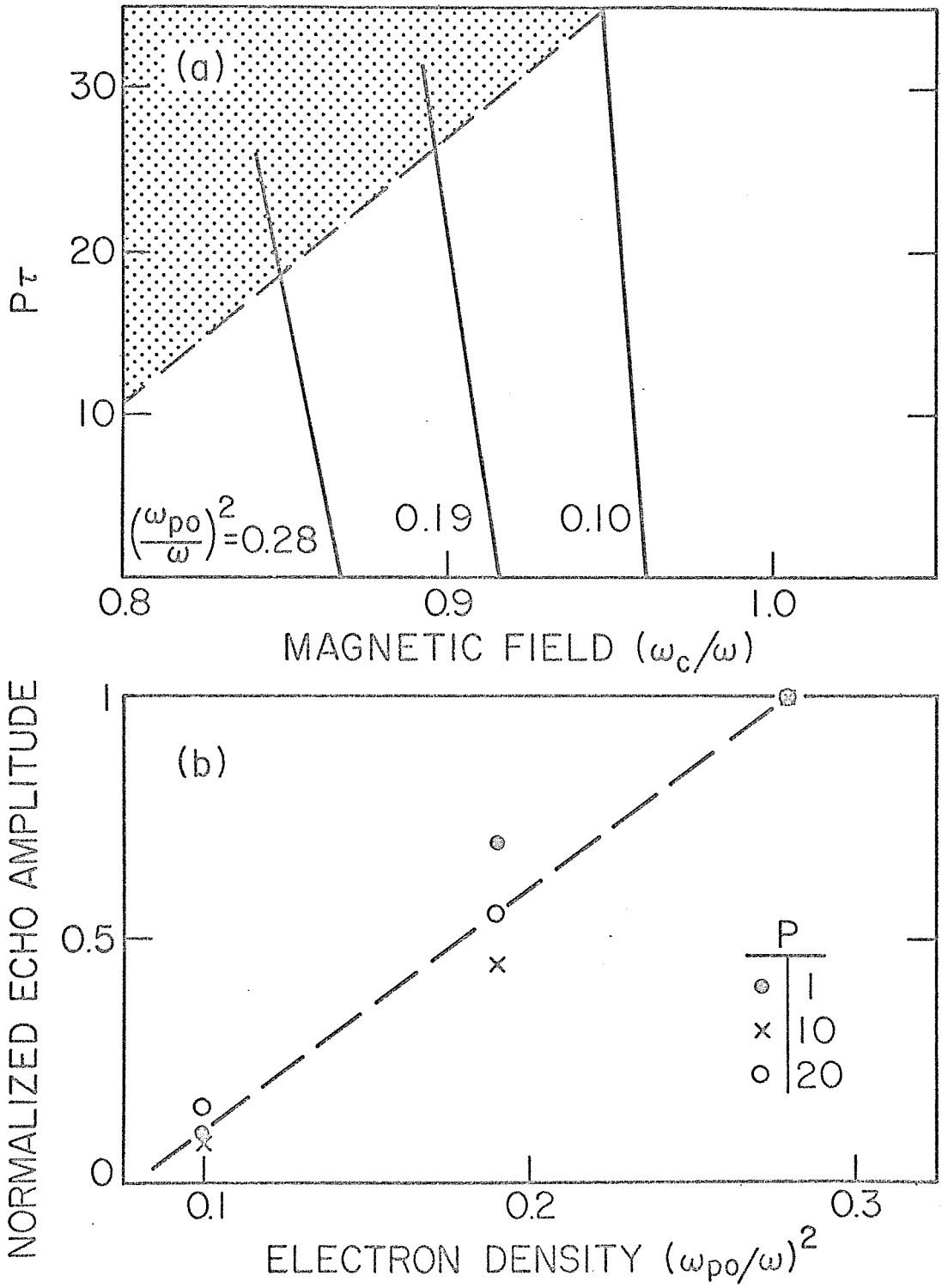

Fig. III.15 Theoretical curves: (a) Loci of peak echo in the [(ω_c/ω), Pτ] plane; (b) Normalized echo amplitude vs. electron density.

convenient to plot other families of curves, particularly in light of certain convenient experimental measurements.

Experimentally it is convenient to measure the echo strength versus input power P while holding other parameters fixed. We will refer to such data as echo power curves. For a fixed electron density Fig. III.16 displays a family of power curves with (ω_c/ω) as a parameter. The values of (ω_c/ω) chosen are near maximum upper hybrid resonance which occurs at 0.9 for this density. As (ω_c/ω) increases, the echo saturates at lower and lower values of input power. This varying saturation phenomenon occurs in the experiments. At low input power the echo increases as P^3 for all values of (ω_c/ω) as one would expect from the results of the previous section (see Eq. 26). Experimentally the echo is generally found to increase as P^n with $3.5 \lesssim n \lesssim 4.5$. Figure III.17a shows a set of power curves with $(\omega_{po}/\omega)^2$ as a parameter. For each value of the electron density (ω_c/ω) was chosen to give the maximum echo at low (P_T). This is a good example of the use of the low power spectrum as a point of reference. The pronounced dip followed by a sharp rise in echo strength has not been observed experimentally, although in some cases one appears to be near the bottom of the dip. Again, failure to observe this rise may result from the limited power available in the experiments. This is consistent with the similar observation concerning multiple peaks (saturation) in the echo spectra, since power saturation effects and spectra saturation effects occur together. The depth of the minimum depends strongly on the density profile. For example, for an x-squared

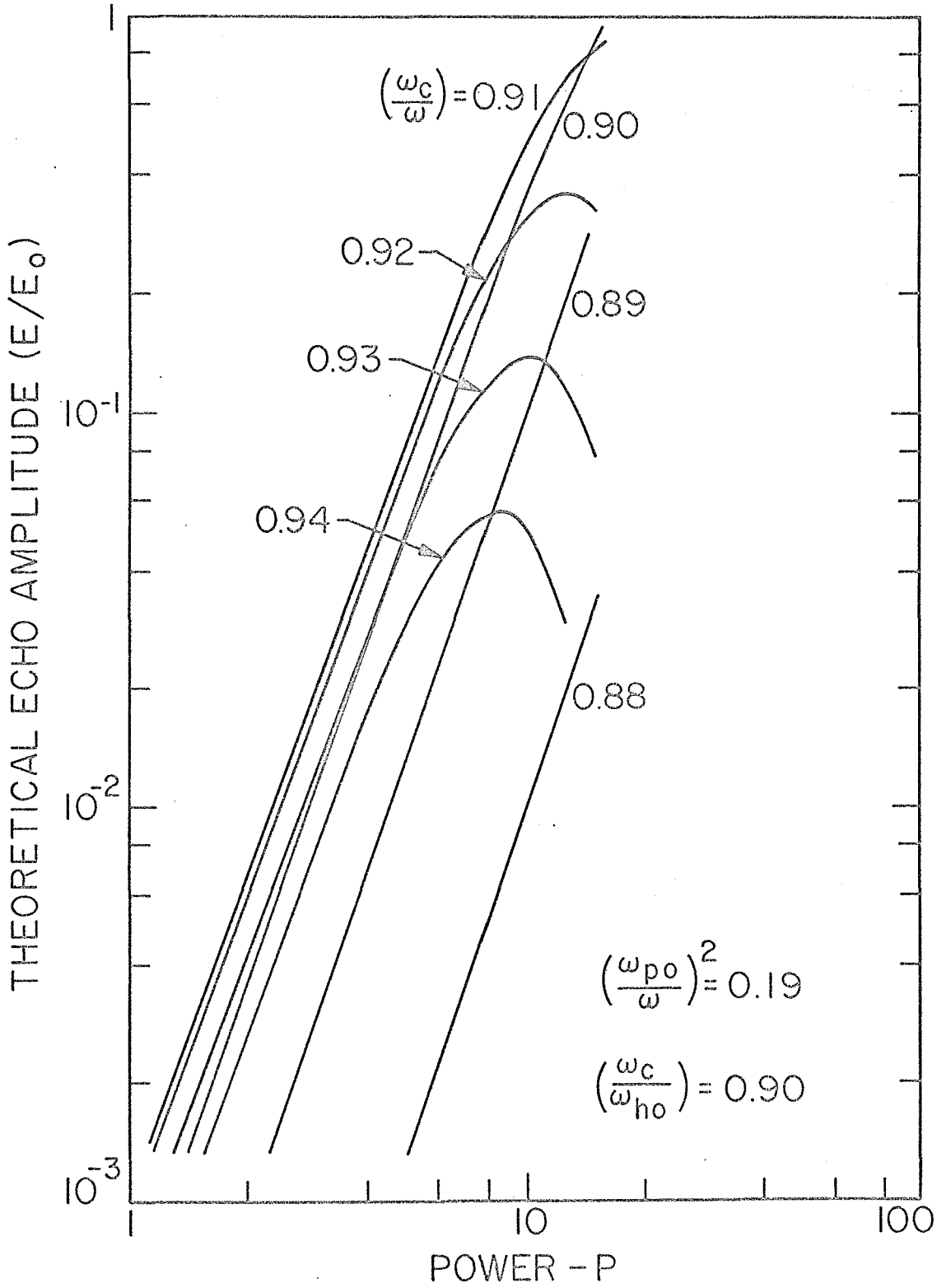

Fig. III.16 Theoretical echo amplitude vs. power with (ω_c/ω) as a parameter.

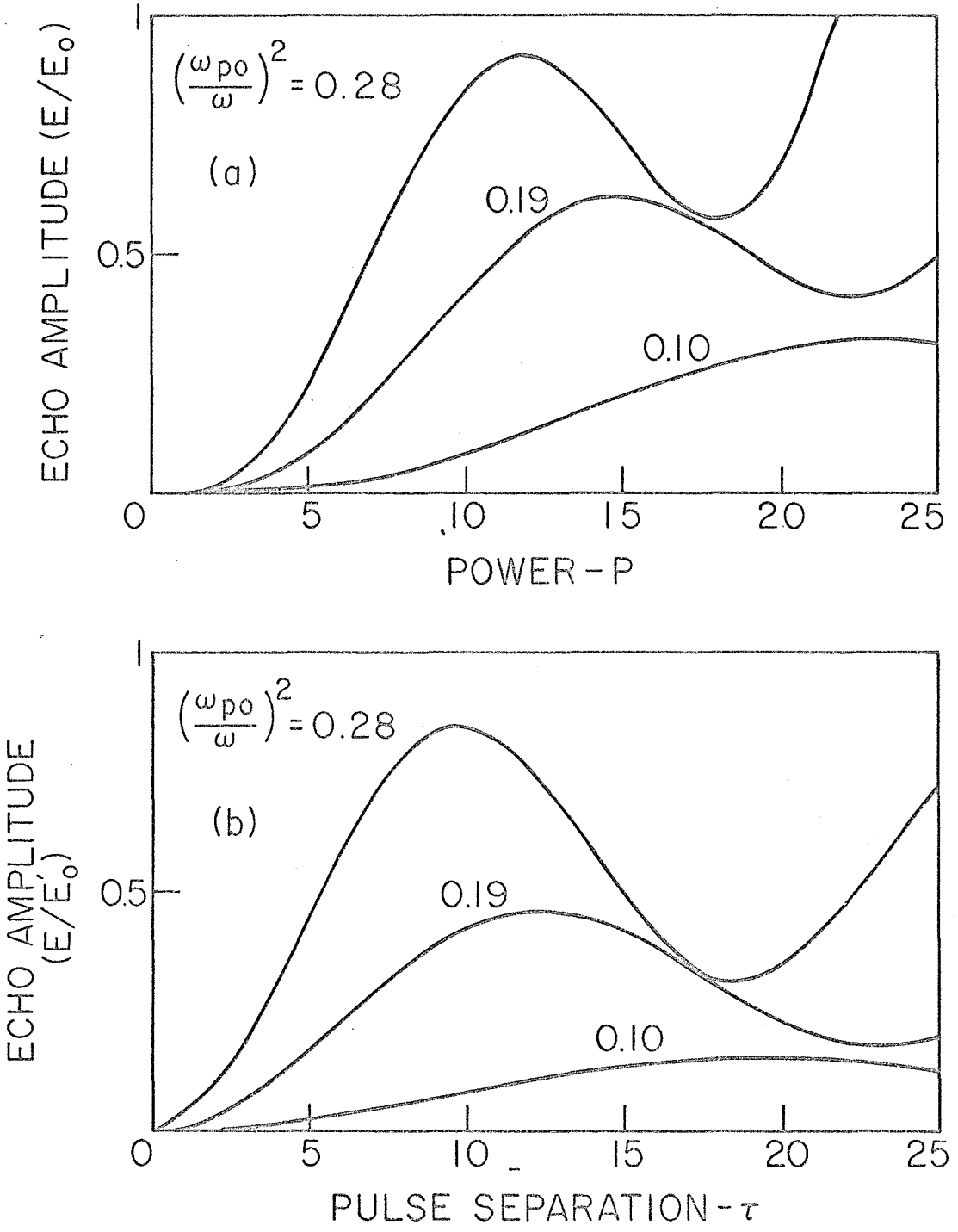

Fig. III.17 Theoretical curves: (a) Echo amplitude vs. power, and (b) echo amplitude vs. pulse separation, with $(\omega_{po}/\omega)^2$ as a parameter $(E'_o = (10^{-3}\ V_o^2\omega^2\Delta t^2)/2)$.

profile, the echo amplitude in the dip can be two orders of magnitude below the echo amplitude at the first power peak.

One other family of curves is typically studied in multiple pulse echo studies. They are plots of echo amplitude versus τ, all other parameters being fixed. These curves are often referred to as echo envelopes, but are not to be confused with the real time envelope of the microwave signal constituting the echo itself. From Eq. 66 it is clear that these echo envelopes will have the same general behavior as the power curves with the exception of the linear factor of P in front of G. Thus, envelopes corresponding to the power curves of Figs. III.16 and III.17a will have the same general features, peaks and valleys being similar. Figure III.17b shows a set of three envelopes under conditions identical to those given for the power curves of Fig. III.17a. Two points are of particular interest. First, as τ goes to zero the echo amplitude goes to zero. This feature is characteristic of all echo systems in which the primary nonlinear effect occurs during the "free decay" evolution of the system, rather than during the excitation pulses (see Section III.B). Second, the position of the maximum echo moves to later τ as the electron density decreases. In practice, the echo envelopes are complicated by the presence of relaxation effects (due to electron-neutral collisions, for example) which have been neglected in our idealized model, but are always present in experiments. As was pointed out in Section III.B, if the relaxation time is T the echo amplitude would be expected to be diminished by a factor $\exp[-\tau/T]$ from that expected in the absence of relaxation. Clearly,

this factor can significantly affect the envelopes, depending on the relation between τ and T. For example, although the collisionless theory indicates that multiple oscillations of a complex nature occur in the echo envelopes, if T were short enough, these oscillations could be strongly damped by the exponential factor. In fact, for a given input power level, when T is short compared to the value of τ necessary to achieve collisionless saturation, the fall off of the envelope for large τ would be expected to be approximately monotonic and determined mainly by the exponential relaxation term. However, even in this extreme case of the influence of relaxation, the qualitative trends in the position of the peak echo (as τ is varied) remain the same. That is, as the electron density decreases the maximum echo occurs at larger τ.

Recalling Eq. 66 and the results given above, we can describe qualitatively the main properties of the upper hybrid echoes. First, consider the electron density to be fixed. Then, for a given P and τ, the echo amplitude is a strong function of (ω_c/ω), being strongest in a narrow band near the maximum upper hybrid frequency of the plasma. As $(P\tau)$ is increased this narrow band moves to higher frequencies (toward lower values of (ω_c/ω)). For a fixed τ and magnetic field, the echo increases as P^3 for low powers, but saturates at higher powers. The onset of this saturation in the power curves occurs at lower values of P as (ω_c/ω) is increased. In the same range of P that the power curves show saturation, the echo spectra begin to exhibit multiple peaks. For fixed (ω_c/ω) and P the echo increases as

τ^2 for small pulse separation, but saturates at large values of τ and shows the same oscillations occurring in the power curves. Now, consider variations in the electron density. The qualitative features described above are the same for all electron densities. There are quantitative differences from one electron density to another. As (ω_{po}/ω) decreases the echoes get weaker. Furthermore, the lower the electron density the higher the value of P required to reach saturation levels. The universal character of the saturation phenomena and their relation to the product $P\tau\ \omega_{po}^2$ (see Eq. 66) should be emphasized. Basically, it is this product which determines the onset of saturation and, indeed the amplitude of the echo to a large extent.

III.C.4 Discussion

The computations of this section are by no means exhaustive with respect to the properties of upper hybrid echoes. As pointed out above, the effect of relaxation on echo envelopes has not been included. No calculations of real time echo shapes were carried out. In actual experiments relaxation effects are important for measurements such as envelopes, and echo half-widths (real time) are found to vary significantly with experimental conditions (10). The variations seen experimentally are roughly what one expects from looking at the theory, but no attempt to compare in detail has been made. Also, no attempt has been made to systematically study the effect on the echo of varying the density profile, H(x). The importance of this profile in determining the echo characteristics is apparent. Only qualitative features have

been established and the functional forms of $H(x)$ were chosen for simplicity and convenience. Furthermore, the spectral width of the escitation pulses was not changed. A value comparable to that used in experiments was chosen and used for all calculations.

The essential nonlinear effect in the upper hybrid echo process manifests itself as an amplitude dependence of the eigenfrequency of a given plasma mode. In general, relaxational nonlinearities also produce echoes. It is interesting to note that some of the characteristics of the upper hybrid echo are not unique to a collisionless model. One could, in principle, include an amplitude dependent phenomenological collision frequency supplying both relaxation and another nonlinear mechanism without qualitatively affecting some features of the results. For example, the echo is strongly peaked near the maximum upper hybrid frequency because of the high density of normal modes there and not because of the nature of the nonlinearity. However, the over-all favorable comparison between theory and experiment, and some of Bauer's (10) experimental measurements suggest strongly that the nonlinear restoring force effects, which yield amplitude dependent frequencies, are of paramount importance and dominate the echo process.

Finally, although the theoretical properties of the upper hybrid echoes are rather complex, we have been able to discern some essential features. Even though the theory borders on being phenomenological and incorporates numerous approximations, it has proved capable of reproducing some of the salient features of the experimental results. For this reason the theory presented can serve as a valuable guide in carrying

out experiments. In fact, in doing experiments one has the tendency at times to attribute certain complexities in the echo properties to error and a lack of control in the experiments, only to find that careful thought, theoretical calculations, and additional measurements produce understanding.

References: Section III

1. R. M. Hill and D. E. Kaplan, Phys. Rev. Letters 14, 1062 (1965).

2. D. E. Kaplan and R. M. Hill, Seventh Annual Meeting of the Plasma Physics Div., Am. Phys. Soc. (Nov. 1965); Bull. Am. Phys. Soc. 11, 496, 538 (1966); G. F. Herrmann, R. M. Hill, and D. E. Kaplan, Phys. Rev. 156, 118 (1967); F. W. Crawford and R. S. Harp, Phys. Letters 21, 292 (1966); J. Appl. Phys. 37, 4405 (1966); D. E. Kaplan, R. M. Hill, and A. Y. Wong, Phys. Letters 22, 585 (1966); R. S. Harp, R. L. Bruce, and F. W. Crawford, J. Appl. Phys. 38, 3385 (1967).

3. L. O. Bauer, F. A. Blum and R. W. Gould, Phys. Rev. Letters 20, 435 (1968).

4. R. W. Gould, Phys. Letters 19, 477 (1965); California Institute of Technology, Tech. Report No. 28, Contract Nonr 220(50), Dec. 1965.

5. W. H. Kegel and R. W. Gould, Phys. Letters 19, 531 (1965); W. H. Kegel, Phys. Letters 23, 317 (1966); Plasma Phys. 9, 23, 339 (1967); L. O. Bauer, R. W. Gould and W. H. Kegel, Bull. Am. Phys. Soc. 12, 756 (1967).

6. G. F. Herrmann and R. F. Whitmer, Phys. Rev. 143, 122 (1966).

7. R. W. Gould, T. M. O'Neil and J. H. Malmberg, Phys. Rev. Letters 19, 219 (1967); R. W. Gould, Phys. Letters 25A, 559 (1967); J. H. Malmberg, C. B. Wharton, R. W. Gould, and T. M. O'Neil, Phys. Rev. Letters 20, 95 (1968).

8. H. Ikezi and N. Takahashi, Phys. Rev. Letters 20, 140 (1968); D.R. Baker, N. R. Ahern and A. Y. Wong, Phys. Rev. Letters 20, 318 (1968).

9. R. W. Gould and F. A. Blum, Eighth International Conference on Phenomena in Ionized Gases, (Springer Verlag, Vienna, 1967), p.405.

10. L. O. Bauer, Ph.D. Thesis, California Institute of Technology, (May 1968).

References: Section III (Continued)

11. D. E. Kaplan, M. Brown and J. A. Cowen, Rev. Sci. Instr. 32, 1182 (1961).

12. L. O. Bauer, F. A. Blum and R. W. Gould, Bull. Am. Phys. Soc. 13, 259 (1968).

13. R. M. Hill and D. E. Kaplan (Private communication).

14. D. E. Kaplan, R. M. Hill and A. Y. Wong, Phys. Letters 22, 585 (1965).

15. G. Bekefi, Radiation Processes in Plasmas (John Wiley, New York, 1966), p. 223.

16. E. L. Hahn, Phys. Rev. 80, 580 (1950).

17. R. P. Feynman, F. L. Vernon and R. W. Hellwarth, Phys. Rev. 28, 49 (1957).

18. For example: (1) solid, J. P. Gordon and K. D. Bowers, Phys. Rev. Letters 1, 368 (1958); (2) liquid, reference (16); (3) gas, R. M. Hill, D. E. Kaplan, G.F. Herrmann, and S. K. Ichiki, Phys. Rev. Letters 18, 105 (1967); and (4) plasma, Reference (1).

19. N. A. Kurnit, I. D. Abella and S. R. Hartmann, Phys. Rev. Letters 13, 567 (1964).

20. D. E. Kaplan, Phys. Rev. Letters 14, 254 (1965).

21. J. J. Stoker, Nonlinear Vibrations in Mechanical and Electrical Systems (Interscience, New York, 1950).

22. A. Papoulis, The Fourier Integral and Its Applications (McGraw-Hill Co., New York, 1962), p. 278.

23. M. Abramowitz and I. A. Stegun, Eds., Handbook of Mathematical Functions, (U. S. Government Printing Office, Washington, D. C., 1964), p. 361.

24. This technique of treatment follows closely that used in independent particle theories of plasma echoes. See, for example,

References: Section III (Continued)

references (4) and (5).

25. A. Y. Wong and O. Judd (to be published).

26. J. M. Dawson, Phys. Rev. 113, 383 (1959).

27. E. M. Barston, Annals Phys. 29, 282 (1964).

28. One could place the plasma in a parallel-plate transmission line as was done in Section II. This procedure was necessary in order to compute reflection and absorption coefficients. However, since we are interested only in studies of the relative echo strength, we will simplify matters by computing only the voltage across the plasma and ignore the circuit factors involving coupling between the plasma and the external load. Furthermore, the plasma impedance is high near the maximum upper hybrid frequency where the echo is strongest and coupling to the plasma should be very effective. In any case, none of the qualitative features of the theoretical results will be changed by this simplification.

29. Actually the motion of the plasma is two-dimensional due to the action of the magnetic field. Since we consider only longitudinal electric fields in the x-direction, the x and y motions are coupled only through the action of $\underline{B}$. This coupling has no effect on the space charge restoring force so that the problem reduces to a one-dimensional one with an additional restoring force in the x-direction which is given by $(\omega_c^2\ \delta x)$.

30. The x-4th density profile is chosen over the x-squared used in Section II because of its ability to reproduce some important qualitative features of the experimental results. In particular, the echo spectra are found power dependent in the experiments. Careful study of Eqs. 60-63 shows that the experimental features can be reproduced theoretically if $z\tau$ is a function of x. For an x-squared profile, the leading term in $(z\tau)$ is independent of x. While for an x-4th profile, the leading term goes like x^2.

References: Section III (Continued)

Other choices for H(x) could serve the same purpose; the x-4th form is chosen only for convenience.

"... Not with a bang but a whimper."
--The Hollow Men, T. S. Eliot

IV. CONCLUSION

One major conclusion to be drawn from this work is that experiment and theory point to a strong relation between the microwave normal mode properties of low temperature laboratory magnetoplasmas and upper hybrid oscillations. Both emission and reflection experiments show what were interpreted as upper hybrid resonance effects and simple cyclotron resonance effects. Although some differences were found between various gases, the basic features and consistent scaling with electron density were always present. The general simplicity and systematic form of the continuous wave data is most noteworthy. The behavior found, particularly the peaks at cyclotron resonance, constitute a completely new observation. The properties of echoes from the same plasmas also show an intimate relation to the upper hybrid frequencies. For example, in the high density case, the echoes were strongest near what was taken to be the maximum upper hybrid frequency of the nonuniform plasma column. Therefore, all the microwave phenomena studied here including the echo processes, are dominated by these collective upper hybrid plasma oscillations.

The theory of a nonuniform cold plasma was found capable of predicting qualitatively many of the effects associated with the upper hybrid oscillations. Most notable is the considerable success of the nonlinear theory in predicting qualitatively many observed properties of the upper hybrid echoes. As is the case experimentally, the upper hybrid echoes were found strongest near the maximum upper hybrid

frequency of the nonuniform slab. Furthermore, the power and pulse separation dependence of the echo spectra proved to agree with experiment, along with other saturation effects. The complexity and number of such properties make a strong case for the general upper hybrid oscillation model. Unfortunately, the cold plasma theory is unable to account for the cyclotron resonance peaks observed in the noise emission and echo spectra. Considering the success of the cold plasma theory in reproducing the upper hybrid phenomena, the consistent failure of the theory to account for the microwave observations made in the immediate vicinity of cyclotron resonance suggests that the theory is inadequate in this domain. One naturally expects that an appropriate hot plasma theory would eliminate this discrepancy. Although this problem with the theory was not resolved, considerable insight concerning the phenomena at hand was gained by consideration of the cold plasma model.

As a supplementary topic, the theory of echoes from a system of anharmonic oscillators not only served as a valuable tool in calculating the properties of upper hybrid echoes, but also gave some new insight concerning the characteristics of echo systems in general. The treatment of finite-pulse-width effects showed clearly the relation between the natural oscillator spectrum and the spectrum of the excitation pulses, further defining the conditions necessary for the observation of echoes in such systems.

The results of this paper also have very important implications concerning the interpretation of cyclotron echo experiments which were carried out previously with plasmas in a nonuniform magnetic field.

The cyclotron echo is strongest when ω is near ω_c. In the low density limit ($\omega_p << \omega_c$) the upper hybrid echo becomes essentially a cyclotron echo, since it is also strongest for $\omega \simeq \omega_c$. Therefore, the independent particle theories which have been used so universally in the interpretation of cyclotron echo experiments cannot be valid in general unless the spread in upper hybrid frequencies due to the spatial dependence of ω_p is considerably less than the spread due to magnetic field inhomogeneity. That is, the experiments must satisfy the condition $(\omega_{po}^2/2\omega_c) << (\Delta\omega_c/\omega_{co})$ where $\Delta\omega_c$ is the spread in cyclotron frequencies and ω_{co} is the value of the local cyclotron frequency at the position where the plasma density is greatest, i.e. where $\omega_p = \omega_{po}$. For typical laboratory experiments this condition places a significant limit on the maximum electron density ($\simeq 10^9 - 10^{10}$ cm^{-3}) for which the echo can be correctly understood on the basis of independent particle theories. The point is, that when the above condition is satisfied the primary restoring force for charge motion is furnished by the externally applied magnetic field. The space charge restoring forces ($\sim \omega_p^2$) are no longer important. The distribution of plasma eigenfrequencies and microwave properties are determined by the external magnetic field. Only under these conditions can an independent particle theory be appropriate.

Finally, it is interesting to note that the unique and profound role of steady state electron density gradients in determining the microwave properties of small laboratory plasmas has once again been demonstrated. These gradients furnished the collection of oscillators

(upper hybrid plasma oscillations) needed to get echoes from a cold plasma. It is clear that any quantitative theoretical description of the experimental results given here will require a detailed knowledge of the equilibrium density profile in discharges such as those studied. Previous studies, particularly of Tonks-Dattner and Buchsbaum-Hasegawa modes, have also shown very clearly this importance of inhomogeneities in bounded plasmas.

APPENDIX A: Calculation of the Cold Plasma Impedance

We wish to evaluate the plasma impedance given in Eq. II.4

$$Z_p = \frac{(\omega_c^2 - \omega^2)}{i\omega\varepsilon_o A} \int_{-a}^{a} \frac{dx}{\omega_c^2 + \omega_p^2(x) - \omega^2} \tag{1}$$

The parabolic density profile such that $\omega_p^2 = \omega_{po}^2(1 - x^2/a^2)$ is assumed. The basic problem is to compute the integral

$$I = \int_0^a \frac{dx}{(\omega_c^2 + \omega_{po}^2 - \omega^2) - \omega_{po}^2 x^2/a^2} \tag{2}$$

particularly when ω is in the range of upper hybrid frequencies, $[\omega_c, \omega_{ho}]$ where $\omega_{ho}^2 = \omega_c^2 + \omega_{po}^2$. Expanding the integrand in Eq. (2) in partial fractions yields

$$I = \frac{a^2}{2\omega_{po}^2 b}\left[\int_0^a \frac{dx}{b - x} + \int_0^a \frac{dx}{b + x}\right] \tag{3}$$

where $b^2 = a^2(\omega_{ho}^2 - \omega^2)/(\omega_{po}^2)$. The problem with the terms of Eq. 3 is that there is some value of x equal to b in the range $[0,a]$ when ω is in the upper hybrid range. Then the integrand of the first term in Eq. 3 has a simple pole at $x = b$. If one considers electron-neutral collision effects, b has a small negative imaginary part (when $\omega_c < \omega < \omega_{ho}$) which goes to zero as the collision frequency goes to zero. Taking this limit of zero collision frequency is the correct way to evaluate the integrals of Eq. 3.

$$I = \frac{a^2}{2\omega_{po}^2 b}\left[\lim_{\varepsilon \to 0}\int_0^a \frac{dx}{b - x + i\varepsilon} + \int_0^a \frac{dx}{b + x}\right] \tag{4}$$

Using the well known Dirac formulation of the first integral in Eq. 4 gives

$$I = \frac{a^2}{2\omega_{po}^2 b}\left[P\int_0^a \frac{dx}{b - x} - i\pi + \int_0^a \frac{dx}{b + x}\right] \tag{5}$$

where P indicates that the Cauchy principal value should be taken. The evaluation of I is now straightforward:

$$I = \frac{a^2}{2\omega_{po}^2 b}\left[\log\left(\frac{a+b}{a-b}\right) - i\pi\right] \quad .$$

For ω outside the upper hybrid range, the expression for Z_p can be found easily using standard integral tables.

$$\omega \leq \omega_c \ , \qquad Z_p = \frac{a}{i\omega\varepsilon_o A}\,\frac{\omega_c^2 - \omega^2}{\omega_{po}\sqrt{\omega_{ho}^2 - \omega^2}}\log\left[\frac{\sqrt{\omega_{ho}^2 - \omega^2} + \omega_{po}}{\sqrt{\omega_{ho}^2 - \omega^2} - \omega_{po}}\right]$$

$$\omega_c \leq \omega \leq \omega_{ho} \ , \qquad Z_p = \frac{a}{i\omega\varepsilon_o A}\,\frac{\omega_c^2 - \omega^2}{\omega_{po}\sqrt{\omega_{ho}^2 - \omega^2}}\left\{\log\left[\frac{\omega_{po} + \sqrt{\omega_{ho}^2 - \omega^2}}{\omega_{po} - \sqrt{\omega_{ho}^2 - \omega^2}}\right] - i\pi\right\}$$

$$\omega > \omega_{ho}, \qquad Z_p = \frac{-2a}{i\omega\varepsilon_o A}\,\frac{\omega_c^2 - \omega^2}{\omega_{po}\sqrt{\omega^2 - \omega_{ho}^2}}\tan^{-1}\left[\frac{\omega_{po}}{\sqrt{\omega^2 - \omega_{ho}^2}}\right]$$

APPENDIX B: Nonlinear Electrostatic Oscillations in Nonuniform, Cold Plasma

Dawson has derived general equations of motion for nonlinear electrostatic oscillations of a cold uniform plasma when there is no magnetic field present (see Reference 26 of Section III). We wish to extend his derivation to the case in which the plasma is nonuniform in the steady state. Consider the displacement of an electron fluid element from its equilibrium position $\underline{r}_o$ (holding the ions fixed).

$$\underline{r} = \underline{r}_o + \underline{R}(\underline{r}_o) \tag{1}$$

Conservation of charge requires

$$\rho_e(\underline{r})\, dV = \rho_i(\underline{r}_o) dV_o \tag{2}$$

where ρ_e is the electron charge density and ρ_i is the ion density. If the transformation given in Eq. 1 is single-valued and regular, dV and dV_o are related by the Jacobian,

$$dV_o = \frac{\partial(x_o, y_o, z_o)}{\partial(x, y, z)}\, dV \tag{3}$$

Then the equation of motion of the fluid element is given by

$$\frac{d^2\underline{R}}{dt^2} = - e \underline{E} , \tag{4}$$

where $\underline{E}$ is the solution of

$$\nabla_r \cdot \underline{E} = \frac{e}{\varepsilon_o}[\rho_i(\underline{r}) - \rho_e(\underline{r})] \tag{5}$$

From Eqs. 2 and 3, we know that

$$\rho_e(\underline{r}) = \rho_i(\underline{r}_o) \frac{\partial(x_o, y_o, z_o)}{\partial(x, y, z)} \tag{6}$$

which yields

$$\nabla_r \cdot \underline{E} = \frac{e}{\varepsilon_o}\left[\rho_i(\underline{r}) - \rho_i(\underline{r}_o) \frac{\partial(x_o, y_o, z_o)}{\partial(x, y, z)}\right] \tag{7}$$

Equations 4 and 7 constitute the desired results. In principle, they describe the nonlinear electrostatic oscillations of a cold inhomogeneous plasma in any number of dimensions which one chooses to cast the problem. They reduce to Dawson's results if the plasma is uniform in the steady state.

Appendix C: Detailed Experimental Conditions for Data Given in Figures

Figure	Neutral Pressure (μ Hg)	CW Power (dbm)	Pulse Power (W)	Pulse Separation (nsec)	Signal Frequency (GHz)
II.2	25	-10	-	-	2.8
II.3	35	-30	-	-	3.0
II.4	21	-23	-	-	3.0
II.5	10	-23	-	-	3.0
II.7	20	-21	-	-	9.0
II.9	18	-	-	-	3.0
II.10	10	-	-	-	3.0
III.2	35	-30	0.5	-	3.0
III.3	35	-30	0.5	100	3.0
III.4	21	-23	0.5	100	3.0
III.5	10	-23	5	150	3.0
III.6	20	-21	1	75	9.0
III.14	20	-	0.3-5	80	3.0